

THESIS ON NATURAL AND EXACT SCIENCES B230

A Computational Approach for Rational Monomer Selection in Molecularly Imprinted Polymer Synthesis

ROMAN BOROZNIJAK



TALLINN UNIVERSITY OF TECHNOLOGY
School of Engineering
Department of Materials and Environmental Technology

This dissertation was accepted for the defence of the degree of Doctor of Philosophy in Natural and Exact Sciences on 05, 2017.

Supervisor: Dr. **Vitali Syritski**, Department of Materials and Environmental Technology, Tallinn University of Technology

Co-supervisors: Prof. **Andres Öpik**, Department of Materials and Environmental Technology, Tallinn University of Technology

Opponents: Prof. **Arunas Ramanavicius**, Faculty of Chemistry, Vilnius University, Lithuania

Dr. **Krzysztof Noworyta**, Department of Physical Chemistry of Supramolecular Complexes, Institute of Physical Chemistry, Polish Academy of Sciences, Poland

Defence of the thesis: May 22, 2017 at 12.00
Lecture hall: U06A-229
Tallinn University of Technology, Ehitajate tee 5,
Tallinn

Declaration:

Hereby I declare that this doctoral thesis, my original investigation and achievement, submitted for the doctoral degree at Tallinn University of Technology, has not previously been submitted for any academic degree.

/Roman Boroznjak/



Copyright: Roman Boroznjak, 2017
ISSN 1406-4723
ISBN 978-9949-83-096-1 (publication)
ISBN 978-9949-83-097-8 (PDF)

LOODUS- JA TÄPPISTEADUSED B230

**Monomeeride valiku protsessi modelleerimine
optimaalse monomeeri leidmiseks molekulaarselt
jälgendatud polümeeride sünteesil**

ROMAN BOROZNIJAK

Contents

List of publications.....	7
The author's contribution to publications.....	7
Other publications	7
List of abbreviations and symbols.....	9
Introduction	11
1. Literature review	14
1.1 Molecularly imprinted polymers	14
1.2 Macromolecular imprinting.....	16
1.2.1 A protein as a macromolecular template.....	16
1.4 Computational Methods in MIP design.....	17
1.4.1 Quantum Chemical Calculations.....	17
1.4.2 Molecular Docking.....	18
1.5 Synthesis of protein-MIPs by electropolymerization	19
1.5.1 Poly (m-phenylenediamine)	19
1.5.2 Polydopamine.....	20
1.5.3 Poly (3,4-ethylenedioxythiophene)	21
1.6 Label-free detection methods	22
1.6.1 Quartz Crystal Microbalance.....	22
1.6.2 Surface Acoustic Wave	24
1.7 Methods for assessment of performance of MIPs in binding assays...	25
1.8 Summary of literature review and objectives of the study	27
1.9 Objective and aims of the study	29
2. Experimental part	30
2.1 Computational approach.....	30
2.1.1 Molecular Docking.....	30
2.1.2 Quantum chemical calculations.....	32
2.2 Polymer synthesis.....	33
2.2.1 Electrode cleaning and IgG immobilization.....	33
2.2.2 Electrochemical deposition of the polymer films.....	33
2.2.3 IgG-MIP preparation and rebinding study	34
3. Results and Discussion.....	36
3.1 Computational simulations.....	36
3.1.1 Molecular docking.....	36
3.1.2 Quantum chemical calculation	40
3.2 Preparation of IgG-MIPs and study of IgG rebinding.....	42
Conclusions	45
Abstract	46
Kokkuvõtte	49
Acknowledgements	51
References	52
APPENDIX A	63

APPENDIX B	99
CURRICULUM VITAE	101
ELULOOKIRJELDUS.....	104

List of publications

The doctoral thesis is based on the following original published papers referred to in the text by the Roman numerals:

Paper I

R. Boroznjak, A. Lomaka, A. Tretjakov, V. Syritski, J. Reut, A. Öpik, A Computational Approach to Study Functional Monomer-Protein Molecular Interactions to Optimize Protein Molecular Imprinting. Accepted for publication in Journal of Molecular Recognition, 2017, DOI: 10.1002/jmr.2635.

Paper II

A. Tretjakov, V. Syritski, J. Reut, R. Boroznjak, O. Volobujeva, A. Öpik, Surface molecularly imprinted polydopamine films for recognition of immunoglobulin G. *Microchim Acta* 2013, 180. 1433-1442, DOI: 10.1007/s00604-013-1039-y.

Paper III

A. Tretjakov, V. Syritski, J. Reut, R. Boroznjak, A. Öpik, Molecularly imprinted polymer film interfaced with Surface Acoustic Wave technology as a sensing platform for label-free protein detection. *Anal Chim Acta* 2016, 902. 182-188, DOI: 10.1016/j.aca.2015.11.004.

Copies of these articles are included in Appendix A.

The author's contribution to publications

The contribution by the author to the papers included in the thesis is as follows:

Paper I: Systematization of the computational approach and its validation for imprinting of a macromolecular template, such as IgG. Major role in writing.

Paper II: Conducting surface chemistry for immobilization of IgG via the linker system with cleavable bond. Performing basic steps of the surface imprinting strategy for polydopamine-based IgG-MIP synthesis taking into account the correlation between calculated size and orientation of the immobilized protein. Minor role in writing.

Paper III: Conducting experimental work to validate the data simulated with the computational approach. Theoretical interpretation of the measurements. Minor role in writing.

Other publications

A.G. Ayankojo, A.Tretjakov, J. Reut, R. Boroznjak, A.Öpik, J. Rappich,

A.Furchner, K.Hinrichs, and V. Syritski. Molecularly Imprinted Polymer Integrated with a Surface Acoustic Wave Technique for Detection of Sulfamethizole. *Anal. Chem.* 2016, 88. 1476–1484.

Performing quantum chemical calculations to select the optimal monomer for SMZ-MIP film synthesis. Minor role in writing.

List of abbreviations and symbols

ADT	Autodock Tools
Ag/AgCl/KCl _{sat}	Silver/Silver Chloride Electrode
4-ATP	4-Aminothiophenol
AM1	Austin model 1
B3LYP	Becke's three-parameter exchange functional combined with gradient corrected functional of Lee-Yang-Parr
BuryP	Penalty for buried polar group
Coul	Electrostatic interactions
CV	Cyclic Voltammetry
DA	Dopamine
DFT	Density functional theory
DMSO	Dimethylsulfoxide
DTSSP	3,3'-dithiobis(sulfosuccinimidyl propionate)
EDOT	3,4-ethylenedioxythiophene
EIS	Electrochemical impedance spectra
EQCM	Electrochemical quartz crystal microbalance
FIA	Flow injection analysis
H-bond	Hydrogen bonds
IDT	Interdigital transducer
IF	Imprinting factor
IgG	Immunoglobulin G
IgG-MI-PEDOT	Poly(3,4-ethylenedioxythiophene) based IgG-imprinted polymer
IgG-MI-PDA	Polydopamine based IgG-imprinted polymer
IgG-MI-PmPD	Poly(meta-phenylene diamine) based IgG-imprinted polymer
IRSE	Infrared spectrometry
Lipo	Hydrophobic contacts
LOD	Limit of detection
MD	Molecular docking
mPD	meta-Phenylene diamine
MIP	Molecularly imprinted polymer
MQ	Millipore (ultrapure) water
NIP	Non-imprinted polymer
NI-PEDOT	Poly(3,4-ethylenedioxythiophene) based non-imprinted polymer
NI-PDA	Polydopamine based non-imprinted polymer
NI-PmPD	Poly(meta-phenylene diamine) based non-imprinted polymer
NMR	Nuclear Magnetic Resonance
oPD	orto-Phenylene diamine
OPLS-2005	Optimized potentials for liquid simulations
PBS	Phosphate buffer saline
PDA	Polydopamine

PEDOT	Poly(3,4-ethylenedioxythiophene)
PEDOT-PSS	Poly(3,4-ethylenedioxythiophene) doped with PSS
PM3	Parameterized model number 3
PmPD	Poly(meta-Phenylene diamine)
pPD	para-Phenylene diamine
PSS	Polystyrene sulfonate
RotB	Freezing rotatable bonds
QC	Quantum Chemistry
QCCs	Quantum Chemical Calculations
QCM	Quartz Crystal Microbalance
QM	Quantum Mechanics
QPLD	Quantum mechanical polarized ligand docking
SAW	Surface Acoustic Wave
SCF	Self-consistent field method
SDS	Sodium Dodecyl sulfate
SE	Semi-empirical
SMZ	Sulfamethizole
SP	Standard precision
vdW	van der Waals
WO	Washing out
XP	Extra-precision

Introduction

Molecular imprinting has become a promising method for the design of synthetic receptors, so-called Molecularly Imprinted Polymers (MIPs), having binding sites with a predetermined selectivity for a given analyte. The method of molecular imprinting consists in the polymerization of a mixture of functional monomers around a target analyte molecule that acts as a molecular template. During polymerization, the template induces binding sites in the reticulated polymer that are capable of selective recognizing the template molecules after removal of the templates from the polymer [1-3]. The major advantages of MIPs, along with their binding affinities to the target analyte comparable to a biological receptor [4], are related to their synthetic nature. Namely, these materials are robust under a wide range of chemical and physical conditions, and their preparation is highly reproducible and cost-effective. Moreover, MIPs can be easily designed for recognition of an almost unlimited number of targets, even those for which biological receptors are not available. Presently, the concept of molecular imprinting has been widely employed for the development of molecular recognition materials and has been applied in various fields where high selectivity toward an analyte is needed. Thus, MIPs have been implemented in chemical analysis and detection [5, 6], affinity separation and purification [7-9], drug delivery [10, 11], and catalysis [12-16].

Essentially, strategies for molecular imprinting can be grouped on the basis of the type of the monomer-template interaction into a covalent and a non-covalent imprinting method. The latter is especially applicable when imprinting a macromolecular template [17, 18]. The prerequisite for the formation of selective binding sites in a MIP supposes the presence of non-covalent interactions (self-assembly), such as hydrogen bonds (H-bonds), van der Waals forces, ionic interactions, and hydrophobic effects in the pre-polymerization complex between a template molecule and functional monomers. It is assumed that the choice of functional monomers capable of forming more stable complexes with the template could result in a MIP with a high selectivity and affinity [9, 19]. Molecular interactions in these complexes are maintained during the polymerization and play a crucial role in the formation of complementary binding sites after the template removal that subsequently provides selective rebinding of the target to the MIP. Thus, performance of the MIP relies first of all on the quantity and strength of pre-existing molecular interactions in those complexes before polymerization of the monomers.

In the last few decades, interest in the field of macromolecular imprinting, resulting in MIPs capable of selective recognition of the specific macromolecules, e.g. proteins, viruses, cells, in a complex medium, has considerably increased due to the great demand in clinical diagnostics and therapies aiming at replacement of expensive and readily degradable biological recognition elements [17, 18, 20-23]. The presence in a macromolecular template like a protein of a considerable amount of different functional groups creates

potential premises for abundant non-covalent interactions between the protein and functional monomers in a pre-polymerization complex before protein-MIP synthesis. Consequently, an estimation of all possible non-covalent interactions as well as their strength in the protein-monomer complex should be seriously considered when aiming to design a protein-MIP with highly selective recognition sites.

Different computational approaches, including molecular mechanics, molecular dynamics [24], quantum chemical calculations (QCCs) [25], and molecular docking (MD), were successfully used for a rational design of MIPs through the prediction, simulation and estimation of molecular interactions between a template molecule and a monomer in a pre-polymerization complex as well as in a polymer matrix [26, 27]. Thus, Piletsky's group created a virtual library of functional monomers, which could be screened by a molecular modelling software against a template molecule of interest aiming at preselecting a group of preferential monomers for the following generation of more selective MIPs [28, 29]. Dong et al. calculated the energy of H-bond interactions in simulated complexes between a template and a monomer using a QCC (density functional theory, DFT) [30]. Maciejewska's group employed 3D alignment methodology to design the structure of the polymerization system by the energy optimization of randomly distributed molecular components. Such a system was able to mimic the formation of the recognition cavities in the polymer matrix as well as its interaction with the various analytes [31]. The hybrid quantum mechanical/molecular mechanical (QM/MM) approach for a rational design of MIPs has been applied by several authors [30, 32].

However, most of these reports describe the computational methods to model complexes of functional monomers with small molecular-weight templates [31]. At the same time, very few attempts have been made to use computational methods to rationally design a protein-MIP. These methods mostly use the molecular mechanics simulations [33], MD [34, 35] and lattice Monte Carlo simulations [36]. Among them, MD is the fastest and less resource-consuming computational method to estimate protein–ligand interactions that is widely used in the field of drug design [37]. This method can also provide reliable predictions of binding poses of a monomer on a protein prior to the polymerization as well as determination of the types of non-covalent interactions taking place by the set of the amino acids present near this binding pocket [34]. QCCs method allows the assessment of the strength of H-bond interactions occurring between the H-bond donor and the acceptor [38]; however, its applicability for the calculation of protein-ligand interaction is limited due to the size of the system.

The aim of this study was to develop a computational modeling approach allowing the selection of a more favorable functional monomer for building a polymer with macromolecular imprints capable of selective rebinding protein-sized analytes. MD combined with QCCs were used for modeling and comparing molecular interactions between a model macromolecular template,

immunoglobulin G (IgG), and one of three electropolymerizable functional monomers: m-phenylenediamine (mPD), dopamine, and 3,4-ethylenedioxythiophene, as well as to predict the probable arrangement of multiple monomers around the protein. MD was applied to find energetically favorable binding poses of a monomer on IgG as well as to predict the probable arrangement of multiple monomer molecules around the IgG molecule. The MD results were complemented with the QCCs, allowing estimation of the cumulative strength of multiple H-bond interactions in the prepolymerization complex between the proton-donor groups of monomers and the accessible proton-acceptor groups of the protein to establish further its influence on the performance of the resulting IgG-MIPs. The theoretical predictions were validated by the experimental data on IgG rebinding to the IgG-MIPs generated from the candidate monomers.

1. Literature review

1.1 Molecularly imprinted polymers

Molecularly imprinted polymers (MIPs) are synthetic “tailor-made materials” that are capable of selective binding/rebinding a predefined target molecule [1]. MIP-based materials are prepared employing the molecular imprinting process (Fig. 1). The process starts by the formation of a pre-polymerization complex between a functional monomer and a target molecule that acts later on as a template. During the subsequent polymerization of the monomers, their functional groups become fixed in well defined positions around the template molecule. Finally, the template molecules, which are now confined in the polymer matrix, are removed by washing with an appropriate solvent, leaving behind the specific molecular-cavities that are complementary to the template molecule in term of size, shape and chemical functionality. The resulting polymeric material, MIP, is able to rebind selectively the target molecule or similar molecular structures. The quality and amount of template-specific cavities in the MIP capable of rebinding the target molecule can be affected due to the incomplete template removal, polymer degradation and/or polymer swelling, and alteration of the specific functional groups (Fig. 2) [39]. To improve the quality of cavities and their amount, it is important to estimate non-covalent interactions between the monomer and the template—that assists to select an optimal monomer and to wash out the solvent for the template removal procedure.

MIPs have been already proven successful in molecular recognition of different analytes in molecular diagnostics [5], biotechnology [1, 40] and chromatography [7-9]. MIPs can be also a promising candidate for the replacement of natural receptors in diagnostic tools that are usually based on biomolecules such as antibodies and enzymes. Despite their excellent selectivity/specificity, exploitation of biological-origin receptors does not always fulfill the expectations due to the fragile nature of these molecules. Therefore, implementing MIP-based synthetic receptors appeared to be a promising alternative to the natural ones due to their chemical and thermal stability and reproducible and cost-effective fabrication.

In general, strategies for molecular imprinting can be classified on the basis of whether the interactions in the pre-polymerization complex between a monomer and a template are covalent or non-covalent:

- In covalent imprinting, the template is covalently bound to the functional monomer. After the polymerization, the template is chemically cleaved and the functional groups remaining in the binding site are capable of binding the target molecule by re-establishing the covalent bond [41]. The advantage of this approach is that the functional groups are only associated with the template site. However, only a limited number of compounds (alcohols, aldehydes, ketones, carboxylic acids and amines) can be imprinted with this approach.

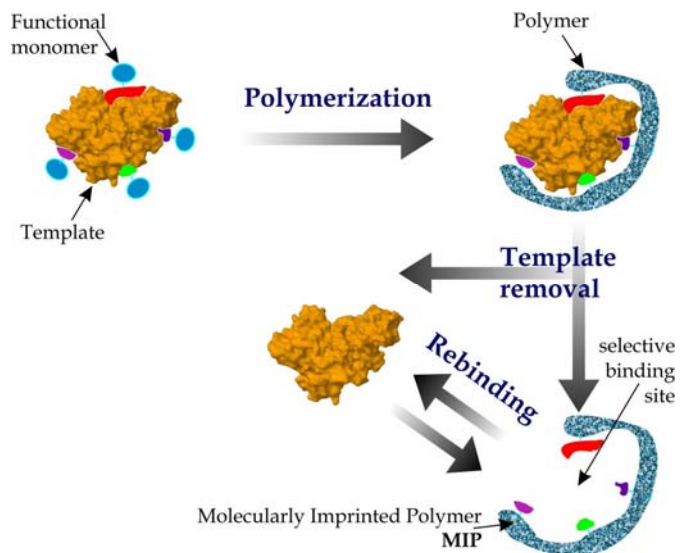


Figure 1. Schematic illustration of the molecular imprinting process.

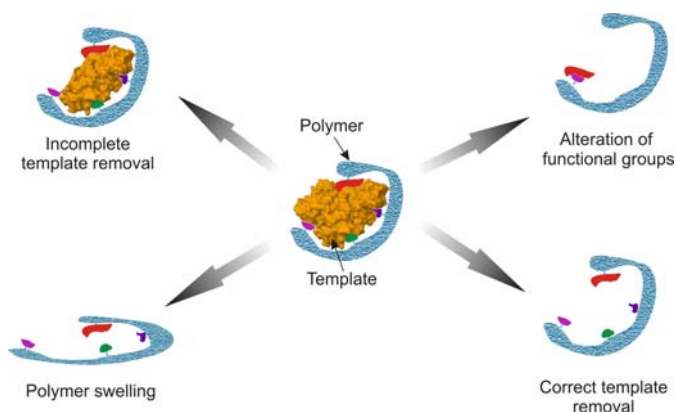


Figure 2. Challenges of template molecule removal for MIP.

- Non-covalent imprinting is based on the non-covalent forces, such as H-bond, ion-pairing, and dipole-dipole interactions between the functional monomer and the template [42]. Due to its simplicity, versatility and adaptability, this method is most widely used to create MIP, particularly MIP with macromolecular imprints [23]. However, a disadvantage of the non-covalent imprinting is the high probability for the formation of heterogeneous binding sites in MIP. Nevertheless, currently, this method is by far the most widely applied and has become a general synthesis strategy for MIPs [43].

1.2 Macromolecular imprinting

In the last few decades, interest in the field of macromolecular imprinting, resulting in MIPs capable of selective recognition of the specific macromolecules, e.g. proteins, viruses, cells, in a complex medium, has considerably increased due to their great demand in clinical diagnostics and therapies aiming at the replacement of expensive and readily degradable biological recognition elements [17, 18, 20-23]. Synthetic receptors based on protein-MIPs offer a promising alternative to biological receptors in biosensors, providing more stable and low-cost recognition elements [44]. However, the major drawback of imprinting macromolecules such as proteins is related to their structural and shape complexity that restricts the molecule mobility within the highly crosslinked polymer matrix, which consequently results in poor rebinding efficiency of MIP. In addition, the risk of conformational changes of protein limits the choice of functional monomers and polymerization solvent.

Considerable success in protein imprinting was achieved by realizing the surface imprinted approach, allowing the formation of MIPs with the selective binding sites located at or close to their surface [45-47]. Examples of successful protein-MIP synthesis for bovine hemoglobin (BHb) [13], lysozyme [48], avidin [49, 50], melittin [4], and cytochrome C [51] have been described. MIP synthesis for more complex macromolecular template such as IgG is not widely described in literature [52].

While different computational approaches including molecular mechanics, molecular dynamics [24], QCCs [25] and MD were successfully used for a rational design of MIPs for small molecular-weight templates, there are very few attempts to rationally design macromolecular MIPs with computational methods mostly using the molecular mechanics simulations [33], MD [34, 35] and lattice Monte Carlo simulations [36].

1.2.1 A protein as a macromolecular template

Proteins are functional biopolymers consisting of one or more ordered sequences of amino acids (polypeptides) and occasionally functional-depending prosthetic groups (organic small molecules and/or metals). Shapes and chemical properties of proteins depend on the nature of amino acid sequence in its polypeptides [53], their folding in bioactive form and any prosthetic groups [54], such as oligosaccharides, metal-chelating groups or lipid acid residues.

In general, amino acids can be classified on the basis of their functional groups in "side-chain": hydrophobic (alanine, valine, isoleucine, leucine, methionine, phenylalanine, and tryptophan), polar uncharged (serine, threonine, glutamine, and asparagine), negatively charged (aspartic acid and glutamic acid), and positively charged (arginine, histidine, lysine). Polar uncharged and negatively charged amino acid residues in a protein have proton-accepting functional groups

able to generate H-bond interactions with a ligand. In addition, the H-bond can be formed between a ligand and a proton-accepting group of a prosthetic group of protein. For example, IgG molecule contains two carbohydrate chains in its Fc-fragment where the hydroxyl group and oxygen atoms in a heterocycle are the major proton-accepting groups capable of forming H-bonds with a ligand.

Thus, the presence in a macromolecular template like a protein of a considerable amount of different functional groups creates potential premises for multiple non-covalent interactions (H-bond, van der Waals, electrostatic and hydrophobic) between the protein and functional monomers in a pre-polymerization complex before protein-MIP synthesis [9, 19]. These interactions are then, to some extent, maintained during polymerization and play a crucial role in the formation of complementary binding sites after the template protein removal, thus providing the subsequent selective rebinding of the target protein to the protein-MIP. Consequently, an estimation of all possible non-covalent interactions as well as their strength in the protein-monomer complex should be seriously considered when aiming at designing a protein-MIP with highly selective recognition sites.

1.4 Computational Methods in MIP design

Different computational approaches including molecular mechanics, molecular dynamics [24], quantum chemical calculation (QCC) [25], and molecular docking (MD) were successfully used for a rational design of MIPs through the prediction, simulation and estimation of molecular interactions between a template molecule and a monomer in a pre-polymerization complex as well as in a polymer matrix [26, 27]. However, most of these reports describe the computational methods to model complexes of functional monomers with low molecular-weight templates. At the same time, there are very few computational studies on macromolecular MIPs that mostly use the molecular mechanics simulations [33], MD [34, 35], and lattice Monte Carlo simulations [36].

A more detailed description of QCCs and MD used in this study for computational modeling is provided in the following section.

1.4.1 Quantum Chemical Calculations

QCCs have been shown to be a promising method for the rational selection of a functional monomer for small molecular-weight template, allowing the estimation of H-bond association energy in template-monomer complexes [30].

The algorithm to calculate the association energy of H-bond interactions between a template molecule and a monomer includes firstly, the geometry optimization of the molecular structures of individual compounds and their complexes by the semi-empirical (SE) parameterization method 3 (PM3) and secondly, the calculation of the energies of the optimized structures by the density functional theory (DFT) method [30]. PM3 and Austin model 1 (AM1) are the

most popular among the different SE methods. Whereas PM3 and AM1 are based on nearly the same equations, PM3 uses a more improved set of parameters than AM1. In the earlier studies, AM1 was reported to calculate the heat of formation [55]. PM3 is more accurate than AM1 at simulating the geometry of H-bond interactions [56] and is commonly used for geometry optimization of the complexes [30]. DFT is a standard method for electronic structure calculations in computational chemistry. The B3LYP (Becke, three parameter, Lee-Yang-Parr) method is a DFT based calculation containing a combined exchange functional and combined correlation functional and is widely used in QCCs [31]. Despite the reported limitations of DFT as compared to the Hartree-Fock method [56], DFT at B3LYP/6-31G(d) level was adopted for molecular optimization [57] and association energy calculation in the MIP design [32], and has become a popular method for simulations of molecular interactions in pre-polymerization complexes between a monomer and a small-molecular weight template [58-61].

Gaussian 09 at B3LYP level using the 6-31G(d) basis set is a widely used software to estimate energies of geometrically optimized molecular structures and complexes [30, 31]. QCC method allows assessment of the strength of H-bond interactions occurring between the H-bond donor and the acceptor [38]; however, its applicability to calculate protein-ligand interaction is limited due to the size of the system.

1.4.2 Molecular Docking

MD is the fastest and least resource-consuming computational method to estimate protein-ligand interactions widely used in the field of drug design [37, 62, 63]. The main goal of protein docking is to predict how a pair of molecules interacts, predicting accurate ligand poses and evaluating the main existing interactions. Molecular docking requires the structures of the molecules that form the complex and aims to predict correctly the binding site on the target, the orientation of the ligand and the conformation of both. Finally, a rank of possible docking poses based on the estimated free energies of binding is given. The poses are scored using the scoring function that approximates the ligand binding free energy and takes into account a number of non-covalent interaction parameters. For example, a widely used Glide software uses an empirical scoring function, GScore, that approximates the ligand binding free energy and takes into account a number of parameters like H-bonds, hydrophobic contacts, van der Waals, electrostatic, polar interactions in the binding site, metal binding term, penalty for buried polar group and freezing rotatable bonds [64, 65]. The scoring of the same receptor and ligand by a different scoring function is the commonly used method to validate binding poses in pharmaceutical chemistry [62, 63].

The application of MD for the computational modelling of protein-MIP has been reported by Kryscio et al. [34]. The authors studied the interactions between albumin and frequently employed functional monomers and used MD to determine the most favorable binding sites for these monomers on albumin and

the types of noncovalent interactions taking place based on the amino acids present near the binding pocket. Thus, MD can be considered as a promising method for protein-MIP computational design, providing reliable predictions of binding poses of a functional monomer on a protein prior to the polymerization. One of the main challenges is that MD provides the energy estimations only for the best-scoring bindings poses while ignores weak interactions between the ligand and the protein, i.e. the H-bond interactions between spatial accessible polar amino acid residues and monomers.

There is a principal difference between the use of MD in drug design and for the selection of an optimal monomer for protein-MIP synthesis. In the drug design, the structure of small molecules is changed to produce the most specific ligand to a protein or a specific binding site aiming at the formation of the most stable complex. However, in the selection of an optimal monomer, MD, uses stable monomer structures, finds their favorable binding poses and arrangements around a protein.

1.5 Synthesis of protein-MIPs by electropolymerization

Among the various approaches for the synthesis of MIP-based recognition element, electrosynthesis has been shown to be a convenient method, allowing rapid and controlled deposition of the MIPs as films with tunable thickness [66-68]. With electrosynthesized MIPs, polymeric films can be easily grown with strict adherence to conducting electrodes of any shape and size and with a thickness controlled by the amount of circulated charge. This feature gives the possibility of creating direct communication between the MIP and the surface of the transducer in a simple way. Moreover, the possibility to carry out the polymerization relatively quickly at room temperature, and in the solutions that are compatible with protein native conformation is especially convenient for protein-MIP synthesis.

Promising results on the application of electrochemical polymerization for protein-MIPs fabrication were shown for a number of different polymers, such as poly (3,4-ethylenedioxythiophene) (PEDOT) [50, 69], poly (o-phenylenediamine) (PoPD) [70], polypyrrole [69, 71], polydopamine (PDA) [47], and poly (m-phenylenediamine) (PmPD) [46].

In this thesis, electrosynthesized polymers, PmPD, PEDOT, and PDA, were used as polymeric matrices to produce IgG-MIP films owing to availability of multiple functional groups, biocompatibility and compatibility with aqueous solutions [72-74]. The properties and polymerization mechanisms of these polymers are discussed below.

1.5.1 Poly (m-phenylenediamine)

The polymers of aromatic diamines, including three isomers of

polyphenylenediamines, oPD, pPD and mPD, have received increased attention due to a unique combination of good multifunctionalities and many useful properties including high permselectivity to electroactive species [75], anticorrosion ability for metal [76], and high capacitivity [77]. The application of polyphenylenediamines in the fabrication of amperometric biosensors and permselective electrode materials has been widely investigated [78-80].

Although only limited information is available about the polymerization mechanism and structure of PmPD, it is suggested that electrosynthesized PmPD structure is comparable with PoPD [81] and has the 1,4-substituted benzenoid–quinoid structure containing both primary and secondary amine groups (-NH₂, -NH- motifs) (Fig. 3) [82-84].

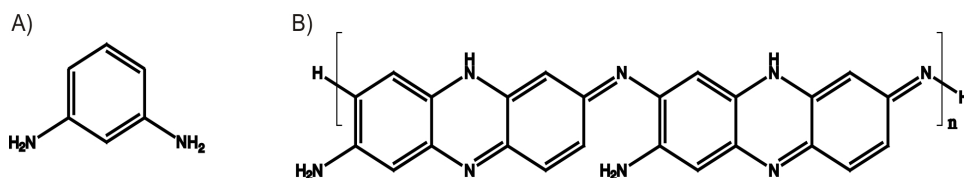


Figure 3. A chemical structure of mPD (A) and benzenoid–quinoid structural unit of PmPD (B).

There are numerous reports on PoPD-based MIP materials intended to QCM sensing of glucose [66], photoelectrochemical sensing of chlorpyrifos molecules [85], detection of DL-phenylalanine by thickness-shear mode acoustic sensor [86], and amperometric sensing of triclosan [87]. However, to our best knowledge, the use of PmPD as polymer matrix for MIP has only recently been reported by Syritski's group [46]. Nevertheless, mPD appeared to be a very attractive material for protein-MIP formation due to its hydrophilicity, compatibility with protein native conformation [88], remarkably high solvent resistance in organic and aqueous solutions, the presence of amine groups that enable the formation of H-bond interactions with accessible polar residues of protein.

1.5.2 Polydopamine

Dopamine is the most widely distributed catecholic compound that contains polar hydroxy- and amino-groups. It is commonly known as a hormone and neurotransmitter. In nature, adhesive proteins secreted by mussels for attachment to almost all types of surfaces consist of dopamine similar structures. Recently, an approach for surface modification, inspired by the mussel adhesive proteins, based on dopamine polymerization to form thin adherent polymer onto a wide range of inorganic and organic materials was reported [73]. Two main methods can be applied to the preparation of PDA films. The most common and the simplest way is a spontaneous self-polymerization of DA under weak alkaline conditions to produce an adherent polymer coating on virtually any substrate and

catechol groups are oxidized to the quinone form. Another way is electrochemical polymerization that offers the possibility of fast and highly controllable PDA films deposition [89]. Moreover, self-limiting growth of insulating PDA ensures the formation of ultrathin films of the nanometer scale. The chemical structures of DA and its polymer unit are presented in Figure 4.

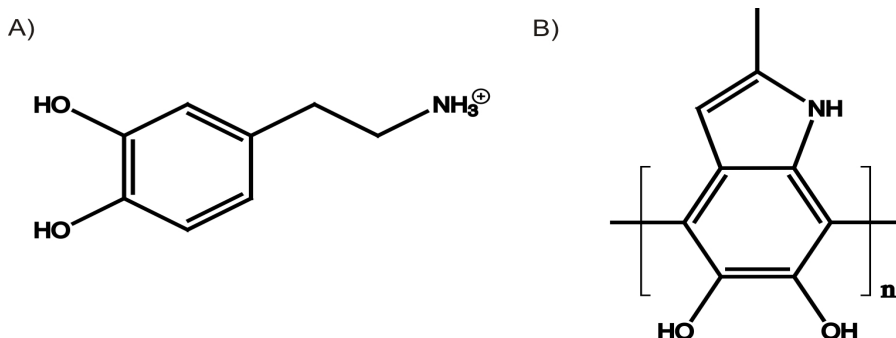


Figure 4. The chemical structure of DA (A) and structural unit of PDA (B).

The existence of polar functional groups, compatibility with aqueous solutions, the possibility of precisely controlled thin film synthesis via electrochemical polymerization make dopamine an attractive monomer for MIP formation. Nevertheless, until now there are only a few reports on the PDA-based MIP films and most of them concern the PDA prepared by self-polymerization of dopamine at weak alkaline pH. The application of electrosynthesized molecularly imprinted PDA films as a recognition element for the capacitive sensing of nicotine was first reported by Liu's group [87]. Recently, Syritski's group has successfully applied PDA for IgG-MIP films synthesis [47].

1.5.3 Poly (3,4-ethylenedioxythiophene)

Poly(3,4-ethylenedioxythiophene) (PEDOT) is an electrically conducting polymer with improved chemical and thermal stability, high conductivity (ca 400-600 S/cm) and high degree of optical transparency [90]. The chemical structures of EDOT and its polymer unit are presented in Figure 5 [91].

PEDOT doped with poly(styrenesulfonate) (PSS) (PEDOT/ PSS) is widely used as an antistatic coating, electronics packaging, transparent conductor in electroluminescent devices, photovoltaics, organic thin film transistors, and sensors [92] [93, 94]. PEDOT has been studied as a promising candidate for biosensing and biomedical application [72, 95].

There are also a few reports on the application of PEDOT for MIP synthesis. For instance, a sensing electrode modified with morphine-imprinted PEDOT was reported in [96]. Syritski's group was the first to report on the PEDOT/PSS application as matrix for protein imprinting by introducing a synthesis approach for producing surface imprinted microrods for avidin selective recognition [50]. Later, the same group developed a novel concept to generate micropatterned

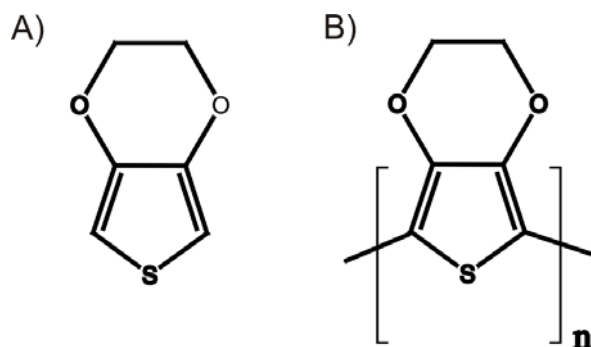


Figure 5. Chemical structures of EDOT (A) and structural units of PEDOT (B).

surface-imprinted PEDOT/PSS for avidin recognition by using standard photolithographic technology [49]. It was revealed that PEDOT/PSS provides a matrix with low nonspecific protein adsorption and, together with the electrochemical synthesis, offers clear advantages in terms of controlling the deposition process and compatibility with aqueous media [Lautner, 2011 #61, 97]. In addition, PEDOT/PSS material has functionalities that are expected to generate H-bonds, as well as electrostatic and p-p interactions with the protein template.

1.6 Label-free detection methods

Label-free detection methods are preferable for the investigation of binding events on MIP surfaces because labeling can change the interfacial activity of the labeled protein and influence the accuracy of measured data [98]. Label-free detection platforms integrated with MIPs are able to provide the relevant information on the target binding. This detection can be performed using various transducer devices, such as Quartz Crystal Microbalance (QCM), Surface Plasmon Resonance (SPR), and Surface Acoustic Waves (SAW). In this thesis, QCM and SAW were used and their principles are described below.

1.6.1 Quartz Crystal Microbalance

QCM is a sensing piezoelectric transducer device for detection in both air and liquid phase. This transducer can be used to monitor mass-change processes in a label-free manner on the sensing surface in the liquid phase via detecting frequency and resistance changes [99]. The sensing part of the QCM consists of a thin disk-shaped quartz crystal covered by gold electrode layers on both sides (Fig. 6) [100]. Internal mechanical stress is being produced by a piezoelectric material when an external electrical potential is applied to it. A resonant oscillation is achieved by including the crystal in an oscillation circuit, which has electric and the mechanical oscillations close to the fundamental frequency of the crystal. The fundamental frequency depends on the thickness of the wafer, its chemical structure, shape and mass plated on it [101].

The first quantitative investigation of the piezoelectric effect was performed by Sauerbrey who derived the relationship for the change in the frequency ΔF (in Hz) caused by the added mass Δm (in g):

$$\Delta m = -\frac{\Delta F}{C_f} \quad (1)$$

$$T_f = \frac{\Delta m}{\rho_f} \quad (2)$$

where ΔF – resonant frequency change (Hz), Δm – mass change (g/cm^2), C_f – sensitivity factor (for 5 MHz quartz crystal, $56.6 \text{ Hz} \cdot \mu\text{g}^{-1} \cdot \text{cm}^2$), T_f – thickness of the film in cm, ρ_f – density of film material in g cm^{-3} [102].

If an increase of the mass takes place on the sensing surface, the oscillation frequency will decrease. According to the Sauerbrey equation, the observed frequency change is directly proportional to the increase in mass and deposited films thickness can be correlated with the amount of analyte binding [103]. The electrodes are connected with the oscillation circuit board and an alternating high frequency electrical field is applied across the plane of the quartz crystal, inducing its vibration in a mechanically resonant shear mode.

As an extremely sensitive surface mass sensor, QCM has been described for the measurement of mass change in a variety of studies, such as underpotential deposition of metals [104], dissolution studies [105], DNA immobilization [106] and subsequent hybridization in solution phase [107, 108], protein adsorption on solid surface [109-111] and immunologic studies [112-114], and studies related to cell-substrate interactions in situ and measurement of the dynamics of exocytosis and vesicle retrieval at cell populations [115, 116]. Applications to the rebinding studies for molecularly imprinted films have been reported in [66, 117].

In this thesis, measurements on QCM were used to optimize synthesis parameters of homogeneous polymer films. The measurement of IgG adsorption on PDA-based IgG-MIP was performed on a QCM sensor combined with the method of Flow Injection Analysis (FIA) for real-time monitoring of the IgG binding [47]. The combination of QCM with electrochemistry (EQCM) was used to control synthesized film thickness during polymerization [46, 47].

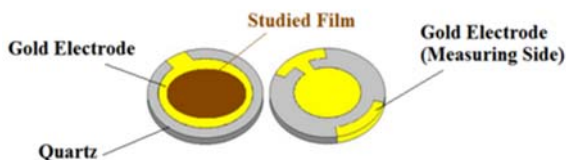


Figure 6. A schematic representation of a QCM sensor.

1.6.2 Surface Acoustic Wave

SAW sensors are acoustic wave-based piezoelectric sensing platforms. Initially, the piezoelectric effect was described by Pierre and Paul-Jacques Curie. Later, the properties of the surface acoustic wave mode of propagation were reported by John William Strutt. A surface acoustic wave (SAW) is an acoustic, mechanical wave that propagates confined to the surface of a cut piezoelectric crystal. Coupling to any medium contacting the surface affects strongly the velocity and/or amplitude of the wave. Further development of photolithographic techniques for computer chips and telecommunication devices to transfer micro- and nanostructure patterns optically onto a substrate, allowed fabrication of micro- and nanostructures implemented in modern biosensors. In a typical approach, an electrical signal is converted at interdigital transducers (IDTs) into polarized transversal waves travelling parallel to the sensing surface, utilizing the piezoelectric properties of the substrate material. This approach is very sensitive to specific biological interactions with the sensor surface [118]. Typically, the wave is transmitted confined to an independent guiding layer and not the substrate. Thus, the acoustic energy is concentrated within the guiding layer rather than in the bulk of the piezoelectric material. The sensitivity of the sensor for surface modifications is increased by the choice of the material and the design of the guiding layer [119, 120] as well as by the structure of the sensor and the transducers [121]. The waves are travelling across the sensitive area, altered by biochemical events at its surface. Afterwards, the wave is converted back at another IDT into an electrical signal. Input and output signals are transformed, for example, into a resulting signal of frequency or phase changes, which can then be correlated to the corresponding mass and mechanical properties in the fluid contacting the sensitive surface. The components necessary for the measurement of aqueous or other fluid components are displayed in Figure 7.

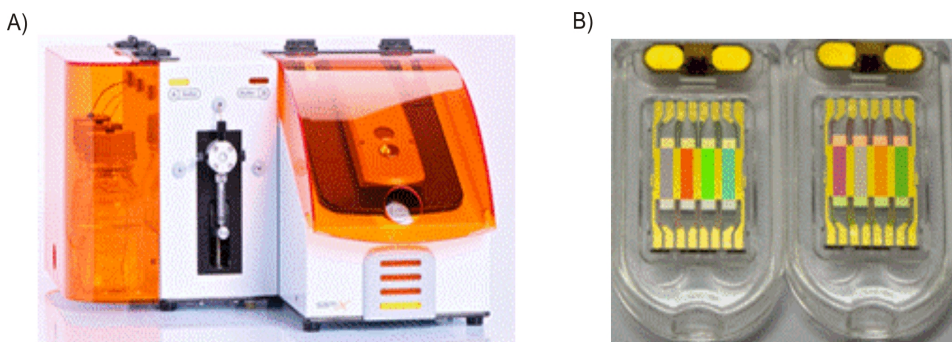


Figure 7. A) The SAW biosensor system. B) SAW chips with four sensor elements each.

Three types of SAW sensors are commonly used: Rayleigh-SAW sensors, Lamb-wave sensors, and Love-wave sensors. The material waves in Rayleigh and Lamb-wave sensors are displaced in the y axis in the direction of the medium. The waves in Rayleigh acoustic wave sensors can be excited at the opposite

surface from the detection surface. The energy is distributed across the complete substrate material and not at the detection surface. Due to liquid medium damped, these medium Rayleigh- and Lamb-wave sensors are commonly used as gas sensors. The Love-Wave sensors are a member of the family of SAW sensors in which acoustic oscillation energy is highly coupled to the wave guiding layer. This additional layer minimizes the energy dissipation losses into environmental media, making these Love-configured sensors, besides their extremely high sensitivity towards surface effects, well suited for operation in aqueous medium [118, 122]. Compared with QCM, the Love-wave SAW sensor has a distinct advantage in extremely high sensitivity due to higher operating frequency (100 MHz to a few GHz). Another remarkable advantage of the SAW technology is a multiplexing capability (combination of multiple sensor elements in a single chip) that allows considerable reduction in experimental time and expenses. Thus, the SAW platform can provide relevant information on binding events on MIP surfaces in real-time and label-free manner to validate the computational predictions.

1.7 Methods for assessment of performance of MIPs in binding assays

A systematic approach that enables the evaluation of the effectiveness of MIPs is very important during their study since it allows finding out which of the fabrication parameters improves the performance of a MIP.

Analysis of the kinetics of the processes following the receptor (MIP) and the ligand (target molecule) reversible association and dissociation in terms of kinetic constant (rate constant) and the amount of an analyte adsorbed at an equilibrium (Q_{eq}) can help to assess the performance of MIPs. The analyte injection period or association phase is characterized by association and dissociation processes, while dissociation phase occurs only by dissociation. The fitting of the association phase to an appropriate kinetic model provides the rate constant of the process (k) and the response at equilibrium conditions. The adsorption kinetics models, pseudo-first-(3) and pseudo-second-order (4) describe the adsorption process as kinetics of active sites (cavity) occupation with adsorbate (target molecule).

$$Q = Q_{eq}[1 - e^{-k_1 t}] \quad (3)$$

$$Q = [Q_{eq}^2 k_2 t] / [1 + Q_{eq} k_2 t] \quad (4)$$

where Q - response upon target rebinding at time t , Q_{eq} - Q value at equilibrium, k_1 - pseudo-first rate constant, k_2 - pseudo-second order rate constant.

In the first order reaction kinetics, only a single active site on the sensor surface

is physically bound by the target molecules. The rate of target molecule occupation of the active sites follows a proportionality to the amount of unoccupied sites [123]. In a pseudo-second order kinetics, the rate-limiting step is a chemisorption process in which case there is exchange of electrons between the target molecules and the sensor. The occupation rate of the adsorbed target is directly related to the square of the remaining number of unoccupied sites [124, 125]. Both kinetic models were successfully applied to the analysis of binding on the MIP surfaces [126].

Adsorption isotherms represent the dependence of the equilibrium concentration of a bound target on the concentration of the target in the solution, providing useful information on the binding properties of the film. The Langmuir isotherm (5) is commonly used to fit various adsorption data. This model is based on the following assumptions: equivalence of adsorption sites (one molecule per one site), homogeneity of the surface, the absence of other interactions in the solution. All these assumptions are rarely observed in practice and to modify for the real experiment, an equation is needed.

$$Q = Q_{\max}C/(C+K_D) \quad (5)$$

where C - concentration of the analyte in the solution, K_D - equilibrium dissociation constant, and Q and Q_{\max} - fractions of bound analyte and its saturation value, respectively. The real MIP has different variations of imprinted cavities. Bi-Langmuir equation takes into account the situation of two types of adsorption sites (6) [126].

$$Q = Q_{\max1}C/(C+K_{D1}) + Q_{\max2}C/(C+K_{D2}) \quad (6)$$

Another challenge of using MIPs as films is a high degree of heterogeneity of the surface. Freundlich (7) and combined Langmuir-Freundlich (8) models can take into account surface roughness, heterogeneity, and interactions in the analyte solution [127, 128]. Thus, Langmuir-Freundlich isotherm models the binding behavior of MIP and NIP films more accurately when the heterogeneity index m is below 1.

$$Q = aC^m \quad (7)$$

$$Q = Q_{\max}C^m/(C^m+K_D) \quad (8)$$

where C - concentration of the analyte in the solution, K_D - equilibrium dissociation constant, and Q and Q_{\max} - fractions of bound analyte and its saturation value, respectively, m - surface heterogeneity index.

Thus, using the values of Q_{eq} and the Langmuir–Freundlich (LF) binding model, the maximum response of the sensors, $Q_{\max}(\text{MIP})$ and $Q_{\max}(\text{NIP})$, is determined [46].

Imprinting factor (IF) indicates the capacity of a MIP towards a target molecule, showing the ratio of target molecule binding on a MIP to a control NIP that was calculated according to the following equation (9):

$$\text{IF} = Q_{\max}(\text{MIP})/Q_{\max}(\text{NIP}) \quad (9)$$

where $Q_{\max}(\text{MIP})$ - the maximum adsorption capacity of MIP and $Q_{\max}(\text{NIP})$ - maximum adsorption capacity of NIP.

To compare performances of MIP films with the applied one concentration, it is acceptable to calculate IF at the equilibrium achieved according to the following equation (10):

$$\text{IF} = Q_{eq}(\text{MIP})/Q_{eq}(\text{NIP}) \quad (10)$$

where $Q_{eq}(\text{MIP})$ - the maximum adsorption capacity of MIP and $Q_{eq}(\text{NIP})$ - maximum adsorption capacity of NIP.

1.8 Summary of literature review and objectives of the study

Molecular imprinting is one of the state-of-the-art techniques allowing generation of robust molecular recognition materials - MIPs that might have antibody-like ability to bind and discriminate between molecules. These materials can be promising alternatives to natural biological receptors in biosensing as they provide selective, stable and renewable recognition elements.

In general, strategies for molecular imprinting can be classified on the basis of whether the interactions in the pre-polymerization complex between a monomer and a template are covalent or non-covalent. The latter is by far the most applied

and has become a general synthesis strategy for MIPs.

In the last few decades, interest in the field of macromolecular imprinting, resulting in MIPs capable of selective recognition of the specific macromolecules, e.g. proteins, viruses, cells, in a complex medium, has considerably increased due to the great demand in clinical diagnostics and therapies aiming at the replacement of expensive and readily degradable biological recognition elements.

However, imprinting macromolecules, in particular proteins, encountered difficulties related to their structural and shape complexity. This limits mass transport of such macromolecules in highly reticulated polymeric networks and leads, thus, to their entrapment during imprinting rather than to binding sites permitting free ligand exchange with the sample solution. Additional challenges arise owing to the flexibility of the protein conformation and its susceptibility to environmental conditions as well as to the inherent complexity and diversity of the interactions between macromolecules and MIPs. The presence in a macromolecular template like a protein of a considerable amount of different functional groups creates potential premises for multiple non-covalent interactions (H-bond, van der Waals, electrostatic and hydrophobic) between the protein and functional monomers in a pre-polymerization complex before protein-MIP synthesis. These interactions are then, to some extent, maintained during polymerization and play a crucial role in the formation of complementary binding sites after the template protein removal, thus providing the subsequent selective rebinding of the target protein to the protein-MIP. Consequently, an estimation of all possible non-covalent interactions as well as their strength in the protein-monomer complex should be seriously considered when aiming at designing a protein-MIP with highly selective recognition sites.

While different computational approaches, including molecular mechanics, molecular dynamics, QCCs and MD, were successfully used for a rational design of MIPs for small molecular-weight templates, there are very few attempts to rationally design macromolecular MIPs by computational approaches.

Among the various approaches for the synthesis of MIP-based recognition element, electrosynthesis has been shown to be a convenient method, allowing rapid and controlled deposition of the MIPs as films with tunable thickness. With electrosynthesized MIPs, polymeric films can be easily grown with strict adherence to conducting electrodes of any shape and size and with a thickness controlled by the amount of circulated charge. This feature gives the possibility of creating a direct communication between the MIP and the surface of the transducer in a simple way.

The label-free sensing platforms, such as SAW, provide relevant information on binding events on MIP surfaces. This platform has high sensitivity towards molecular interactions happening on its surface and thus, is considered very

suitable for the study of binding properties of the MIP films in real-time and label-free manner to validate the developed computational approach.

1.9 Objective and aims of the study

The main objective of this thesis was to develop a computational modeling approach allowing the rational selection of a functional monomer for building a polymer with binding sites capable of selective capturing of macromolecular analytes. This approach has to provide criteria to select an optimal functional monomer for building the macromolecular MIP considering the intrinsic energy of the monomers-macromolecule complex. Thus, the specific aims of the thesis are as follows:

- To find the energetically favorable binding poses of a candidate monomer and their distribution over a model protein (IgG) and to estimate the energy of non-covalent interactions in these binding poses;
- To estimate the cumulative strength of multiple H-bond interactions between the sterically accessible polar amino acid or monosaccharide residues of IgG and candidate monomers;
- To generate IgG-MIPs from the candidate monomers by electrochemical polymerization and study their ability of selective rebinding of IgG by the label-free detection method;
- To validate the results of the computational modeling approach by finding a correlation between the theoretical predictions and performance of the IgG-MIPs.

2. Experimental part

2.1 Computational approach

The computational modeling approach was used for the rational selection of a more advantageous functional monomer for building a MIP with macromolecular imprints capable of selective rebinding of protein-sized analytes. In this approach, the interactions between IgG as a model protein, and mPD, DA, EDOT as functional monomers in the pre-polymerization complex were modeled by using: (i) MD of each of the monomers in IgG to determine the energetically favorable binding poses, and (ii) QCCs to assess the cumulative strength of H-bond interactions between the monomers and the sterically accessible proton-acceptor groups of IgG, such as polar amino acid and sugar residues.

2.1.1 Molecular Docking

To find energetically favorable binding poses of candidate monomers on a model IgG and to predict the probable arrangement of multiple monomer molecules around IgG, MD was performed. To overcome MD limitations, quantum mechanical polarized ligand docking (QPLD) was used. This software is capable of estimating binding energies in simulated poses using an inner QCC tool to increase the accuracy of performance [129]. The QCC tool of QPLD is based on the DFT method using the 6-31G*/LACVP* basis set, B3LYP density functional, and “Ultrafine” SCF accuracy level (iacc=1, iacscf=2) to estimate atom charges of monomers in the field of the receptor. This MD software calculates the charges for monomer atoms by these internal QCCs and after charge reassignment to the monomer, performs more accurate energy estimation in the binding poses. Thus, MD studies were carried out by using the QPLD workflow based on Glide [65, 129, 130] using Optimized Potentials for Liquid Simulations (OPLS-2005) force field [131, 132] and for comparison with Autodock. The crystal structure of IgG (1HZH) deposited in Protein Data Bank (PDB) was processed within the Protein Preparation Wizard in Maestro [133], performing progressive minimizations until the average root mean square deviation of the non-hydrogen atoms reached 0.3 Å. The structures of the monomers (mPD, EDOT, and DA) were generated in Maestro [133] and processed within the Ligand Preparation Wizard [134]. The monomers and the protein were converted to MAE format (Maestro). For rigid docking, a rigid receptor grid defined by an inner box of 50x50x50 Å³ was generated in the different fragments of IgG, such as Fab-fragment with the center at 94.725; 86.582; 94.166 Å; hinge fragment with the center at 76.565; 111.963; 136.892 Å and Fc-fragment with the center at 53.311; 128.675; 112.692 Å. All candidate monomers were docked in the protein structure using standard precision (SP) QPLD (quantum mechanics–polarized ligand docking implemented in the Schrödinger suite (<http://www.schrodinger.com/>), including initial docking, monomer charge estimation via implemented QCCs and docking on the basis of estimated charges.

The energy-minimized poses were scored using an empirical scoring function, GScore that approximates the ligand binding free energy and takes into account a number of parameters like H-bonds, hydrophobic contacts (Lipo), van der Waals (vdW), electrostatic (Coul), polar interactions in the binding site (Site), metal binding term (Metal), penalty for buried polar group (BuryP), and freezing rotatable bonds (RotB) (11) [64, 65]:

$$\text{GScore} = 0.065 * \text{vdW} + 0.130 * \text{Coul} + \text{Lipo} + \text{H-bonds} + \text{Metal} + \text{BuryP} + \text{RotB} + \text{Site} \quad (11)$$

The hydration effect has a key role in ligand-protein interactions as well in controlling the stability and conformation of protein structure. This effect term has become an integral part of many scoring functions used in protein-ligand docking including GScore, as stated by Schrödinger, the software provider. Thus, GScore already includes the specific term that accounts the solvation effect and the results of the docking simulations presented in this study comprises the solvent effects.

To validate the simulated geometries, Autodock4.2.6 (from the Scripps Research Institute) was applied to the same fragments of IgG as QPLD with the same rigid receptor grid-box. Docking procedures with Autodock4.2.6 were performed on the grid-centers used by QPLD. For Autodock, the crystal structure of IgG (1HZH) deposited in Protein Data Bank (PDB) and monomer structures were processed within the AutoDockTools (ADT) software performing structure preparation procedures. The monomers and the protein were converted to ADT format (into .pdbqt files). The initial files for grid-box generation (.gpf) and docking procedure (.dpf) were prepared with ADT and processed with the software. The predicted poses were geometrically agreed with QPLD results with selection spacing 0.375 Å, Grid 50x50x50Å³ and genetic algorithm with population 150. This software uses a scoring function ΔGScore (12).

$$\Delta\text{GScore} = \text{vdW} + \text{Coul} + \text{Hbond} + \text{Desolv} + \text{Tors} \quad (12)$$

The geometry of a pose validated by two different scoring functions are more realistic than predicted by only one software. To compare compatibility and preferability of using both softwares in terms of docking to IgG, the resulting scoring energies were compared. To determine conformational risks, the flexible variant of Autodock was used (no published data) and to improve the accuracy of energy estimation QPLD software was used with the same receptor grids and ligands that were prepared for geometry simulations by Glide.

It should be noted that GScore already includes the specific term that accounts for the solvation effect [64]. The monomer, which formed the lowest-energy

(GScore) docked complex with the selected IgG regions, was considered as more favorable for the formation of an IgG-MIP in terms of its selectivity towards IgG.

To predict the probable arrangement of multiple monomer molecules around the protein, the sequential docking protocol was applied using the same parameters as initial docking; however, each successive docking of the monomer was performed to the complex of IgG and the monomer resulting from the previous docking step [135]. The sequential docking was repeated until the software was unable to predict a binding pose for the next monomer in the previously simulated protein and monomer complex.

2.1.2 Quantum chemical calculations

Since MD estimates only preferable bindings and ignores other interactions, we performed QCCs to estimate hydrogen binding energies between IgG and monomers. QCCs were used to assess the cumulative strength of H-bond interactions between the monomers and the sterically accessible proton-acceptor groups of IgG, such as polar amino acid and sugar residues.

The binding energies of hydrogen interactions between proton-accepting groups of template molecule and candidate monomers were estimated using Gaussian09 (GaussView 5.0.9 software). To begin with, all structures and complexes were geometrically optimized with the PM3 SE method. The optimized objects were subjected to binding energies, ΔE , and Mulliken charge calculations using the DFT method at level B3LYP/6-31G(d) level [32]. Binding energies were computed as the difference between the energy of the complex and the energy of each molecule by equation (13) [31, 32, 136].

$$\Delta E = E_{X+M} - (E_X + E_M) \quad (13)$$

where E_{X+M} , E_X and E_M are the potential energies of the complex (X+M) and its isolated molecular components, the amino acid or monosaccharide (X) and monomer (M), respectively. E_{X+M} , E_X and E_M were computed by Gaussian 09 at Becke's three-parameter exchange functional combined with gradient corrected functional of Lee-Yang-Parr (B3LYP) level using the 6-31G(d) basis set.

The strength of H-bond interactions between IgG and the monomers was calculated as a sum of association energies ($\sum \Delta E$) between the amino acid or monosaccharide associated with the residues found and the monomer (14):

$$\sum \Delta E = \sum [E_{X+M} - (E_X + E_M)] \quad (14)$$

It is necessary here to clarify that QCCs were performed in vacuum and no solvent effect on the simulated complexes was considered. It is assumed that in the complex of the monomer with the isolated polar residue, the solvent effect would strongly differ from that occurring in the complex with the same residue in the protein chain.

2.2 Polymer synthesis

2.2.1 Electrode cleaning and IgG immobilization

The gold electrode of SAW chip (NanoTemper Technologies, GmbH, München, Germany) was cleaned by immersion in fresh ammonium-hydrogen peroxide solution (30% NH_3 : 30% H_2O_2 :MQ 1:1:5 volume ratio) with heating for 20 min, followed by a cleaning step in a UV/ozone cleaner. Then the electrode was rinsed with distilled water and dried in a nitrogen stream. The gold electrodes of a 5 MHz QCM sensor (Maxtek, Inc.) were cleaned by fresh piranha solution (97% H_2SO_4 : 30% H_2O_2 , 3:1 volume ratio) for 10 min and then rinsed abundantly with MQ water.

Then the clean electrodes were immersed in the ethanolic solution of 0.1 M 4-ATP for 1 h to form the amine-terminated self-assembled monolayer, after which the electrode was thoroughly rinsed with ethanol to remove the unreacted thiols. The amine-modified electrode was subsequently incubated in the PBS buffer (pH 7.4) containing 10 mM of a cleavable amine-reactive cross-linker, DTSSP, for 30 min followed by rinsing with MQ water. Then, the IgG-modified electrode was achieved by subsequent incubation in PBS buffer (pH 7.4) containing 1 mg mL^{-1} of IgG for 30 min, followed by rinsing with MQ water.

2.2.2 Electrochemical deposition of the polymer films

EQCM measurements were performed using the QCM system (QCM100, Stanford Research Systems, Inc., Sunnyvale, CA, USA) connected to the potentiostat (Reference 600TM, Gamry Instruments, Inc.) and the frequency counter (PM6680B, Fluke Corporation). Electrochemical syntheses were performed in a three-electrode 1 mL Teflon electrochemical cell. Gold plated SAW or QCM sensor chip was used as a working electrode, while a rectangular shaped platinum plate ($4 \times 1.5 \text{ cm}^2$) and Ag/AgCl/ KCl_{sat} as a counter and a reference electrode, respectively.

The electrochemical polymerization of three functional monomers: mPD, EDOT, and DA, on IgG-modified as well as non-modified gold electrodes of QCM sensor were studied by the EQCM technique. Synthesis parameters for producing homogeneous polymer films are described in Table 1.

Table 1. Synthesis parameters used for the electrochemical polymerization of the mPD, EDOT, and DA on the IgG-modified gold surface

Monomer	Polymerization solution	Electrochemical technique	Potential, V (vs Ag/AgCl/KCl _{sat})	Synthesis time for 11 nm film, s
mPD	10 mM mPD in PBS	Chronocoulometry	0.9	3
EDOT	10 mM EDOT in 25 mM PSS/MQ	Chronocoulometry	0.8	21
DA	5 mM DA in PBS	Cyclic Voltammetry	-0.45 to 0.55 (50 mV/s)	840

2.2.3 IgG-MIP preparation and rebinding study

IgG-MIP films were prepared according to the surface imprinting strategy developed by Syritski's group (Paper I and II). Thus, the electrodeposition of the PmPD films was performed on the IgG-modified SAW chip in PBS containing 10 mM of mPD by applying potential 0.9 V for 3 s vs Ag/AgCl. Other polymers were synthesized under the following conditions: PDA from 5 mM dopamine solution in PBS by cyclic voltammetry -0.45 to 0.55 V vs Ag/AgCl for 42 cycles and PEDOT-PSS from 10 mM EDOT/25 mM PSS solution in MQ by applying potential 0.8 V for 21 s vs Ag/AgCl. The thicknesses of the deposited films are expected at 11 nm.

IgG was removed from the polymer by the incubation of the polymer-modified SAW chip in 100 mM solution of 2-mercaptoethanol in PBS buffer for 1h to cleave DTSSP disulfide bond, followed by washing in DMSO for 15 min with stirring. DMSO is an appropriate H-bond disrupting solvent for biomolecules. Finally, the resulting IgG-MIP sensor was washed thoroughly with ultrapure water and subjected to protein rebinding studies using SAW instrument. IgG rebinding to the IgG-MIP-modified SAW chip was carried out using the SAW technique. A constant flow of filtered and degassed PBS buffer solution (pH 7.4) flowed over the sensor until a constant baseline with a flow rate of 25 $\mu\text{L min}^{-1}$. Subsequently, PBS buffer solutions containing IgG at the concentration of $8 \times 10^{-3} \text{ mg mL}^{-1}$ were injected into the flow stream via an injection loop (500 μL) and allowed to interact with the IgG-MIP or NIP modified sensor chip.

To compare the IgG-MIPs in terms of their affinity to IgG molecule, a non-imprinted polymer (NIP) structure was also tested. NIP films were synthesized under the same conditions as IgG-MIP, but excluding the cleavage step. In this case, the polymer film, even if it contains the template protein, has no cavities on its surface.

The real-time label-free protein binding measurements were performed using Surface Acoustic Wave (SAW) sensing system Sam®X (NanoTemper Technologies, GmbH, München, Germany) comprising an autosampler with a six-port injection valve, a small volume (8 µl) flow cell and two sensor chips with eight sensing channels. The software packages SensMaster and SequenceMaster (SAW Instruments GmbH) were used to control the sensing system Sam®X. The data were recorded with a time resolution of 1.2 sec. Data analysis was performed using the Origin 9.0 (Originlab corp.) software. A constant flow of filtered and degassed PBS buffer solution (pH 7.4) flowed over the sensor until a constant baseline with a flow rate of 25 µL min⁻¹. Subsequently, PBS buffer solutions containing IgG at the range of concentrations of IgG (6.4×10^{-5} - 8×10^{-3} mg mL⁻¹) were injected into the flow stream via an injection loop (500 µL) and allowed interaction with the IgG-MIP or NIP modified sensor chip.

3. Results and Discussion

3.1 Computational simulations

It is widely accepted that non-covalent interactions, such as H-bonds, van der Waals, electrostatic and hydrophobic interactions occurring between monomer and protein in the prepolymerization complex, all play a role in specific binding poses formation during the imprinting process. Consequently, the success of a protein-MIP strongly depends on the stability and strength of its monomer-template complex prior to polymerization. Thus, simulating all noncovalent interactions in a protein-MIP prepolymerization mixture can provide a more accurate insight into the molecular-level events underlying the imprinting process.

In this study, the computational approach to model the interactions between IgG as a model template and a monomer was based on the two main steps: (i) determination of the energetically favorable binding poses for a monomer on protein body by MD and (ii) prediction of hydrogen-bonding ability of the spatially accessible proton-accepting groups of IgG such as polar amino acid residues and a carbohydrate moiety, with the monomer by QCCs. The simulation approach allowed determination of the amino acids surrounding the monomer when it is at its most favorable binding pose on IgG as well as the types of interactions that are likely to occur considering the distance between the polar atoms of the amino acid and the monomer and the type of the side chain group of the amino acid residue. In addition, the hydrogen bonding probability between the monomer and the spatially accessible proton-accepting groups of IgG were taken into account.

3.1.1 Molecular docking

Considering a complex structure of IgG and docking software limitations, the MD of a monomer was performed separately to the three selected fragments of the IgG molecule: Fab, a hinge, and a Fc-fragment (Fig. 8) using both software (QPLD and Autodock) (Table 2).

Table 2. Binding energy estimation for IgG-mPD by QPLD and Autodock , kJ mol⁻¹

Fragment of IgG	GScore energies, kJ mol ⁻¹	
	QPLD	Autodock (optimized parameters)
Fab-fragment	-20.01 ÷ -17.49	-14.35 ÷ -13.68
Hinge-fragment	-19.54 ÷ -16.28	-13.35 ÷ -12.13
Fc-fragment	-21.17 ÷ -20.21	-16.61 ÷ -16.23

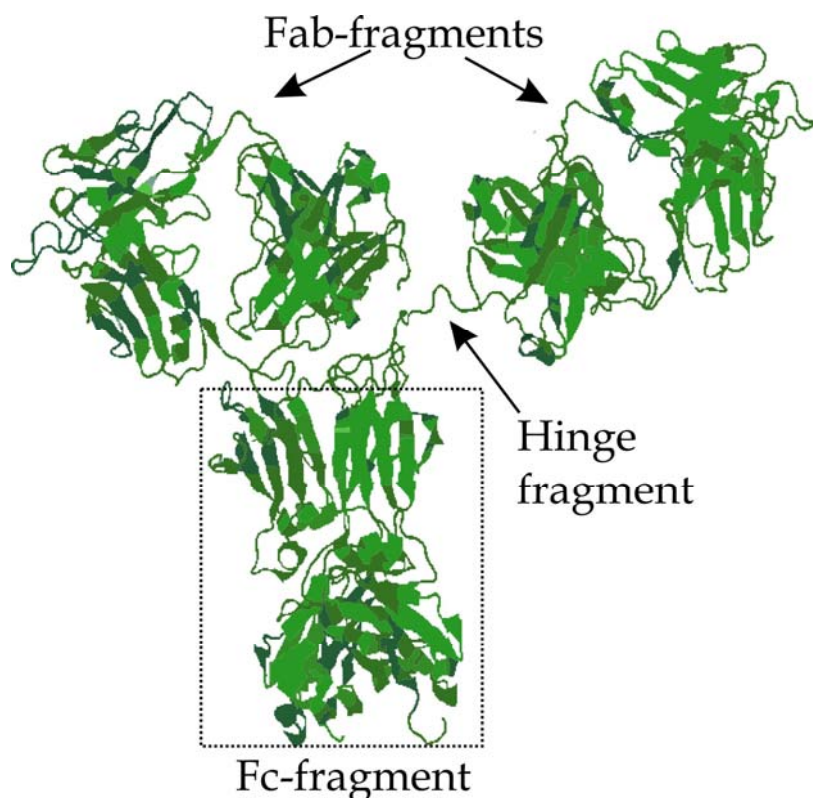


Figure 8. Schematic diagram of IgG, showing the Fab, Fc and Hinge fragments.

The lowest scoring energy (GScore) for each monomer in the selected fragment of IgG as well as the energies of van der Waals, lipophilic, electrostatic interactions taking place in these binding poses were specified by QPLD. The results are summarized in Table 3.

The monomers with lower interaction energies (GScore) in the studied fragment can be considered as the most favorable for polymer matrix formation. The GScore values for the best-scoring binding poses of all three monomers docked to the selected regions of IgG had almost similar ranging between -19.54 and -22.38 kJ mol $^{-1}$, besides EDOT, which demonstrated no interaction with the hinge region (Article I). This indicates that both mPD and DA are able to form more stable pre-polymerization complexes with IgG through the non-covalent interactions, and can be considered as more appropriate functional monomers for IgG-MIP fabrication than EDOT.

It is expected that if a protein solution contains a monomer at a high molar excess, there is far more than one ligand per protein molecule. Since MD gives an indication of the ligand preferential pose in the protein, sequential docking protocol of each of these grids will demonstrate the saturation by ligand when all favorable places have already been occupied [135]. Thus, IgG was docked with each of monomer to achieve full saturation using QPLD (Table 4).

Table 3. Energies of interactions and GScore values (kJ mol⁻¹) for the best-scoring binding poses of mPD, DA and EDOT docked to the selected regions of IgG (averaged QPLD data)

Monomer	Van der Waals interaction, kJ mol ⁻¹	Lipophilic Interaction, kJ mol ⁻¹	Electrostatic Interaction, kJ mol ⁻¹	Hydrogen interaction, kJ mol ⁻¹	GScore, kJ mol ⁻¹
Fab-fragment					
mPD	-52.46	-6.42	-5.20	-1.19	-20.01
DA	-67.78	-8.84	-7.91	-1.23	-20.56
EDOT	-57.28	-8.17	-2.70	-1.27	-22.02
Hinge-fragment					
mPD	-50.67	-6.97	-0.25	-1.26	-19.54
DA	-63.37	-7.87	-15.14	-1.17	-20.79
EDOT	-	-	-	-	-
Fc-fragment					
mPD	-38.76	-7.26	-0.38	-2.52	-21.17
DA	-73.93	-10.26	-0.54	-1.54	-22.38
EDOT	-62.75	-7.36	-1.44	-1.21	-20.64

It was found that EDOT and DA are distributed non-uniformly over IgG, being preferably concentrated in the Fc (9 molecules of EDOT) and hinge (9 molecules of DA) regions, while mPD tends to be arranged more uniformly (6 molecules - on Fab, 6 molecules - on hinge, 2 molecules - on Fc regions) (Article I).

Table 4. The distribution of various monomers on IgG as a result of the sequential docking by QPLD.

Fragment of IgG	Monomer (number of docked molecules)		
	mPD	DA	EDOT
Fab-fragment	3	4	4
Hinge-fragment	6	9	0
Fc-fragment	2	1	9

Obviously, a more uniform arrangement of mPD around IgG would facilitate cavities for IgG than those of IgG-MI-PDA and IgG-MI-PEDOT. In summary, mPD is considered as an optimal monomer for the formation of IgG-MIP. The poses of mPD simulated by QPLD demonstrate the important role of polar groups in amino acids (glutamic/aspartic acid, serine, rarely by threonine, tyrosine) and monosaccharides in the formation of non-covalent interactions between mPD and IgG (Table 5).

Table 5. The non-covalent interactions of mPD in the poses predicted by QPLD

Number of docked mPD	Amino acid/monosaccharides around associated monomer, estimated for 4 Å
Fab-fragment (3)	
1	LYS62K, TYR96M, THR97M, PHE98M
2	ARG44K, GLU46K, LYS62K
3	GLN39K, ARG44K, GLN43K, TYR87M, GLN100M
Hinge fragment (6)	
1	LYS228K, PRO227K, PRO240H, PRO241H, ASP232K, CYS230K
2	PRO240H, SER195K, ALA138K
3	PRO240H, CYS239H, CYS239K, PRO240K, PRO241K
4	ASN314H, ALA244K, CYS242K, PRO243K, PRO243H, PRO245H
5	CYS239H, PRO240H, PRO241H, PRO243H, PRO241K, PRO243K
6	PRO240H, CYS242H, PRO241H
XP	SER127K, ASP232K, PRO241H, NMA127K
Fc-fragment (2)	
1	MAN485H, BMA481H, GAL484H, MAN482H, NAG483H, BMA481K, MAN482K
2	NAG483H, MAN482H, NAG479K

3.1.2 Quantum chemical calculation

The MD results were complemented with the QCCs, allowing estimation of the cumulative strength of multiple H-bond interactions in the prepolymerization complex between the proton-donor groups of monomers and the accessible proton-acceptor groups of IgG.

Figure 9 visualizes the positions of the sterically accessible polar O-atoms of the amino acids and sugars (monosaccharide) in the residues of IgG, which might be engaging in strong H-bond interactions with proton-donor groups of the monomers. It is interesting to note that O-atoms, which are associated with the amino acids, are uniformly distributed around the protein, while those associated with sugars are predominantly concentrated in the carbohydrate moiety of the Fc-fragment.

Since usage of QCCs for the study of protein-monomer interaction is limited due to the size of the system, the calculations were performed for the isolated complexes of the monomer-polar residue and the results were eventually summarized to represent the total strength of H-bond interactions in the IgG-monomer complex. Although the approach neglects the contribution of the

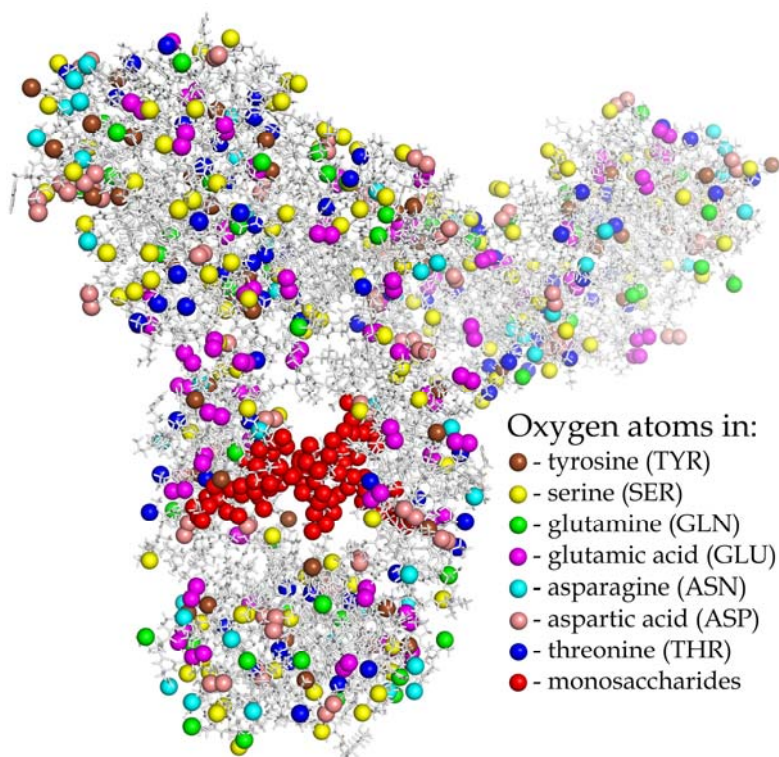


Figure 9. 3D map of steric accessible proton-accepting (oxygen) atoms in the polar amino acid of IgG.

summarized to represent the total strength of H-bond interactions in the IgG-monomer complex. Although the approach neglects the contribution of the neighboring residues surrounding the polar residue in the polypeptide chain of IgG to the association energy of the isolated complex, the validity of its application has been proved by the additional calculations, revealing only insignificant or no difference in the association energies of the complexes of the monomer-amino acid and the monomer-tripeptide, comprising the polar amino acid joined with two neighboring residues on N- and C- terminals (Table 6).

Table 6. The association energies of complexes of mPD-amino acid and mPD-tripeptide comprising the amino acid joined with two neighboring residues on N- and C- terminal

Amino acid or tripeptide-mPD	Association energy (ΔE), kJ mol ⁻¹	Amino acid or tripeptide-mPD	Association energy (ΔE), kJ mol ⁻¹
ASN	39.38	GLU	28.88
Ser-ASN-Phe	41.08	Ile-GLU-Gly	28.89
Ile-ASN-Pro	39.38	Gly-GLU-Asn	28.80
Tyr-ASN-Gly	39.38	Phe-GLU-Gly	29.19
Gly-ASN-Lys	39.38	Tyr-GLU-Lys	29.09
SER	36.75	GLN	39.38
Asn-SER-Phe	36.76	Asn-GLN-Phe	39.00
Ile-SER-Pro	36.79	Ile-GLN-Pro	39.50
Tyr-SER-Gly	36.71	Tyr-GLN-Lys	40.00
Gly-SER-Lys	36.75	Gly-GLN-Asn	39.67
TYR	26.25	ASP	34.13
Ser-TYR-Gly	26.26	Ile-ASP-Gly	34.71
Ile-TYR-Pro	26.30	Phe-ASP-Asn	34.89
Gly-TYR-Lys	26.29	Tyr-ASP-Lys	34.24
Asn-TYR-Phe	26.22	Gly-ASP-Pro	34.50
THR	49.88		
Asn-THR-Phe	49.88		
Ile-THR-Pro	50.51		
Gly-THR-Lys	49.91		
Tyr-THR-Gly	51.00		

Table 7 summarizes the association energies (ΔE) of interaction between the polar amino acid or monosaccharide residues of IgG and the different monomers (mPD, DA, EDOT), as calculated by QCC. The comparison of these values shows that mPD forms the strongest network of H-bond interactions around IgG molecule, as compared to the other two monomers. Thus, one can expect that the IgG-MI-PmPD might possess stronger H-bonding ability with IgG than IgG-MI-PEDOT and IgG-MI-PDA. Moreover, the detected presence of multiple H-bond interactions between IgG and monomer might necessitate the optimization of IgG removal procedure from the formed polymer by means of complementary treatment of the polymer with a solvent, which readily dissociates the H-bonds in order to further facilitate the release of IgG from the polymer and convert it efficiently into IgG-MIP (Article I).

Table 7. The association energy of the complexes (ΔE) between polar amino acid or monosaccharide residues of IgG and the monomers (mPD, DA, EDOT) as estimated by QCC

Polar residue of IgG	Association energy (ΔE), kJ mol ⁻¹		
	mPD	DA	EDOT
Glu (64*, violet**)	1848.32	1680.64	39.38
Tyr (51, brown)	1338.75	803.25	0.53
Ser (146, yellow)	5365.50	383.98	18.38
Gln (54, green)	2126.52	1134.00	24.94
Asp (51, salmon)	1740.63	267.75	39.38
Asn (50, cyan)	1969.00	656.50	93.47
Thr (90, blue)	4489.20	1181.70	26.26
Carbohydrate OH (47, red)	617.11	4195.69	17.59
Carbohydrate CO (8, red)	147.04	63.04	-
Carbohydrate O in heterocycle (18, red)	614.34	661.68	-
Carbohydrate O between cycles (16, red)	84.00	651.04	-
Total ***($\sum \Delta E$)	20340.41	11679.27	16449.60

*Number of sterically accessible units in the IgG.

**See 3D map of IgG representing the color-coded positions of the polar residues with the proton acceptor groups (Fig. 9).

***The total association energy was taken as the sum of the individual association energies of the sterically accessible residues in IgG. This $\sum \Delta E$ estimates the cumulative strength of H-bond interactions between the monomers and IgG, but neglects solvent effect. Fig. 10

3.2 Preparation of IgG-MIPs and study of IgG rebinding

To further support the MD and QCCs results, the PmPD-, PDA- and PEDOT-based IgG-MIPs and NIPs were synthesized electrochemically and their performances were compared (Article I). The electrochemical synthesis parameters and polymer film thickness were optimized (Articles II and III).

Additionally, the different solvents such as HCl, NaOH, and DMSO were applied separately in order to elucidate their capability to disrupt the multiple H-bond interactions between IgG and the polymer matrix.

Because of numerous H-bonds simulated between a monomer and the protein, washing out process was optimized by DMSO as effective aprotic H-bonds disruptive reagent successfully used to dissociate H-bonds in biomolecules [137]. DMSO is a polar aprotic solvent that can accept H-bonds to oxygen but lacks polar hydrogen to donate in an H-bond. DMSO can form an H-bond with an amino group in the PmPD backbone, replacing the H-bond between the protein and PmPD, while it cannot form an H-bond with itself or with another proton-donor group. Thus, DMSO can be an appropriate H-bond disrupting solvent for the protein-PmPD system acting via the competitive mechanism.

Among the IgG-MIPs washed out with different procedures, the most pronounced imprinting effect (IF 2.68) was observed for the IgG-MIP washed with DMSO. In this case, the value of K_D , which is considered as a measure of IgG affinity towards the MIP, was found to be approximately one order of magnitude higher for the IgG-MIP than that for the corresponding NIP (Article III). Based on the performed experiments, DMSO appeared to be an optimal agent assisting IgG removal from the polymer matrix, increasing the number of the complementary cavities, but at the same time treating the NIP gently, making it well-suited for the reference purpose, as demonstrated by the highest IF value (2.68) of IgG-MI-PmPD(DMSO) (Fig. 10, Table 8).

It was decided, therefore, to use DMSO in the following experiments where the PmPD, PDA and PEDOT-based IgG-MIPs/NIPs were synthesized, and their Q_{eq} and IF (Eq. 10) values upon the single injection of IgG (53.3 nM, Fig. S4 in Article III) were compared (Fig. 11). In the same way, the IgG-MI-PmPD(DMSO) was given the highest IF that agrees well with the results predicted above by MD and QCCs, showing the advantage of mPD as a functional monomer for the synthesis of IgG-MIP (see section 3.1).

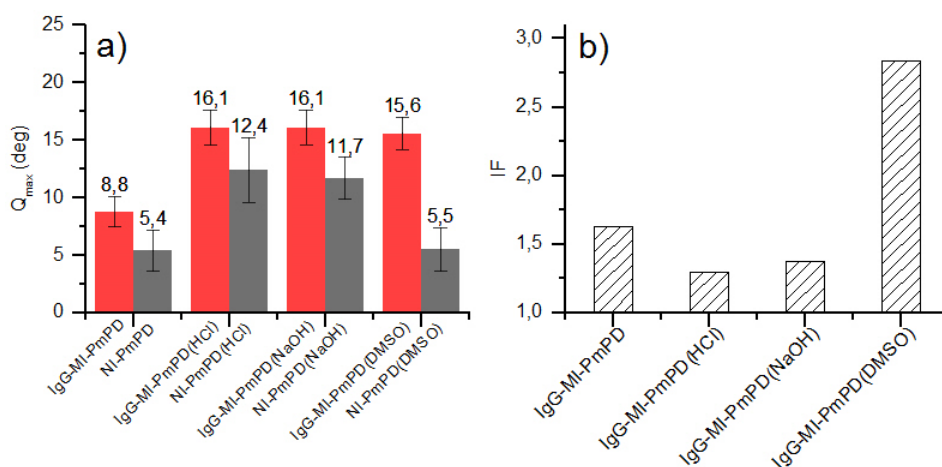


Figure 10. (a) Q_{max} values derived from the binding isotherms, as measured by SAW for the IgG-MI-PmPD NI-PmPD-modified sensor surfaces and for those additionally treated in either HCl, NaOH or DMSO (IgG-MI-PmPD(HCl), IgG-MI-PmPD(NaOH), IgG-MI-PmPD(DMSO)), and for the reference NIP systems (NI-PmPD(HCl), NI-PmPD(NaOH), NI-PmPD(DMSO)). (b) The values of IFs for the respective pairs of IgG-MIPs and NIPs were calculated by Eq. (9).

Table 8. Rebinding data recalculated for MIP-surfaces with different washing out solvents

Treatment	Qmax(MIP)	Qmax(NIP)	IF
Standart WO	8.8±1.3	5.4±1.8	1.66
Standart WO + SDS	8.4±1.3	7.5±2.5	1.12
Standart WO + HCl	16.1±5.5	12.4±2.8	1.33
Standart WO + NaOH	16.1±7.5	11.7±5.8	1.38
Standart WO + DMSO	15.6±1.4	5.5±1.9	2.68

In addition, comparison of the dissociation constants, K_D s, derived from binding kinetics, might shed light on the binding affinity between IgG and the synthesized IgG-MIPs [50, 138, 139]. The calculated K_D values (3.1 nM, 4.8 nM and 5.0 nM for IgG-MI-PmPD, IgG-MI-PDA, IgG-MI-PEDOT, respectively) were consist with the conclusions above, demonstrating somewhat higher binding affinity of IgG to IgG-MI-PmPD. However, the K_D values did not differ enough to justify reliably which of the polymers provided IgG-MIP having the higher affinity to IgG.

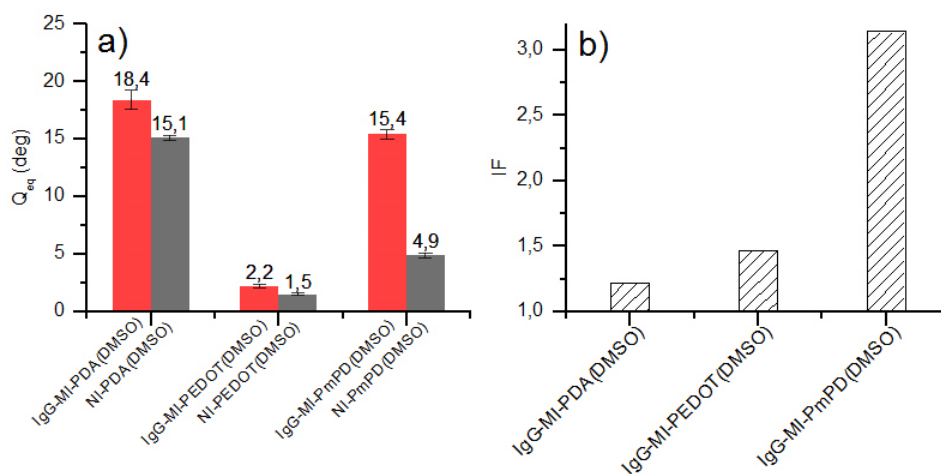


Figure 11. (a) Q_{eq} values derived from the kinetic analysis of the sensorgram association phase upon injection of IgG (53.3 nM), as measured by SAW for the IgG-MIP (IgG-MI-PDA(DMSO), IgG-MI-PEDOT(DMSO), IgG-MI-PmPD(DMSO)) and for the reference NIP films. The respective films were synthesized from either DA, EDOT or mPD and subjected to the additional DMSO treatment. (b) The values of IFs for the respective pairs of IgG-MIPs and NIP films, as calculated by Eq. (10). All signal data were adopted from cleaved films (MIP), subtracting background signal measured from the films washed without the cleavage procedure (NIP).

Conclusions

The aim of this thesis was to develop a computational modeling approach allowing the rational selection of a functional monomer for building a MIP having binding sites capable of selective capturing of macromolecular analytes. In this approach, MD combined with QCC were used for modelling and comparing molecular interactions between a model macromolecular template (IgG) and one of three electropolymerizable functional monomers (mPD, DA, EDOT). The approach allows us to draw the following conclusions:

- The energetically favorable binding poses of the monomer on the different regions of IgG, their distribution over the whole molecule of IgG, and energies of non-covalent interactions (GScore) at these poses can be readily estimated using MD. Although all three studied monomers demonstrated almost similar GScore values, ranging between -19.54 and -22.38 kJ mol⁻¹, mPD molecules were found to be arranged more uniformly around IgG as compared to DA and EDOT.
- The association energies (ΔE) of hydrogen interaction between the polar amino acid or monosaccharide residues of IgG and the different monomers can be calculated by QCC. The results showed that mPD formed the strongest network of H-bond interactions around IgG molecule as compared with the other two monomers.
- According to the above mentioned computational predictions, mPD can be considered as a more optimal monomer for the synthesis of IgG-MIP than DA or EDOT.
- The computational predictions were validated experimentally comparing performances of the IgG-MIPs synthesized from mPD, DA or EDOT. Namely, the PmPD-based IgG-MIPs (IgG-MI-PmPD) had relatively higher binding capacity towards IgG than those generated from PDA (IgG-MI-PDA) and PEDOT (IgG-MI-PEDOT), as judged by their IF values, which were 3.1, 1.5 and 1.8 for IgG-MI-PmPD, IgG-MI-PDA and IgG-MI-PEDOT, respectively.
- It was revealed that among the solvents, NaOH, HCl and DMSO, the latter was found to be a more suitable solvent to disrupt the multiple H-bond interactions between IgG and the polymer matrix, while minimally affecting the binding properties of the control polymer. This was judged by the IF value, which was the highest for IgG-MIP films additionally treated in DMSO (IgG-PmPD(DMSO)).

Finally, the computational approach presented in this thesis is novel, valid and reasonable. The approach provides means for understanding macromolecular imprinting phenomena, i.e. potency of the MIPs to selective recognizing of macromolecules such as proteins. Therefore, future work will be substantially facilitated by the developed approach to design MIPs for the detection of the range of clinically relevant proteins, such as prostate specific antigen (PSA), neurotrophic factor proteins (CDNF, BDNF) and other proteins.

Abstract

Molecular imprinting is one of the state-of-the-art techniques to generate robust molecular recognition materials with antibody-like ability to bind and discriminate between molecules. The technique can be defined as the process of template-induced formation of selective molecular recognition sites in a polymer matrix material. In this process, a mixture of functional monomers is polymerized around a target analyte molecule that acts as a molecular template. During the polymerization, the template induces binding sites in the reticulated polymer that are capable of selective recognition of the target analyte molecules after removal of the templates from the formed polymer. The main benefits of these polymers, so-called Molecularly Imprinted Polymers (MIPs), are related to their synthetic nature, i.e. excellent chemical and thermal stability associated with reproducible, cost-effective fabrication. MIP materials have been shown to be a promising alternative to natural biological receptors in biosensors providing paths to synthesize more stable and low-cost recognition elements.

The prerequisite for the formation of selective binding sites for a macromolecular target in a MIP supposes the presence of non-covalent interactions (self-assembly), such as H-bonds, van der Waals forces, ionic interactions, and hydrophobic effects in the pre-polymerization complex between the macromolecular template molecule and the functional monomers. It is assumed that the choice of functional monomers capable of forming more stable non-covalent complexes with the template could result in a MIP with a high selectivity and affinity. Thus, performance of the MIP relies first of all on the quantity and strength of pre-existing molecular interactions in those complexes before the polymerization of the monomers. This aspect is particularly crucial for the formation of selective binding sites in a MIP for a macromolecular structure, such as, e.g., a protein (protein-MIP) where a considerable amount of different functional groups enables multiple non-covalent interactions between the protein and a functional monomer in the pre-polymerization complex. Therefore, an estimation of all possible non-covalent interactions as well as their strength in the protein-monomer complex should be seriously considered when aiming to design a protein-MIP with highly selective recognition sites.

Different computational approaches, including molecular mechanics, molecular dynamics, quantum chemical calculation (QCC) and molecular docking (MD), were successfully used for a rational design of MIPs through the prediction, simulation and estimation of molecular interactions between a small molecular weight molecule and a monomer in a pre-polymerization complex. However, there are very few computational studies on MIPs that are selective towards a macromolecular molecule. These studies mostly use the molecular mechanics simulations, MD and lattice Monte Carlo simulations. Among them, MD is the fastest and least resource-consuming computational method to estimate protein-ligand interactions, and it is widely used in the field of drug design. MD provides reliable predictions of binding poses of a monomer on a protein prior to

the polymerization, as well as determination of the types of non-covalent interactions taking place by the set of the amino acids present near this binding pocket. However, MD limits estimation of energy only for interactions happening in the areas with the best-scoring bindings poses ignoring as well weak interactions between the ligand and the protein, i.e. the H-bond interactions between spatial accessible polar amino acid residues and monomers. At same time, QCC allows precise assessing of such H-bond interactions; however, its applicability to the calculation of the protein-ligand complex is limited due to the size of the system.

Therefore, the main objective of this thesis was to develop a computational modeling approach allowing the rational selection of a functional monomer for building a polymer with binding sites capable of selectively capturing macromolecular analytes. In this approach, MD combined with QCC were used for modeling and comparing molecular interactions between a model macromolecular template (IgG), and one of three electropolymerizable functional monomers (mPD, DA, EDOT). MD was applied to find the energetically favorable binding poses of the monomer on IgG as well as to predict the probable arrangement of the multiple monomer molecules around IgG. Although all three studied monomers demonstrated almost similar GScore values ranging between -19.54 and -22.38 kJ mol^{-1} , mPD molecules were found to be arranged more uniformly around IgG as compared to DA and EDOT. The MD results were complemented with the QCC, allowing estimation of the cumulative strength of multiple H-bond interactions in the prepolymerization complex between the proton-donor groups of the monomers and the accessible proton-acceptor groups of IgG to establish further its influence on the performance of the resulting IgG-MIPs. The comparison of the association energies (ΔE) of interaction between the polar amino acid or monosaccharide residues of IgG and the different monomers calculated by QCC showed that mPD formed the strongest network of H-bond interactions around IgG molecule, versus the other two monomers that further justified the selection of mPD as an optimal monomer for the synthesis of IgG-MIP.

The computational predictions were validated experimentally by the SAW biosensing platform, which was used to compare performances of the IgG-MIPs synthesized from the candidate monomers. The experimental results showed that the PmPD-based IgG-MIPs (IgG-MI-PmPD) had a relatively higher binding capacity towards IgG than that generated from PDA (IgG-MI-PDA) and PEDOT (IgG-MI-PEDOT), as judged by their IF values, which were 3.1, 1.5 and 1.8 for IgG-MI-PmPD, IgG-MI-PDA and IgG-MI-PEDOT, respectively. It was revealed that among the solvents, NaOH, HCl and DMSO, the latter was found to be a more suitable solvent to disrupt the multiple H-bond interactions between IgG and the polymer matrix, while minimally affecting the binding properties of the control polymer.

Therefore, the computational approach presented in this thesis is novel and provides means for understanding the macromolecular imprinting phenomena, i.e. potency of the MIPs to recognize selectively macromolecules such as proteins.

Kokkuvõte

Molekulaarne jäljendamine on kaasaegne tehnoloogia antikeha-analoogsete materjalide valmistamiseks molekulaarsel tasemel teatud sihtmolekulide sidumiseks ja eristamiseks. Molekulaarse jäljendamise tehnoloogia põhineb sihtmolekulide suhtes tundlike „mälupesade“ loomises polümeeri maatriksis. Selleks polümeriseeritakse monomeer koos vastava sihtmolekuliga moodustades polümeerse kompleksi sihtmolekuli ja monomeeri vahel. Järgnevalt eemaldatakse sihtmolekul polümeeri maatriksist nii, et polümeeri maatriksis säilib sihtmolekuli jälend, mis on võimeline uuesti siduma uuritavast keskkonnast sihtmolekuli. Selliselt valmistatud molekulaarselt jäljendatud polümeeride (MJP) eeliseks võrreldes looduslike retseptoritega on võimalus neid laboritingimustes sünteesida, tagades sellega parema keemiliste omaduste stabiilsuse, hea temperatuuritaluvuse, omaduste reprodutseeritavuse ja odavama hinna võrreldes looduslike analoogide – retseptoritega.

MJP efektiivsus sõltub olulisel määral sihtmolekuli ja monomeer polümerisatsioonil tekkivate mittekovalentsete sidemete – vesiniksidemete, van der Waalsi, ioonsete aga ka hüdrofoobsete sidemete - iseloomust. Polümerisatsioonil tekkivad sidemed peavad olema stabiilsed molekulaarselt jäljendatud polümeeri püsivuse tagamiseks, kuid samal ajal peavad ka võimaldama eemaldada sihtmolekuli polümeeri maatriksist nii, et säiliks tervena sihtmolekuli „mälupesa“ ja polümeeri maatriks.

Sihtmolekuli ja monomeeri vahel tekkivate võimalike sidemete arvu, liigi ja tugevuse prognoosimisel arvutimodelleerimise abi kasutatakse tavaliselt molekulaarmehaanilist ja molekulaardünaamilist lähendust, molekulaarsildamist (molecular docking, MD) ja kvantkeemilisi arvutusi (quantum chemical calculations, QCCs). Selline prognoosimine enne praktilist polümerisatsiooni annab väga olulist teavet optimaalse monomeeri valikuks ja kui seda teha arvutil modelleerimise abil siis on võimalik märkimisväärselt hoida kokku töömahukate katsete ja kallite reagentide arvelt. Peab märkima, et suurem osa kirjanduse allikatest kirjeldab molekulaarmodelleerimise protsessi funktsionaalsete monomeeride ja madalmolekulaarsete sihtmolekulide vahel, kuid väga vähe on uuritud sidemete arvu, liigi ja tugevuse prognoosimise võimalusi makromolekulaarsete sihtmolekulide (proteiinide) korral. Makromolekulaarsete sihtmolekulidega MJP molekulaarmodelleerimisel on kasutatud peamiselt molekulaarmehaanilist lähendust, MD ja Monte Carlo simulatsioone. Üldnimetatud meetoditest on MD kõige kiirem ja säästlikum arvutil modelleerimise meetod proteiin-ligandi vaheliste sidemete prognoosimiseks ning seda kasutatakse peamiselt ravimite molekulaardisainis. Meetod võimaldab prognoosida võimalikku sidemete teket polümerisatsioonil aga ka ennustada eeldatavate sidemete iseloomu. Samas on MD meetodil teatud puudused. MD toob välja vaid eelistatud sidemed ja ei võimalda täpselt hinnata kõikide võimalike sidemete tekkeenergiaid. Näiteks ei arvestata vesiniksidemeid monomeeri ja võimalike proteiinis esinevate polaarsete aminohapete ja suhkrute

prooton-aktseptor rühmade vahel. Kvantkeemiliste arvutustega on küll võimalik hinnata paremini erinevate sideme tüüpide energiasid, kuid selle meetodi rakendamine proteiin-ligandi vaheliste sidemete hindamiseks on raskendatud süsteemi suurte mõõtmete tõttu.

Käesoleva doktoritöö eesmärgiks oli monomeeride valiku protsessi molekulaarne modelleerimine optimaalse monomeeri leidmiseks MJP valmistamiseks proteiini selektiivseks määramiseks. Mudelproteiiniks (sihtmolekuliks) valiti Immuunoglobuliin G (IgG) kui üks enim esindatud antikehi inimese seerumis. Polümeermaatriksi moodustamiseks analüüsi kolme elektrokeemiliselt polümeriseeritavat monomeeri – m-fenüleendiamiini (mPD), dopamiini (DA) ja 3,4-etiüleendioksiotiofeeni (EDOT). MD ja kvantkeemiliste arvutuste abil modelleeriti kõigi kolme monomeeri ja sihtmolekuli polümerisatsioonil tekkivate eelistatud sidemete teket ja paigutust proteiini suhtes ning samuti tekkivate sidemete energiasid. Modelleerimisel kasutati MD meetodit eelistatud sidemete prognoosimiseks monomeeri ja IgG vahel ja nende jaotus monomeeride ja erinevate IgG molekuli fragmentide suhtes, samuti tekkivate mittekovalentsete sidemete energiasid. Kõigi kolme analüüsitud monomeeri ja IgG vahelised sidemeenergiad langesid vahemikku -19.54 and -22.38 kJ mol⁻¹, kuid mPD molekulid jaotusid IgG molekuli suhtes kõige ühtlasemalt. MD meetodit täiendati kvantkeemiliste arvutustega võttes arvesse vesiniksidemete summaarset energiasid, mis tekib monomeeri prooton- doonor gruppide ja proteiini prooton- aktseptor gruppide vahel. Näidati, et kõige stabiilsemad sidemed moodustatakse IgG molekuli suhtes polümerisatsioonil monomeeri m-fenüleendiamiiniga (mPD). Arvutusliku modelleerimise kokkuvõtteks leiti, et optimaalseks monomeeriks IgG sidumiseks molekulaarselt jälgendatud tehnoloogia abil on m-fenüleendiamiin (mPD).

Arvutusliku modelleerimise tulemusi kontrolliti eksperimentaalselt hinnates IgG sidumise efektiivsust uuritud monomeeridest valmistatud MJP (IgG-MIP) kiledel pinna akustilise laine (surface acoustic wave, SAW) meetodil. IgG sidumise efektiivsuse parandamiseks uuriti täiendavalt erinevate lahustite kasutamise efektiivsust sihtmolekuli väljapesemisel mälupesade arvu suurendamiseks. Analüüsi kolme lahustaja: NaOH, HCl ja DMSO kasutamise mõju mälupesade tekitamiseks, määraes erinevate lahustajatega töödeldud IgG-MIP efektiivsust ja leiti, et ülalnimetatud lahustajatest toimib kõige efektiivsemalt DMSO seejuures kõige vähem kahjustades polümeeri maatriksit. IgG-MIP efektiivsuse võrdlemine SAW meetodil erinevate monomeeride korral näitas, et DMSO lahustaja kasutamisel saadi monomeeri mPD kasutamisel IgG-MI-PmPD spetsiifilise sidumise efektiivsuseks IF=3.1 võrreldes IgG-MI-PDA (IF=1.5) ja IgG-MI-PEDOT (IF=1.8).

Kokkuvõtteks järeldati, et doktoritöös välja pakutud molekulaarse modelleerimise meetod optimaalse monomeeri leidmiseks makromolekulaarsete sihtmolekulide (IgG) jaoks töötab hästi mida kinnitasid ka IgG-MIP sidumise efektiivsuse analüüsi tulemused.

Acknowledgements

I am heartily thankful to my supervisor, Dr. Vitali Syritski for the patient guidance, encouragement and advice he has provided throughout my time as his student. I have been extremely lucky to have a supervisor who cared so much about my work, enabled me to develop an understanding of the subject and responded to my questions and queries so promptly.

I would like to express my sincere gratitude to my co-supervisor Prof. Andres Öpik for his support and supervision.

Also, I would like to express my deepest gratitude to my co-supervisor Dr. Jekaterina Reut for all her help, support, interest and valuable advice.

I wish to thank Dr. Malle Krunks, Head of the Department of Materials Science up to 2015, for providing an excellent opportunity to carry out my studies and research at the Chair of Physical Chemistry of Tallinn University of Technology and for the opportunity to use high-end research equipment within the Department.

I thank Dr. Andre Lomaka for his assistance in the interpretation of computational modelling results.

In addition, I would like to thank my colleagues Alexei Tretjakov and Akinrinade George Ayankajo as well as everybody whom I worked with in the Department of Materials Science.

Finally, I am grateful to my family and all the people who have supported me during my doctoral studies.

This research was carried out at the Chair of Physical Chemistry, Department of Materials Science. The work was financially supported by Estonian Science Foundation (**PUT150**), Estonian Ministry of Education and Research (SF0140033s12), European Social Fund's Doctoral Studies and Internationalization Program (DoRa8), FMTDK graduate school "Functional materials and technologies" (European Social Fund under Project 1.2.0401.09-0079 in Estonia).

References

- [1] K. Mosbach, O. Ramstrom, The emerging technique of molecular imprinting and its future impact on biotechnology, *Bio-Technology* 14(2) (1996) 163-170.
- [2] K. Haupt, Biomaterials: Plastic antibodies, *Nature materials* 9(8) (2010) 612-4.
- [3] C.S. Mahon, D.A. Fulton, Mimicking nature with synthetic macromolecules capable of recognition, *Nature chemistry* 6(8) (2014) 665-72.
- [4] Y. Hoshino, T. Kodama, Y. Okahata, K.J. Shea, Peptide imprinted polymer nanoparticles: a plastic antibody, *Journal of the American Chemical Society* 130(46) (2008) 15242-3.
- [5] E.L. Holthoff, F.V. Bright, Molecularly templated materials in chemical sensing, *Analytica Chimica Acta* 594(2) (2007) 147-61.
- [6] L. Uzun, A.P. Turner, Molecularly-imprinted polymer sensors: realising their potential, *Biosensors & Bioelectronics* 76 (2016) 131-44.
- [7] F.G. Tamayo, E. Turiel, A. Martin-Esteban, Molecularly imprinted polymers for solid-phase extraction and solid-phase microextraction: recent developments and future trends, *Journal of chromatography. A* 1152(1-2) (2007) 32-40.
- [8] W.J. Cheong, S.H. Yang, F. Ali, Molecular imprinted polymers for separation science: a review of reviews, *Journal of separation science* 36(3) (2013) 609-28.
- [9] H. Zhang, L. Ye, K. Mosbach, Non-covalent molecular imprinting with emphasis on its application in separation and drug development, *Journal of molecular recognition : JMR* 19(4) (2006) 248-59.
- [10] C. Alvarez-Lorenzo, A. Concheiro, Molecularly imprinted polymers for drug delivery, *Journal of chromatography. B, Analytical technologies in the biomedical and life sciences* 804(1) (2004) 231-45.
- [11] F. Puoci, G. Cirillo, M. Curcio, O.I. Parisi, F. Iemma, N. Picci, Molecularly imprinted polymers in drug delivery: state of art and future perspectives, *Expert opinion on drug delivery* 8(10) (2011) 1379-93.
- [12] G. Wulff, J. Liu, Design of biomimetic catalysts by molecular imprinting in synthetic polymers: the role of transition state stabilization, *Accounts of chemical research* 45(2) (2012) 239-47.
- [13] X. Kan, Q. Zhao, D. Shao, Z. Geng, Z. Wang, J.-J. Zhu, Preparation and Recognition Properties of Bovine Hemoglobin Magnetic Molecularly Imprinted Polymers, *Journal of Physical Chemistry B* 114(11) (2010) 3999-4004.
- [14] N. Kirsch, J. Hedin-Dahlstrom, H. Henschel, M.J. Whitcombe, S. Wikman, I.A. Nicholls, Molecularly imprinted polymer catalysis of a Diels-Alder reaction. , *J. Mol. Catal. B-Enzym.* 58(1-4) (2009) 110-117.
- [15] S.J. Li, Y. Ge, A.P.F. Turner, A catalytic and positively thermosensitive molecularly imprinted polymer., *Adv. Funct. Mater.* 21(6) (2011) 1194-1200.
- [16] K.J. Tong, S. Xiao, S.J. Li, J. Wang, Molecular recognition and catalysis by molecularly imprinted polymer catalysts: Thermodynamic and kinetic surveys on the specific behaviors, *J. Inorg. Organomet. Polym. Mater.* 18(3) (2008) 426-433.
- [17] D.R. Kryscio, N.A. Peppas, Critical review and perspective of macromolecularly imprinted polymers, *Acta Biomaterialia* 8(2) (2012) 461-73.

- [18] M.J. Whitcombe, I. Chianella, L. Larcombe, S.A. Piletsky, J. Noble, R. Porter, A. Horgan, The rational development of molecularly imprinted polymer-based sensors for protein detection, *Chem. Soc. Rev.* 40(3) (2011) 1547-1571.
- [19] K. Karim, F. Breton, R. Rouillon, E.V. Piletska, A. Guerreiro, I. Chianella, S.A. Piletsky, How to find effective functional monomers for effective molecularly imprinted polymers?, *Advanced drug delivery reviews* 57(12) (2005) 1795-808.
- [20] C. Alexander, H.S. Andersson, L.I. Andersson, R.J. Ansell, N. Kirsch, I.A. Nicholls, J. O'Mahony, M.J. Whitcombe, Molecular imprinting science and technology: a survey of the literature for the years up to and including 2003, *Journal of Molecular Recognition* 19(2) (2006) 106-180.
- [21] S.J. Li, S.S. Cao, M.J. Whitcombe, S.A. Piletsky, Size matters: Challenges in imprinting macromolecules., *Prog. Polym. Sci.* 39(1) (2014) 145-163.
- [22] H.Q. Zhang, Water-compatible molecularly imprinted polymers: Promising synthetic substitutes for biological receptors, *Polymer* 55(3) (2014) 699-714.
- [23] M.J. Whitcombe, N. Kirsch, I.A. Nicholls, Molecular imprinting science and technology: a survey of the literature for the years 2004-2011, *Journal of Molecular Recognition* 27(6) (2014) 297-401.
- [24] G.D. Olsson, K. Niedergall, M. Bach, B.C.G. Karlsson, G. Tovar, I.A. Nicholls, Simulation of imprinted emulsion prepolymerization mixtures, *Polym. J.* 47(12) (2015) 827-830.
- [25] A. Azimi, M. Javanbakht, Computational prediction and experimental selectivity coefficients for hydroxyzine and cetirizine molecularly imprinted polymer based potentiometric sensors, *Analytica Chimica Acta* 812 (2014) 184-90.
- [26] S. Subrahmanyam, A. Guerreiro, A. Poma, E. Moczko, E. Piletska, S. Piletsky, Optimisation of experimental conditions for synthesis of high affinity MIP nanoparticles, *European Polymer Journal* 49(1) (2013) 100-105.
- [27] T. Cowen, K. Karim, S. Piletsky, Computational approaches in the design of synthetic receptors - A review, *Analytica Chimica Acta* 936 (2016) 62-74.
- [28] S.A. Piletsky, K. Karim, E.V. Piletska, C.J. Day, K.W. Freebairn, C. Legge, A.P.F. Turner, Recognition of ephedrine enantiomers by molecularly imprinted polymers designed using a computational approach, *Analyst* 126(10) (2001) 1826-1830.
- [29] S. Piletsky, E. Piletska, K. Karim, G. Foster, C. Legge, A. Turner, Custom synthesis of molecular imprinted polymers for biotechnological application - Preparation of a polymer selective for tylosin, *Analytica Chimica Acta* 504(1) (2004) 123-130.
- [30] C. Dong, X. Li, Z. Guo, J. Qi, Development of a model for the rational design of molecular imprinted polymer: Computational approach for combined molecular dynamics/quantum mechanics calculations, *Analytica Chimica Acta* 647(1) (2009) 117-124.
- [31] M. Sobiech, T. Zolek, P. Lulinski, D. Maciejewska, A computational exploration of imprinted polymer affinity based on voriconazole metabolites, *Analyst* 139(7) (2014) 1779-1788.

- [32] W.G. Dong, M. Yan, M.L. Zhang, Z. Liu, Y.M. Li, A computational and experimental investigation of the interaction between the template molecule and the functional monomer used in the molecularly imprinted polymer, *Analytica Chimica Acta* 542(2) (2005) 186-192.
- [33] C.Y. Hsu, H.Y. Lin, J.L. Thomas, B.T. Wu, T.C. Chou, Incorporation of styrene enhances recognition of ribonuclease A by molecularly imprinted polymers, *Biosensors & Bioelectronics* 22(3) (2006) 355-363.
- [34] D.R. Kryscio, Y. Shi, P.Y. Ren, N.A. Peppas, Molecular Docking Simulations for Macromolecularly Imprinted Polymers, *Industrial & Engineering Chemistry Research* 50(24) (2011) 13877-13884.
- [35] J. Pan, X.H. Xue, J.H. Wang, H.M. Me, Z.Y. Wu, Recognition property and preparation of *Staphylococcus aureus* protein A-imprinted polyacrylamide polymers by inverse-phase suspension and bulk polymerization, *Polymer* 50(11) (2009) 2365-2372.
- [36] L. Levi, S. Srebnik, Simulation of Protein-Imprinted Polymers. 1. Imprinted Pore Properties, *Journal of Physical Chemistry B* 114(1) (2010) 107-114.
- [37] A. Unzue, K. Lafleur, H. Zhao, T. Zhou, J. Dong, P. Kolb, J. Liebl, S. Zahler, A. Caflisch, C. Nevado, Three stories on Eph kinase inhibitors: From in silico discovery to in vivo validation, *European Journal of Medicinal Chemistry* 112 (2016) 347-66.
- [38] M.H. Hao, Theoretical Calculation of Hydrogen-Bonding Strength for Drug Molecules, *Journal of chemical theory and computation* 2(3) (2006) 863-72.
- [39] R.A. Lorenzo, A.M. Carro, C. Alvarez-Lorenzo, A. Concheiro, To Remove or Not to Remove? The Challenge of Extracting the Template to Make the Cavities Available in Molecularly Imprinted Polymers (MIPs), *International Journal of Molecular Sciences* 12(7) (2011) 4327-4347.
- [40] B. Mattiasson, L. Ye, Molecularly Imprinted Polymers in Biotechnology Preface, in: B. Mattiasson, L. Ye (Eds.), *Molecularly Imprinted Polymers in Biotechnology*, Springer Int Publishing Ag, Cham, 2015, pp. V-VI.
- [41] A. Sarhan, G. Wulff, The use of polymers with enzyme-analogous structures for the resolution of racemates., *Angewandte Chemie International Edition* 11(1) (1972) 341.
- [42] R. Arshady, K. Mosbach, SYNTHESIS OF SUBSTRATE-SELECTIVE POLYMERS BY HOST-GUEST POLYMERIZATION, *Macromolecular Chemistry and Physics-Makromolekulare Chemie* 182(2) (1981) 687-692.
- [43] L.X. Chen, S.F. Xu, J.H. Li, Recent advances in molecular imprinting technology: current status, challenges and highlighted applications, *Chem. Soc. Rev.* 40(5) (2011) 2922-2942.
- [44] L. Ye, K. Mosbach, Molecular imprinting: Synthetic materials as substitutes for biological antibodies and receptors, *Chemistry of Materials* 20(3) (2008) 859-868.
- [45] H.Q. Shi, W.B. Tsai, M.D. Garrison, S. Ferrari, B.D. Ratner, Template-imprinted nanostructured surfaces for protein recognition, *Nature* 398(6728) (1999) 593-597.
- [46] A. Tretjakov, V. Syritski, J. Reut, R. Boroznjak, A. Opik, Molecularly

imprinted polymer film interfaced with Surface Acoustic Wave technology as a sensing platform for label-free protein detection, *Analytica Chimica Acta* 902 (2016) 182-188.

[47] A. Tretjakov, V. Syritski, J. Reut, R. Boroznjak, O. Volobujeva, A. Opik, Surface molecularly imprinted polydopamine films for recognition of immunoglobulin G, *Microchimica Acta* 180(15-16) (2013) 1433-1442.

[48] W. Zhang, L. Qin, X. He, W. Li, Z. Y., Novel surface modified molecularly imprinted polymer using acryloyl-beta-cyclodextrin and acrylamide as monomers for selective recognition of lysozyme in aqueous solution., *J Chromatogr A*. 1216(21) (2009) 4560-4567.

[49] G. Lautner, J. Kaev, J. Reut, A. Öpik, J. Rappich, V. Syritski, G. R., Selective artificial receptors based on micropatterned surface-imprinted polymers for label-free detection of proteins by SPR imaging., *Adv Funct Mater* 21(3) (2011) 591-597.

[50] A. Menaker, V. Syritski, J. Reut, A. Opik, V. Horvath, R.E. Gyurcsanyi, Electrosynthesized Surface-Imprinted Conducting Polymer Microrods for Selective Protein Recognition, *Adv. Mater.* 21(22) (2009) 2271-+.

[51] Y. Li, H.H. Yang, Q.H. You, Z.X. Zhuang, X.R. Wang, Protein recognition via surface molecularly imprinted polymer nanowires, *Analytical Chemistry* 78(1) (2006) 317-320.

[52] A. Nematollahzadeh, W. Sun, C.S.A. Aureliano, D. Lutkemeyer, J. Stute, M.J. Abdekhodaie, A. Shojaei, B. Sellergren, High-Capacity Hierarchically Imprinted Polymer Beads for Protein Recognition and Capture, *Angewandte Chemie-International Edition* 50(2) (2011) 495-498.

[53] A. Kulandaisamy, V. Lathi, K. ViswaPoorani, K. Yugandhar, M.M. Gromiha, Important amino acid residues involved in folding and binding of protein-protein complexes, *International Journal of Biological Macromolecules* 94 (2017) 438-444.

[54] P. Towner, W. Gaertner, B. Walckhoff, D. Oesterhelt, H. Hopf, Alpha-retinal as a prosthetic group in bacteriorhodopsin, *Febs Letters* 117(1) (1980) 363-367.

[55] M.J.S. Dewar, E.G. Zoebisch, E.F. Healy, J.J.P. Stewart, AM1 - a new general-purpose quantum-mechanical molecular model, *Journal of the American Chemical Society* 115(12) (1993) 5348-5348.

[56] A. van der Vaart, K.M. Merz, The role of polarization and charge transfer in the solvation of biomolecules, *Journal of the American Chemical Society* 121(39) (1999) 9182-9190.

[57] A. van der Vaart, D. Suarez, K.M. Merz, Critical assessment of the performance of the semiempirical divide and conquer method for single point calculations and geometry optimizations of large chemical systems, *Journal of Chemical Physics* 113(23) (2000) 10512-10523.

[58] K. Raha, K.M. Merz, A quantum mechanics-based scoring function: Study of zinc ion-mediated ligand binding, *Journal of the American Chemical Society* 126(4) (2004) 1020-1021.

[59] K.T. Simons, C. Kooperberg, E. Huang, D. Baker, Assembly of protein

tertiary structures from fragments with similar local sequences using simulated annealing and Bayesian scoring functions, *Journal of Molecular Biology* 268(1) (1997) 209-225.

[60] B.J. McConkey, V. Sobolev, M. Edelman, Discrimination of native protein structures using atom-atom contact scoring, *Proceedings of the National Academy of Sciences of the United States of America* 100(6) (2003) 3215-3220.

[61] J. Tsai, R. Bonneau, A.V. Morozov, B. Kuhlman, C.A. Rohl, D. Baker, An improved protein decoy set for testing energy functions for protein structure prediction, *Proteins-Structure Function and Genetics* 53(1) (2003) 76-87.

[62] C. Hetenyi, U. Maran, M. Karelson, A comprehensive docking study on the selectivity of binding of aromatic compounds to proteins, *Journal of Chemical Information and Computer Sciences* 43(5) (2003) 1576-1583.

[63] L.G. Ferreira, R.N. dos Santos, G. Oliva, A.D. Andricopulo, *Molecular Docking and Structure-Based Drug Design Strategies*, *Molecules* 20(7) (2015) 13384-13421.

[64] Glide5.5 User Manual, (2009).

[65] R.A. Friesner, J.L. Banks, R.B. Murphy, T.A. Halgren, J.J. Klicic, D.T. Mainz, M.P. Repasky, E.H. Knoll, M. Shelley, J.K. Perry, D.E. Shaw, P. Francis, P.S. Shenkin, Glide: A new approach for rapid, accurate docking and scoring. 1. Method and assessment of docking accuracy, *Journal of Medicinal Chemistry* 47(7) (2004) 1739-1749.

[66] C. Malitesta, I. Losito, P.G. Zambonin, Molecularly imprinted electrosynthesized polymers: new materials for biomimetic sensors, *Analytical chemistry* 71(7) (1999) 1366-70.

[67] C. Malitesta, E. Mazzotta, R.A. Picca, A. Poma, I. Chianella, S.A. Piletsky, MIP sensors - the electrochemical approach, *Analytical and Bioanalytical Chemistry* 402(5) (2012) 1827-1846.

[68] P.S. Sharma, A. Pietrzyk-Le, F. D'Souza, W. Kutner, Electrochemically synthesized polymers in molecular imprinting for chemical sensing, *Analytical and Bioanalytical Chemistry* 402(10) (2012) 3177-3204.

[69] J. Orozco, A. Cortes, G.Z. Cheng, S. Sattayasamitsathit, W. Gao, X.M. Feng, Y.F. Shen, J. Wang, Molecularly Imprinted Polymer-Based Catalytic Micromotors for Selective Protein Transport, *Journal of the American Chemical Society* 135(14) (2013) 5336-5339.

[70] Y. Wang, T.X. Wei, Surface plasmon resonance sensor chips for the recognition of bovine serum albumin via electropolymerized molecularly imprinted polymers, *Chinese Chemical Letters* 24(9) (2013) 813-816.

[71] X.W. Kan, Z.L. Xing, A.H. Zhu, Z. Zhao, G.L. Xu, C. Li, H. Zhou, Molecularly imprinted polymers based electrochemical sensor for bovine hemoglobin recognition, *Sensors and Actuators B-Chemical* 168 (2012) 395-401.

[72] S.M. Richardson-Burns, J.L. Hendricks, B. Foster, L.K. Povlich, D.H. Kim, D.C. Martin, Polymerization of the conducting polymer poly(3,4-ethylenedioxythiophene) (PEDOT) around living neural cells, *Biomaterials* 28(8) (2007) 1539-1552.

[73] H. Lee, S.M. Dellatore, W.M. Miller, P.B. Messersmith, Mussel-inspired

surface chemistry for multifunctional coatings, *Science* 318(5849) (2007) 426-430.

[74] Y.W. Zhang, H.L. Li, Y.L. Luo, X. Shi, J.Q. Tian, X.P. Sun, Poly(m-Phenylenediamine) Nanospheres and Nanorods: Selective Synthesis and Their Application for Multiplex Nucleic Acid Detection, *Plos One* 6(6) (2011).

[75] S.J. Killoran, R.D. O'Neill, Characterization of permselective coatings electrosynthesized on Pt-Ir from the three phenylenediamine isomers for biosensor applications, *Electrochimica Acta* 53(24) (2008) 7303-7312.

[76] B. Duran, G. Bereket, M. Duran, Electrochemical synthesis and characterization of poly(m-phenylenediamine) films on copper for corrosion protection, *Progress in Organic Coatings* 73(2-3) (2012) 162-168.

[77] H. Zhu, X. Wang, X. Liu, X. Yang, Integrated synthesis of poly(o-phenylenediamine)-derived carbon materials for high performance supercapacitors, *Adv. Mater.* 24(48) (2012) 6524-9.

[78] Q.L. Yang, P. Atanasov, E. Wilkins, An integrated needle-type biosensor for intravascular glucose and lactate monitoring, *Electroanalysis* 10(11) (1998) 752-757.

[79] P.C. Nien, P.Y. Chen, K.C. Ho, Fabricating an Amperometric Cholesterol Biosensor by a Covalent Linkage between Poly(3-thiopheneacetic acid) and Cholesterol Oxidase, *Sensors* 9(3) (2009) 1794-1806.

[80] S.A. Rothwell, S.J. Killoran, R.D. O'Neill, Enzyme Immobilization Strategies and Electropolymerization Conditions to Control Sensitivity and Selectivity Parameters of a Polymer-Enzyme Composite Glucose Biosensor, *Sensors* 10(7) (2010) 6439-6462.

[81] M.M. Rhemrev-Boom, M.A. Jonker, K. Venema, G. Jobst, R. Tiessena, J. Korf, On-line continuous monitoring of glucose or lactate by ultraslow microdialysis combined with a flow-through nanoliter biosensor based on poly(m-phenylenediamine) ultra-thin polymer membrane as enzyme electrode, *The Analyst* 126(7) (2001) 1073-9.

[82] I. Losito, E. De Giglio, N. Cioffi, C. Malitesta, Spectroscopic investigation on polymer films obtained by oxidation of o-phenylenediamine on platinum electrodes at different pHs, *Journal of Materials Chemistry* 11(7) (2001) 1812-1817.

[83] J. Yano, Electrochemical and structural studies on soluble and conducting polymer from o-phenylenediamine, *J. Polym. Sci. Pol. Chem.* 33(14) (1995) 2435-2441.

[84] X.G. Li, W. Duan, M.R. Huang, L.N.J. Rodriguez, Electrocopolymerization of meta-phenylenediamine and ortho-phenetidine, *Reactive & Functional Polymers* 62(3) (2005) 261-270.

[85] P.P. Wang, W.J. Dai, L. Ge, M. Yan, S.G. Ge, J.H. Yu, Visible light photoelectrochemical sensor based on Au nanoparticles and molecularly imprinted poly(o-phenylenediamine)-modified TiO₂ nanotubes for specific and sensitive detection chlorpyrifos, *The Analyst* 138(3) (2013) 939-945.

[86] H. Peng, Y.Y. Zhang, J.H. Zhang, Q.J. Xie, L.H. Nie, S.Z. Yao, Development of a thickness shear mode acoustic sensor based on an

electrosynthesized molecularly imprinted polymer using an underivatized amino acid as the template, *The Analyst* 126(2) (2001) 189-194.

[87] Y. Liu, Q.J. Song, L. Wang, Development and characterization of an amperometric sensor for triclosan detection based on electropolymerized molecularly imprinted polymer, *Microchemical Journal* 91(2) (2009) 222-226.

[88] R. Haas, T.L. Rosenberry, Protein denaturation by addition and removal of acetonitrile - application to tryptic digestion of acetylcholinesterase, *Analytical Biochemistry* 224(1) (1995) 425-427.

[89] B. Stockle, D.Y.W. Ng, C. Meier, T. Paust, F. Bischoff, T. Diemant, R.J. Behm, K.E. Gottschalk, U. Ziener, T. Weil, Precise Control of Polydopamine Film Formation by Electropolymerization, *Macromolecular Symposia* 346(1) (2014) 73-81.

[90] Y. Wang, Research progress on a novel conductive polymer-poly(3,4-ethylenedioxythiophene) (PEDOT), *Journal of Physics: Conference Series* 152(1) (2009) 1-10.

[91] A. Lenz, H. Kariis, A. Pohl, P. Persson, L. Ojamae, The electronic structure and reflectivity of PEDOT:PSS from density functional theory, *Chemical Physics* 384(1-3) (2011) 44-51.

[92] F. Jonas, W. Krafft, B. Muys, Poly(3,4-ethylenedioxythiophene) - conductive coatings, technical applications and properties, *Macromolecular Symposia* 100 (1995) 169-173.

[93] L.S. Roman, M.R. Andersson, T. Yohannes, O. Inganas, Photodiode performance and nanostructure of polythiophene/C-60 blends, *Adv. Mater.* 9(15) (1997) 1164-&.

[94] A.C. Arias, M. Granstrom, D.S. Thomas, K. Petritsch, R.H. Friend, Doped conducting-polymer-semiconducting-polymer interfaces: Their use in organic photovoltaic devices, *Physical Review B* 60(3) (1999) 1854-1860.

[95] X.Y. Cui, D.C. Martin, Electrochemical deposition and characterization of poly(3,4-ethylenedioxythiophene) on neural microelectrode arrays, *Sensors and Actuators B-Chemical* 89(1-2) (2003) 92-102.

[96] C.H. Weng, W.M. Yeh, K.C. Ho, G.B. Lee, A microfluidic system utilizing molecularly imprinted polymer films for amperometric detection of morphine, *Sensors and Actuators B-Chemical* 121(2) (2007) 576-582.

[97] C.T. Wu, P.Y. Chen, J.G. Chen, V. Suryanarayanan, K.C. Ho, Detection of nicotine based on molecularly imprinted TiO₂-modified electrodes, *Analytica Chimica Acta* 633(1) (2009) 119-126.

[98] E. Kolodziejczyk, V. Petkova, J.J. Benattar, M.E. Leser, M. Michel, Effect of fluorescent labeling of beta-lactoglobulin on film and interfacial properties in relation to confocal fluorescence microscopy, *Colloids and Surfaces a-Physicochemical and Engineering Aspects* 279(1-3) (2006) 159-166.

[99] C. Gabrielli, M. Keddah, R. Torresi, Calibration of the electrochemical quartz crystal microbalance, *Journal of the Electrochemical Society* 138(9) (1991) 2657-2660.

[100] C.K. O'Sullivan, G.G. Guilbault, Commercial quartz crystal microbalances - theory and applications, *Biosensors & Bioelectronics* 14(8-9) (1999) 663-670.

- [101] J. Rickert, A. Brecht, W. Gopal, QCM operation in liquids: Constant sensitivity during formation of extended protein multilayers by affinity, *Analytical Chemistry* 69(7) (1997) 1441-1448.
- [102] S.M. Chang, H. Muramatsu, C. Nakamura, J. Miyake, The principle and applications of piezoelectric crystal sensors, *Materials Science & Engineering C-Biomimetic and Supramolecular Systems* 12(1-2) (2000) 111-123.
- [103] Y.G. Lee, K.S. Chang, Application of a flow type quartz crystal microbalance immunosensor for real time determination of cattle bovine ephemeral fever virus in liquid, *Talanta* 65(5) (2005) 1335-1342.
- [104] M. Seo, M. Aomi, K. Yoshida, A combined piezoelectric and eqcm study of underpotential deposition of silver on gold electrodes, *Electrochimica Acta* 39(8-9) (1994) 1039-1044.
- [105] M. Benje, M. Eiermann, U. Pittermann, K.G. Weil, An improved quartz microbalance - applications to the electrocrystallization and electro dissolution of nickel, *Berichte Der Bunsen-Gesellschaft-Physical Chemistry Chemical Physics* 90(5) (1986) 435-439.
- [106] K. Niikura, H. Matsuno, Y. Okahata, Direct monitoring of DNA polymerase reactions on a quartz-crystal microbalance, *Journal of the American Chemical Society* 120(33) (1998) 8537-8538.
- [107] R.C. Ebersole, J.A. Miller, J.R. Moran, M.D. Ward, Spontaneously formed functionally active avidin monolayers on metal-surfaces - a strategy for immobilizing biological reagents and design of piezoelectric biosensors, *Journal of the American Chemical Society* 112(8) (1990) 3239-3241.
- [108] F. Caruso, E. Rodda, D.F. Furlong, K. Niikura, Y. Okahata, Quartz crystal microbalance study of DNA immobilization and hybridization for nucleic acid sensor development, *Analytical Chemistry* 69(11) (1997) 2043-2049.
- [109] M. Muratsugu, F. Ohta, Y. Miya, T. Hosokawa, S. Kurosawa, N. Kamo, H. Ikeda, Quartz-crystal microbalance for the detection of microgram quantities of human serum-albumin - relationship between the frequency change and the mass of protein adsorbed, *Analytical Chemistry* 65(20) (1993) 2933-2937.
- [110] F. Hook, J. Voros, M. Rodahl, R. Kurrat, P. Boni, J.J. Ramsden, M. Textor, N.D. Spencer, P. Tengvall, J. Gold, B. Kasemo, A comparative study of protein adsorption on titanium oxide surfaces using in situ ellipsometry, optical waveguide lightmode spectroscopy, and quartz crystal microbalance/dissipation, *Colloids and Surfaces B-Biointerfaces* 24(2) (2002) 155-170.
- [111] M. Tanaka, A. Mochizuki, T. Motomura, K. Shimura, M. Onishi, Y. Okahata, In situ studies on protein adsorption onto a poly(2-methoxyethylacrylate) surface by a quartz crystal microbalance, *Colloids and Surfaces a-Physicochemical and Engineering Aspects* 193(1-3) (2001) 145-152.
- [112] A. Hengerer, C. Kosslinger, J. Decker, S. Hauck, I. Queitsch, H. Wolf, S. Dubel, Determination of phage antibody affinities to antigen by a microbalance sensor system, *Biotechniques* 26(5) (1999) 956-+.
- [113] I.S. Park, W.Y. Kim, N. Kim, Operational characteristics of an antibody-immobilized QCM system detecting *Salmonella* spp, *Biosensors & Bioelectronics* 15(3-4) (2000) 167-172.

- [114] Y.S. Fung, Y.Y. Wong, Self-assembled monolayers as the coating in a quartz piezoelectric crystal immunosensor to detect salmonella in aqueous solution, *Analytical Chemistry* 73(21) (2001) 5302-5309.
- [115] J. Wegener, A. Janshoff, C. Steinem, The quartz crystal microbalance as a novel means to study cell-substrate interactions in situ, *Cell Biochemistry and Biophysics* 34(1) (2001) 121-151.
- [116] A.S. Cans, F. Hook, O. Shupliakov, A.G. Ewing, P.S. Eriksson, L. Brodin, O. Orwar, Measurement of the dynamics of exocytosis and vesicle retrieval at cell populations using a quartz crystal microbalance, *Analytical Chemistry* 73(24) (2001) 5805-5811.
- [117] B. Deore, Z.D. Chen, T. Nagaoka, Potential-induced enantioselective uptake of amino acid into molecularly imprinted overoxidized polypyrrole, *Analytical Chemistry* 72(17) (2000) 3989-3994.
- [118] T.M.A. Gronewold, Surface acoustic wave sensors in the bioanalytical field: Recent trends and challenges, *Analytica Chimica Acta* 603(2) (2007) 119-128.
- [119] Y.L. Rao, G.G. Zhang, Enhancing the sensitivity of SAW sensors with nanostructures, *Current Nanoscience* 2(4) (2006) 311-318.
- [120] F. Martin, M.I. Newton, G. McHale, K.A. Melzak, E. Gizeli, Pulse mode shear horizontal-surface acoustic wave (SH-SAW) system for liquid based sensing applications, *Biosensors & Bioelectronics* 19(6) (2004) 627-632.
- [121] L.A. Francis, J.M. Friedt, P. Bertrand, Influence of electromagnetic interferences on the mass sensitivity of Love mode surface acoustic wave sensors, *Sensors and Actuators a-Physical* 123-24 (2005) 360-369.
- [122] J.X. Cui, J. Iturri, U. Gotz, M. Jimenez, A. del Campo, Analysis of Responsive Polymer Films Using Surface Acoustic Waves, *Langmuir* 29(22) (2013) 6582-6587.
- [123] G. Vasapollo, R. Del Sole, L. Mergola, M.R. Lazzoi, A. Scardino, S. Scorrano, G. Mele, Molecularly Imprinted Polymers: Present and Future Prospective, *International Journal of Molecular Sciences* 12(9) (2011) 5908-5945.
- [124] W. Plazinski, W. Rudzinski, A. Plazinska, Theoretical models of sorption kinetics including a surface reaction mechanism: A review, *Advances in Colloid and Interface Science* 152(1-2) (2009) 2-13.
- [125] Y.S. Ho, Review of second-order models for adsorption systems, *Journal of Hazardous Materials* 136(3) (2006) 681-689.
- [126] X. Li, S.M. Husson, Adsorption of dansylated amino acids on molecularly imprinted surfaces: A surface plasmon resonance study, *Biosensors & Bioelectronics* 22(3) (2006) 336-348.
- [127] R.J. Umpleby, S.C. Baxter, Y.Z. Chen, R.N. Shah, K.D. Shimizu, Characterization of molecularly imprinted polymers with the Langmuir-Freundlich isotherm, *Analytical Chemistry* 73(19) (2001) 4584-4591.
- [128] G.T. Rushton, C.L. Karns, K.D. Shimizu, A critical examination of the use of the Freundlich isotherm in characterizing molecularly imprinted polymers (MLPs), *Analytica Chimica Acta* 528(1) (2005) 107-113.

- [129] A.E. Cho, V. Guallar, B.J. Berne, R. Friesner, Importance of accurate charges in molecular docking: Quantum mechanical/molecular mechanical (QM/MM) approach, *Journal of Computational Chemistry* 26(9) (2005) 915-931.
- [130] QMPL. Schrödinger, LLC, New York, NY, USA.
- [131] W.L. Jorgensen, J. Tiradorives, The Opls Potential Functions for Proteins - Energy Minimizations for Crystals of Cyclic-Peptides and Crambin, *Journal of the American Chemical Society* 110(6) (1988) 1657-1666.
- [132] G.A. Kaminski, R.A. Friesner, J. Tirado-Rives, W.L. Jorgensen, Evaluation and reparametrization of the OPLS-AA force field for proteins via comparison with accurate quantum chemical calculations on peptides, *Journal of Physical Chemistry B* 105(28) (2001) 6474-6487.
- [133] Maestro v10.4. Schrodinger, LLC, New York, NY, USA.
- [134] LigPrep v3.6. Schrodinger, LLC, New York, NY, USA.
- [135] M. Vass, A. Tarcsay, G.M. Keseru, Multiple ligand docking by Glide: implications for virtual second-site screening, *Journal of Computer-Aided Molecular Design* 26(7) (2012) 821-834.
- [136] A.G. Ayankojo, A. Tretjakoy, J. Reut, R. Boroznjak, A. Ouml;pik, J. Rappich, A. Furchner, K. Hinrichs, V. Syritski, Molecularly Imprinted Polymer Integrated with a Surface Acoustic Wave Technique for Detection of Sulfamethizole, *Analytical Chemistry* 88(2) (2016) 1476-1484.
- [137] K.R. Srivastava, A. Kumar, B. Goyal, S. Durani, Stereochemistry and Solvent Role in Protein Folding: Nuclear Magnetic Resonance and Molecular Dynamics Studies of Poly-L and Alternating-L,D Homopolypeptides in Dimethyl Sulfoxide, *Journal of Physical Chemistry B* 115(20) (2011) 6700-6708.
- [138] I. Chernov, H. Greb, U. Janssen-Bienhold, J. Parisi, R. Weiler, E. von Hauff, Binding and potential-triggered release of L-glutamate with molecularly imprinted polypyrrole in neutral pH solutions, *Sensors and Actuators B-Chemical* 203 (2014) 327-332.
- [139] V. Ratautaite, D. Plausinaitis, I. Baleviciute, L. Mikoliunaite, A. Ramanaviciene, A. Ramanavicius, Characterization of caffeine-imprinted polypyrrole by a quartz crystal microbalance and electrochemical impedance spectroscopy, *Sensors and Actuators B-Chemical* 212 (2015) 63-71.

APPENDIX A

PAPER I

R. Boroznjak, A. Lomaka, A. Tretjakov, V. Syritski, J. Reut, A. Öpik, A Computational Approach to Study Functional Monomer-Protein Molecular Interactions to Optimize Protein Molecular Imprinting. Accepted for publication in *Journal of Molecular Recognition*, 2017, DOI: 10.1002/jmr.2635.

RESEARCH ARTICLE

A computational approach to study functional monomer-protein molecular interactions to optimize protein molecular imprinting

R. Boroznjak¹ | J. Reut¹ | A. Tretjakov¹ | A. Lomaka² | A. Öpik¹ | V. Syritski¹ 

¹Department of Materials and Environmental Technology, Tallinn University of Technology, Tallinn, Estonia

²Department of Chemistry and Biotechnology, Tallinn University of Technology, Tallinn, Estonia

Correspondence

Vitali Syritski, Department of Materials and Environmental Technology, Tallinn University of Technology, Ehitajate tee 5, 19086 Tallinn, Estonia.

Email: vitali.syritski@ttu.ee

Funding Information

Eesti Teadusagentuur, Grant/Award Number: PUT150

Abstract

Molecular imprinting has become a promising approach for synthesis of polymeric materials having binding sites with a predetermined selectivity for a given analyte, the so-called molecularly imprinted polymers (MIPs), which can be used as artificial receptors in various application fields. Realization of binding sites in a MIP involves the formation of prepolymerization complexes between a template molecule and monomers, their subsequent polymerization, and the removal of the template. It is believed that the strength of the monomer-template interactions in the prepolymerization mixture influences directly on the quality of the binding sites in a MIP and consequently on its performance. In this study, a computational approach allowing the rational selection of an appropriate monomer for building a MIP capable of selectively rebinding macromolecular analytes has been developed. Molecular docking combined with quantum chemical calculations was used for modeling and comparing molecular interactions among a model macromolecular template, immunoglobulin G (IgG), and 1 of 3 electropolymerizable functional monomers: m-phenylenediamine (mPD), dopamine, and 3,4-ethylenedioxythiophene, as well as to predict the probable arrangement of multiple monomers around the protein. It was revealed that mPD was arranged more uniformly around IgG participating in multiple H-bond interactions with its polar residues and, therefore, could be considered as more advantageous for synthesis of a MIP for IgG recognition (IgG-MIP). These theoretical predictions were verified by the experimental results and found to be in good agreement showing higher binding affinity of the mPD-based IgG-MIP toward IgG as compared with the IgG-MIPs generated from the other 2 monomers.

KEYWORDS

computational approach, IgG, molecular docking, molecularly imprinted polymers, quantum chemical calculations, surface acoustic wave

1 | INTRODUCTION

The principles of molecular recognition, as one of the fundamental mechanisms found in nature, inspire modern molecular engineering science to design synthetic receptors capable of binding various analytes with affinity and selectivity comparable to their biological counterparts. Today, the concept of molecular imprinting is widely recognized as a promising strategy for developing robust molecular recognition materials—the so-called molecularly imprinted polymers (MIPs)—with high specificity toward the analyte.^{1–7} The process of molecular imprinting consists in polymerization of a mixture of

functional monomers around a target molecule that acts as a molecular template (Figure S1). During polymerization, the template induces binding sites in the reticulated polymer that are capable of selectively recognizing the target molecules after removal of the templates from the polymer. Essentially, strategies for molecular imprinting can be grouped on the basis of the type of the monomer-template interaction into a covalent and a noncovalent imprinting approach. The latter is especially applicable when imprinting a macromolecular template.^{8,9} The prerequisite for the formation of selective binding sites in a MIP supposes the presence of noncovalent interactions (self-assembly) such as hydrogen bonds (H-bonds), van der Waals forces, ionic

interactions, and hydrophobic effects in the prepolymerization complex between a template molecule and functional monomers. It is assumed that the choice of functional monomers capable of forming more stable complexes with the template could result in a MIP with a high selectivity and affinity.^{7,10} Thus, performance of the MIP relies first of all on the quantity and strength of preexisting molecular interactions in those complexes before polymerization of the monomers.

The main benefits of MIPs, along with their binding affinities to the target analyte, sometimes comparable to a biological receptor,¹¹ are related to their synthetic nature, ie, robustness and stability under a wide range of chemical and physical conditions, combined with reproducible, cost-effective fabrication. Moreover, MIPs can be easily designed for recognition of an almost unlimited number of targets, even those the biological receptors of which are unavailable. Similarly to biological receptors, the molecular recognition in MIPs is mainly governed by the multiple noncovalent interactions occurring in their binding sites. Consequently, the potential applications of MIPs are related to the areas, where the role of noncovalent interactions is well established.^{7,12-14} A wide variety of review papers can be found focusing on applications of MIPs, including those on the topics of chemical analysis and detection,^{15,16} affinity separation and purification,^{7,17,18} drug delivery,^{19,20} and catalysis.²¹⁻²⁵

In the last few decades, the interest in the field of macromolecular imprinting, resulting in MIPs capable of selective recognition of the specific macromolecules, eg, proteins, viruses, and cells, in a complex medium, has considerably increased because of the great demand in clinical diagnostics and therapies aiming at replacement of expensive and readily degradable biological recognition elements.^{1,8,9,26-28} The presence in a macromolecular template like a protein of a considerable amount of different functional groups creates potential premises for multiple noncovalent interactions (H-bond, van der Waals, electrostatic, and hydrophobic) between the protein and functional monomers in a prepolymerization complex before protein-MIP synthesis. These interactions are then, to some extent, maintained during polymerization and play a crucial role in the formation of complementary binding sites after the template protein removal, thus providing the subsequent selective rebinding of the target protein to the protein-MIP. Consequently, an estimation of all possible noncovalent interactions as well as their strength in the protein-monomer complex should be seriously considered when aiming at designing a protein-MIP with highly selective recognition sites.

Different computational approaches including molecular mechanics, molecular dynamics,²⁹ quantum chemical calculation (QCC),³⁰ and molecular docking (MD) were successfully used for a rational design of MIPs through the prediction, simulation, and estimation of molecular interactions between a template molecule and a monomer in a prepolymerization complex as well as in a polymer matrix.³¹⁻³³ Thus, Piletsky's group created a virtual library of functional monomers, which could be screened by a molecular modeling software against a template molecule of interest aiming at preselecting a group of preferential monomers for the following generation of more selective MIPs.^{34,35} Dong et al calculated energy of H-bond interactions in simulated complexes between a template and a monomer using a QCC (density functional theory). The atoms forming the H-bond interactions between the monomer and template molecules were determined by their

Mulliken charges.³⁶ Maciejewska's group used 3-D alignment methodology to design the structure of the polymerization system by the energy optimization of randomly distributed molecular components. Such a system was able to mimic the formation of the recognition cavities in the polymer matrix as well as its interaction with the various analytes.³⁷ The hybrid quantum-mechanical/molecular mechanical approach for a rational design of MIPs was applied by several authors.^{36,38-41} However, most of these reports describe the computational methods to model complexes of functional monomers with low molecular-weight templates. At the same time, there are very few computational studies on macromolecular MIPs that mostly use the molecular mechanics simulations,⁴² MD,^{43,44} and lattice Monte Carlo simulations.⁴⁵ Among them, MD is the fastest and least resource-consuming computational method to estimate protein-ligand interactions that is widely used in the field of drug design.⁴⁶ This method can also provide reliable predictions of binding poses of a monomer on a protein prior to the polymerization, as well as determination of the types of noncovalent interactions taking place by the set of the amino acids present near this binding pocket.⁴³ At the same time, the possibility of multiple H-bond interactions between a monomer and the accessible proton-acceptor groups of polar amino acid and sugar residues of the protein should also be considered. Quantum chemical calculation method allows assessment of the strength of H-bond interactions occurring between H-bond donor and acceptor⁴⁷; however, its applicability to calculation of protein-ligand interaction is limited because of the size of the system.

The aim of this study was to develop a computational modeling approach allowing the selection of a more favorable functional monomer for building a polymer with macromolecular imprints capable of selectively rebinding protein-sized analytes. Molecular docking was applied to find energetically favorable binding poses of a monomer on a model protein as well as to predict the probable arrangement of multiple monomer molecules around the protein. The MD results were complemented with the QCC allowing estimation of the cumulative strength of multiple H-bond interactions in the prepolymerization complex between the proton-donor groups of monomers and the accessible proton-acceptor groups of the protein to establish further its influence on the performance of the resulting immunoglobulin G-molecularly imprinted polymers (IgG-MIPs). Three electropolymerizable monomers (Figure S2), *m*-phenylenediamine (mPD), dopamine (DA), and 3,4-ethylenedioxythiophene (EDOT), were used as candidates for formation of a MIP matrix and immunoglobulin G (IgG) as a model template protein. The theoretical predictions were validated by the experimental data on IgG rebinding to the IgG-MIPs generated from the candidate monomers.

2 | COMPUTATIONAL APPROACH

2.1 | Molecular docking

The crystal structure of IgG (1HZH) deposited in Protein Data Bank was processed within the Protein Preparation Wizard in Maestro⁴⁸ performing progressive minimizations until the average root mean square deviation of the non-hydrogen atoms reached 0.3 Å. The

structures of the monomers (mPD, EDOT, and DA) were generated in Maestro⁴⁸ and processed within the Ligand Preparation Wizard.⁴⁹ The monomers and the protein were converted to MAE format (Maestro). Molecular docking studies were performed by using the quantum mechanically polarized ligand docking workflow based on Glide⁵⁰⁻⁵² using optimized potentials for liquid simulations–2005 force field.^{53,54} The technique allows for charge polarization of the ligands induced by the protein environment. Quantum mechanically polarized ligand docking improves the partial charges on the ligand atoms in Glide docking run by replacing them with charges generated from a quantum-mechanical (QM) calculation on the ligand in the field of the receptor. Initial charges for each ligand were generated with a semiempirical method and were rigidly docked in Glide standard precision mode with van der Waals radii scaled by 0.8. For rigid docking, a rigid receptor grid defined by inner box of $50 \times 50 \times 50 \text{ \AA}^3$ was generated for the different regions of IgG: the Fab region with the center at 94.725, 86.582, and 94.166 Å; the hinge region with the center at 76.565, 111.963, and 136.892 Å; and the Fc region with the center at 53.311, 128.675, and 112.692 Å. The QM charges were calculated using density functional theory at the B3LYP/3-21G level of theory by Jaguar program.⁵⁵ The generated poses from the initial docking stage were subsequently redocked rigidly in Glide standard precision mode by using the calculated QM charges for the ligands. The poses were scored using Glide empirical scoring function, GScore, that approximates the ligand-binding free energy and takes into account a number of parameters like H-bond interactions (Hbond), lipophilic interactions (Lipo), van der Waals (vdW), electrostatic (Coul), polar interactions in the binding site (Site), metal-binding term (Metal), penalty for buried polar group (BuryP), and freezing rotatable bonds (RotB) according to^{52,56} Equation 1:

$$\text{GScore} = 0.065 \cdot \text{vdW} + 0.130 \cdot \text{Coul} + \text{Lipo} + \text{Hbond} + \text{Metal} + \text{BuryP} + \text{RotB} + \text{Site}. \quad (1)$$

It should be noted that GScore already includes the specific term that accounts for the solvation effect.⁵⁶ The monomer, which formed the lowest energy (GScore) docked complex with the selected IgG regions, was considered as more favorable for the formation of an IgG-MIP in terms of its selectivity toward IgG.

To predict the probable arrangement of multiple monomer molecules around the protein, the sequential docking protocol was applied using the same parameters as initial docking; however, each successive docking of the monomer was performed to the complex of IgG and the monomer resulting from the previous docking step.⁵⁷ The sequential docking was repeated until the software was unable to predict a binding pose for the next monomer in the previously simulated protein and monomer complex.

2.2 | Quantum chemical calculations

The aim of QCCs was to estimate the cumulative strength of multiple H-bond interactions in the prepolymerization complex between the multiple monomers and IgG. The sterically accessible proton-acceptor groups in the polar amino acid and sugar residues of IgG were considered as capable of forming such interactions with the proton-donor groups of the monomers. The program RasMol (version 2.7.5.2) was

used to analyze the structure of IgG (1HZH file from Protein Data Bank) aiming at finding the residues and determining their steric accessibility, ie, the distance between the polar oxygen atom in each residue found and the nearest atom of the protein was calculated, and if the distance was greater than the size of the monomer, the found residue was considered as sterically accessible for the given monomer. The strength of H-bond interactions between IgG and the monomers was calculated as a sum of association energies ($\sum \Delta E$) between the amino acid or monosaccharide, associated with the residues found, and the monomer (Equation 2):

$$\sum \Delta E = \sum [E_{X+M} - (E_X + E_M)], \quad (2)$$

where E_{X+M} , E_X , and E_M are the potential energies of the complex (X + M) and its isolated molecular components, the amino acid or monosaccharide (X), and monomer (M), respectively. E_{X+M} , E_X , and E_M were computed by Gaussian 09 at Becke 3-parameter exchange functional combined with gradient-corrected functional of Lee-Yang-Parr (B3LYP) level using the 6-31G basis set. Before the computation, all molecular structures and their complexes were geometrically optimized by the parameterized model number 3 semiempirical method. It is necessary here to clarify that QCCs were performed in vacuum and no solvent effect on the simulated complexes was considered. It is assumed that in the complex of the monomer with the isolated polar residue, the solvent effect would strongly differ from that occurring in the complex with the same residue in the protein chain.

3 | EXPERIMENTAL PART

3.1 | Chemicals

Immunoglobulin G from human serum, 4-aminothiophenol, 2-mercaptoethanol, phosphate buffer saline tablets, sodium chloride, mPD, EDOT, poly(sodium 4-styrenesulfonate), and dimethyl sulfoxide (DMSO) were purchased from Sigma-Aldrich. Dopamine was obtained from Fluka. Sodium hydroxide and hydrochloric acid were purchased from Riedel-de Haën AG. 3,3'-Dithiobis [sulfosuccinimidylpropionate] was purchased from Thermo Fisher Scientific Inc. Glycerol, sulfuric acid, hydrogen peroxide, and ammonium hydroxide were purchased from Lach-Ner, s.r.o. All chemicals were of analytical grade or higher and were used as received without any further purification. Ultrapure water (resistivity, 18.2 MΩ cm at 25°C, EMD Millipore) was used for the preparation of all aqueous solutions. Phosphate buffer saline solution (0.01 M, pH 7.4) was used to prepare synthesis and analyte solutions.

3.2 | IgG-MIP preparation and IgG-rebinding study

Immunoglobulin G-molecularly imprinted polymer films were fabricated directly on the surface acoustic wave (SAW) chips (NanoTemper Technologies GmbH, München, Germany). The IgG-MIP films based on polydopamine (IgG-MI-PDA) and poly(m-phenylenediamine) (IgG-MI-PmPD) were synthesized as described elsewhere.^{58,59} The polymer matrix for the poly(3,4-ethylenedioxythiophene) (PEDOT)-based

IgG-MIP (IgG-MI-PEDOT) was electrodeposited chronocoulometrically at 0.8 V (vs Ag/AgCl/KCl_{sat}) during 21 seconds from 10 mM EDOT/25 mM poly(sodium 4-styrenesulfonate) solution. The synthesis parameters used for electrodeposition of the 11 nm films are provided in the Table S1. To remove the IgG confined in the electrodeposited polymers and form the IgG-MIP, the ethanolic solution of 0.1M 2-mercaptoethanol was applied for 15 minutes with heating in a water bath to cleave 3,3'-dithiobis [sulfosuccinimidylpropionate] disulfide bond. To provide additional stimulus for IgG removal, the IgG-MI-PmPDs were further separately treated in 0.1 M HCl, 0.1 M NaOH, or DMSO with stirring for 15 minutes. To assess the IgG-MIPs in their affinity to IgG molecule, control nonimprinted polymer (NIP) structures were also fabricated using the very same conditions as for the IgG-MIP but excluding the linker cleavage stage by mercaptoethanol. In this case, the NIP films still contained the covalently bound target protein, but had no specific cavities on its surface.

Thus, the SAW chips modified with films of IgG-MI-PmPD, IgG-MI-PmPD(HCl), IgG-MI-PmPD(NaOH), IgG-MI-PmPD(DMSO) and the respective reference, nonimprinted films of NIP, NI-PmPD(HCl), NI-PmPD(NaOH), NI-PmPD(DMSO) were washed thoroughly with ultrapure water and subjected to the rebinding studies using SAW sensor system (SamX, NanoTemper Technologies GmbH, München, Germany) in the previously described manner applying the range of concentrations of IgG (6.4×10^{-5} to 8×10^{-3} mg mL⁻¹) in phosphate buffer saline buffer.⁵⁸ Briefly, the association phase of the sensorgrams was analyzed with the pseudo second-order kinetic equation to determine Q_{eq} (MIP) and Q_{eq} (NIP)—the equilibrium response of the sensors at a particular concentration of IgG for IgG-MIP and the NIP surfaces, respectively. Later, adsorption isotherms were produced using the values of Q_{eq} and fitted to Langmuir-Freundlich binding model to determine the maximum response of the sensors, Q_{max} (MIP) and Q_{max} (NIP), ie, when all binding sites were occupied by IgG on IgG-MIP and the respective NIP surfaces. The imprinting factor (IF), showing the ratio of IgG binding on a MIP to a control NIP, was calculated according to Equation 3:

$$IF = Q_{max}(MIP)/Q_{max}(NIP). \quad (3)$$

To compare performances of IgG-MIP films, formed from the different monomers, only 1 concentration of IgG (53.3 nM) was applied, and IF was calculated according to Equation 4:

$$IF = Q_{eq}(MIP)/Q_{eq}(NIP). \quad (4)$$

The equilibrium dissociation constant values, K_d , were calculated from Equation 5:

$$K_d = k_{off}/k_{on}, \quad (5)$$

where the association and dissociation rate constants, k_{on} and k_{off} , were derived from the analysis of adsorption and desorption processes, respectively, upon injection of 53.3 nM of IgG on IgG-MIPs.

4 | RESULTS AND DISCUSSION

4.1 | Computational approach

The computational modeling approach was used for the rational selection of a more advantageous functional monomer for building a MIP with macromolecular imprints capable of selectively rebinding protein-sized analytes. In this approach, the interactions between IgG, as a model protein, and mPD, DA, and EDOT as functional monomers, in the prepolymerization complex, were modeled separately and, subsequently, to support the validity of the approach, correlated with the performance of the IgG-MIPs prepared from their respective functional monomers (Section 3.2).

The approach was based on using (1) MD of each of the monomers in IgG to determine the energetically favorable binding poses and (2) QCCs to assess the cumulative strength of H-bond interactions between the monomers and the sterically accessible proton-acceptor groups of IgG, such as polar amino acid and sugar residues (Figure 1). This approach might allow a more comprehensive estimation of the association energy arising in a prepolymerization complex between a selected functional monomer and a macromolecular template by taking into consideration all types of the noncovalent interactions occurring in the best-scoring binding poses as well as those involving the sterically accessible proton-acceptor groups of a macromolecule.

By considering the complex structure of IgG and the limitations of the software, MD of the monomers was performed separately to the selected regions of IgG: Fab, Fc, and hinge (Figure S3). The GScore values for the best-scoring binding poses of all 3 monomers docked to the selected regions of IgG were almost similar ranging between -19.54 and -22.38 kJ mol⁻¹, besides EDOT, which demonstrated no interaction with the hinge region (Table 1). This indicates that both mPD and DA are able to form more stable prepolymerization complexes with IgG through the noncovalent interactions and can be considered as more appropriate functional monomers for IgG-MIP fabrication than EDOT. Since the synthesis solution contained the monomer at a high-molar excess over IgG, it was reasonable to expect that there would be far more than one monomer per IgG molecule capable of noncovalent complex formation. Therefore, an attempt to predict a probable arrangement of multiple monomer molecules around IgG was performed by applying the sequential docking protocol. As it can be seen in Figure 2, EDOT and DA are distributed nonuniformly over IgG being preferably concentrated in the Fc (9 molecules of EDOT) and hinge (9 molecules of DA) regions, while mPD tends to be arranged more uniformly (6 molecules—on Fab, 6 molecules—on hinge, and 2 molecules—on Fc regions). Obviously, a more uniform arrangement of mPD around IgG would facilitate formation of a polymer matrix more accurately confining the shape of IgG and, subsequently, resulting in IgG-MI-PmPD having more specific complementary cavities for IgG than those of IgG-MI-PDA and IgG-MI-PEDOT.

At the same time, for a rational selection of a monomer for IgG-MIP design, dozens of possibilities for H-bond interactions occurring between the respective monomers and the protein in the prepolymerization mixture should also be considered. Figure 3 visualizes the positions of the sterically accessible polar O-atoms of the

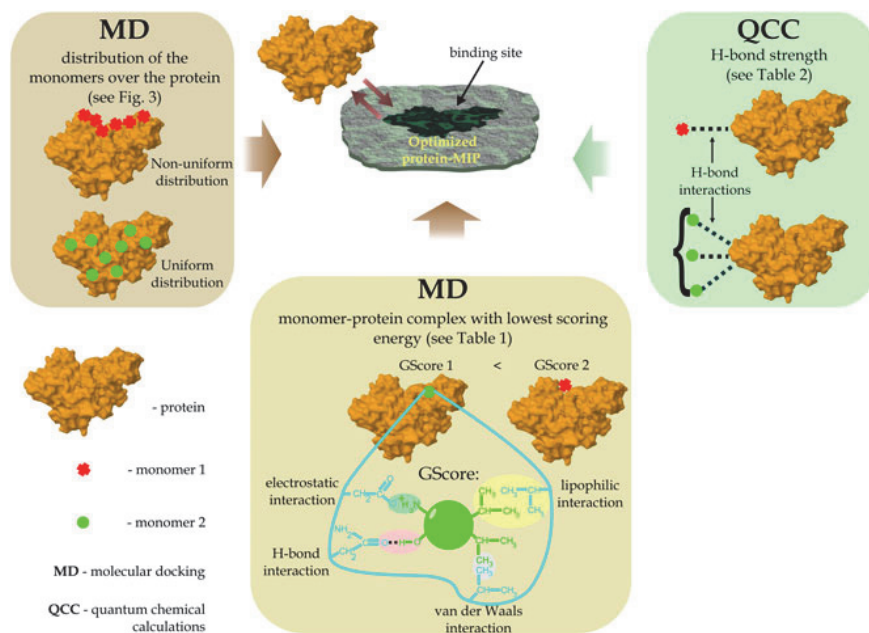


FIGURE 1 A graphical summary of the computational approach to rational selection of a monomer for protein-imprinted film synthesis. GScore indicates Glide empirical scoring function; MD, molecular docking; QCC, quantum chemical calculation

TABLE 1 The GScore values (kJ mol^{-1}) for the best-scoring binding poses of mPD, DA, and EDOT docked to the selected regions of IgG (averaged data from QPLD)

Region of IgG	mPD	DA	EDOT
Fab	-20.01	-20.56	-22.02
Hinge	-19.54	-20.79	No interaction
Fc	-21.17	-22.38	-20.64

Abbreviations: DA, dopamine; EDOT, 3,4-ethylenedioxythiophene; GScore, Glide empirical scoring function; IgG, immunoglobulin G; mPD, m-phenylenediamine; QPLD, quantum mechanically polarized ligand docking.

amino acids and sugars (monosaccharide) in the residues of IgG, which might be engaging in strong H-bond interactions with proton-donor groups of the monomers. O-atoms, which are associated with the amino acids, are uniformly distributed around the protein, while those associated with sugars are predominantly concentrated in the carbohydrate moiety Fc region of IgG.

Since use of QCC for study of protein-ligand interaction is limited because of the size of the system, the calculations were performed for the isolated complexes of the monomer-polar residue, and the results were eventually summarized to represent the total strength of H-bond interactions in the IgG-monomer complex. Although the approach neglects the contribution of the neighboring residues surrounding the polar residue in the polypeptide chain of IgG to the association energy of the isolated complex, the validity of its application has been proved by the additional calculations (Table S2). These calculations show only insignificant or no difference in the association energies of the complexes of monomer-amino acid and monomer-tripeptide

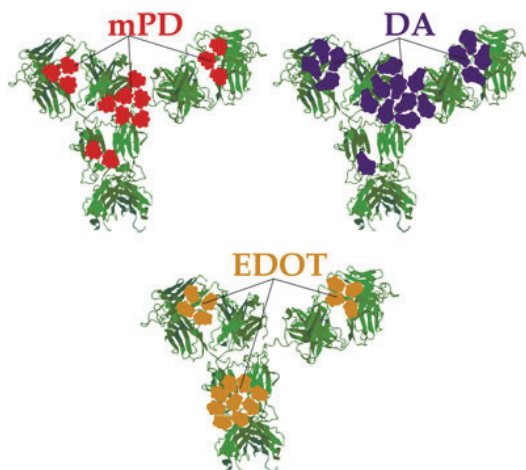


FIGURE 2 The schematic representation of the distribution of the various monomers on IgG as a result of the sequential docking by QPLD. DA indicates dopamine; EDOT, 3,4-ethylenedioxythiophene; IgG, immunoglobulin G; mPD, m-phenylenediamine; QPLD, quantum mechanically polarized ligand docking

comprising polar amino acid joined with 2 neighboring residues on N- and C- terminals.

Table 2 summarizes the association energies (ΔE) of interaction between the polar amino acid or monosaccharide residues of IgG and the different monomers (mPD, DA, and EDOT) as calculated by QCC. The comparison of these values shows that mPD forms the strongest

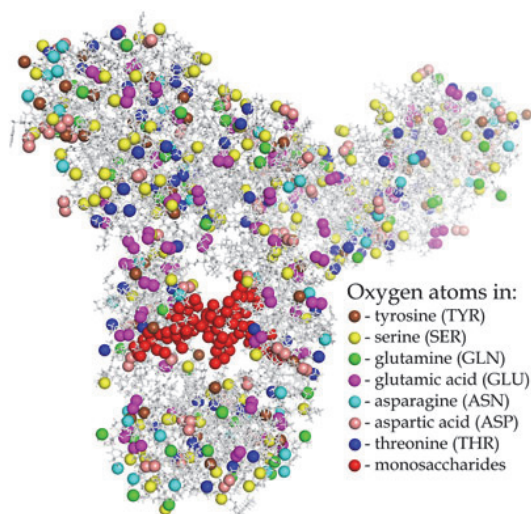


FIGURE 3 Three-dimensional map of the sterically accessible polar residues in immunoglobulin G

network of H-bond interactions around IgG molecule, as compared to the other 2 monomers. Thus, one can expect that the IgG-MI-PmPD might possess stronger H-bonding ability with IgG as compared to

TABLE 2 The association energy of the complexes (ΔE) between polar amino acid or monosaccharide residues of IgG and the monomers (mPD, DA, and EDOT) as estimated by QCC

Polar Residue of IgG	Association Energy (ΔE), kJ mol^{-1}		
	mPD	DA	EDOT
Glu (64 ^a , violet ^b)	1848.32	1680.64	39.38
Tyr (51, brown)	1338.75	803.25	0.53
Ser (146, yellow)	5365.5	383.98	18.38
Gln (54, green)	2126.52	1134	24.94
Asp (51, salmon)	1740.63	267.75	39.38
Asn (50, cyan)	1969	656.5	93.47
Thr (90, blue)	4489.2	1181.7	26.26
Carbohydrate OH (47, red)	617.11	4195.69	17.59
Carbohydrate CO (8, red)	147.04	63.04	—
Carbohydrate O in heterocycle (18, red)	614.34	661.68	—
Carbohydrate O between cycles (16, red)	84	651.04	—
Total ^c ($\sum \Delta E$)	20 340.41	11 679.27	16 449.6

Abbreviations: DA, dopamine; EDOT, 3,4-ethylenedioxythiophene; IgG, immunoglobulin G; mPD, m-phenylenediamine; QCC, quantum chemical calculation.

^aNumber of sterically accessible units in the IgG.

^bSee 3-D map of IgG representing the color-coded positions of the polar residues with the proton-acceptor groups (Figure 3).

^cThe total association energy was taken as the sum of the individual association energies of the sterically accessible residues in IgG. This $\sum \Delta E$ estimates the cumulative strength of H-bond interactions between the monomers and IgG, but neglects solvent effect.

IgG-MI-PEDOT and IgG-MI-PDA. Moreover, the detected presence of multiple H-bond interactions between IgG and the monomer might necessitate the optimization of IgG removal procedure. Thus, a complementary treatment of the polymer with a solvent, which readily dissociates the H-bonds, would facilitate further the release of IgG from the polymer and convert it efficiently into IgG-MIP.

4.2 | Comparison of theoretical predictions of the computational approach with the experimental results

To further support the MD and QCCs results, the PmPD-, PDA-, and PEDOT-based IgG-MIPs and NIPs were synthesized, and their performances were compared. Additionally, the different solvents such as HCl, NaOH, and DMSO were applied separately to elucidate their capability to disrupt the multiple H-bond interactions between IgG and the polymer matrix. Figure 4A graphically represents Q_{max} values

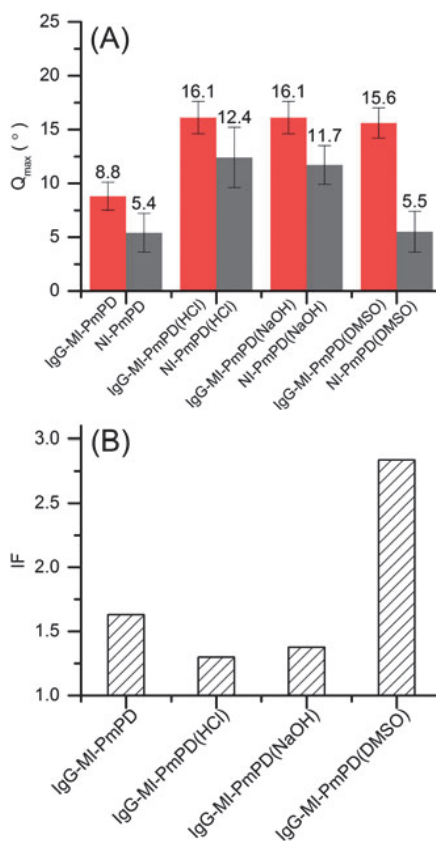


FIGURE 4 A, Q_{max} values derived from the binding isotherms (Figure S4) as measured by surface acoustic wave for the IgG-MI-PmPD NI-PmPD-modified sensor surfaces and for those additionally treated in either HCl, NaOH, or dimethyl sulfoxide (DMSO) (IgG-MI-PmPD(HCl), IgG-MI-PmPD(NaOH), and IgG-MI-PmPD(DMSO)) and for the reference nonimprinted polymer systems (NI-PmPD(HCl), NI-PmPD(NaOH), and NI-PmPD(DMSO)). B, The values of imprinting factors for the respective pairs of immunoglobulin G-molecularly imprinted polymers and nonimprinted polymers as calculated by Equation 3

derived from the binding isotherms (Figure S4) for the IgG-MI-PmPD and the IgG-MIPs undergone such treatments (IgG-MI-PmPD(HCl), IgG-MI-PmPD(NaOH), IgG-MI-PmPD(DMSO)) and for the respective reference NIPs (NI-PmPD(HCl), NI-PmPD(NaOH), NI-PmPD(DMSO)), IgG-MI-PmPD(HCl), IgG-MI-PmPD(NaOH), and IgG-MI-PmPD(DMSO) have rather comparable values of Q_{\max} (approximately 16°) leaving behind IgG-MI-PmPD (approximately 9°). The values of Q_{\max} , however, are considerably different for the corresponding NIPs. The DMSO treatment keeps the nonspecific IgG binding on the NI-PmPD (DMSO) exactly similar to that occurring on the NI-PmPD missing such treatment (5.5° vs 5.4°), while NI-PmPD(HCl) and NI-PmPD(NaOH) tend to display IgG rebinding less distinguished from those on the respective MIPs. This may be rationalized by assuming that HCl and NaOH can equally with DMSO wash out IgG from the polymer matrix

dissociating the H-bond interactions. The respective NIP matrices are, however, irreversibly affected in these solvents, ie, the NIPs, still confining the template molecule, might release it upon the HCl and NaOH treatment probably because of the partial hydrolysis of the protein and become IgG-MIP-like. In the given experiments, DMSO appeared to be an optimal agent assisting IgG removal from the polymer matrix, increasing the number of the complementary cavities, but at the same time treating the NIP gently, making it well suited for the reference purpose, as demonstrated by the highest IF value (2.68) of IgG-MI-PmPD(DMSO) (Figure 4B). Dimethyl sulfoxide, being a polar aprotic solvent that accepts H-bonds to oxygen but lacks polar hydrogens to donate in an H-bond, can act as an H-bond disrupting solvent via the competitive mechanism. It was decided, therefore, to use DMSO in the following experiments, where the PmPD-, PDA-, and PEDOT-based IgG-MIPs/NIPs were synthesized and their Q_{eq} and IF values (Figure 5) upon the single injection of IgG (53.3nM, Figure S5) were compared. In the same way, the IgG-MI-PmPD(DMSO) was given the highest IF value (3.1) that agrees well with the results predicted above by MD and QCCs showing the advantage of mPD as a functional monomer for the synthesis of IgG-MIP (see Section 3.2).

In addition, comparison of the dissociation constants, K_{d} s, derived from binding kinetics might shed light on binding affinity between IgG and the synthesized IgG-MIPs.⁶⁰⁻⁶² The calculated K_{d} values (3.1nM, 4.8nM, and 5.0nM for IgG-MI-PmPD, IgG-MI-PDA, and IgG-MI-PEDOT, respectively) were in consistency with the conclusions above, demonstrating somewhat higher binding affinity of IgG to IgG-MI-PmPD. However, the K_{d} values did not differ enough to justify reliably, which of the polymers provided IgG-MIP having the higher affinity to IgG.

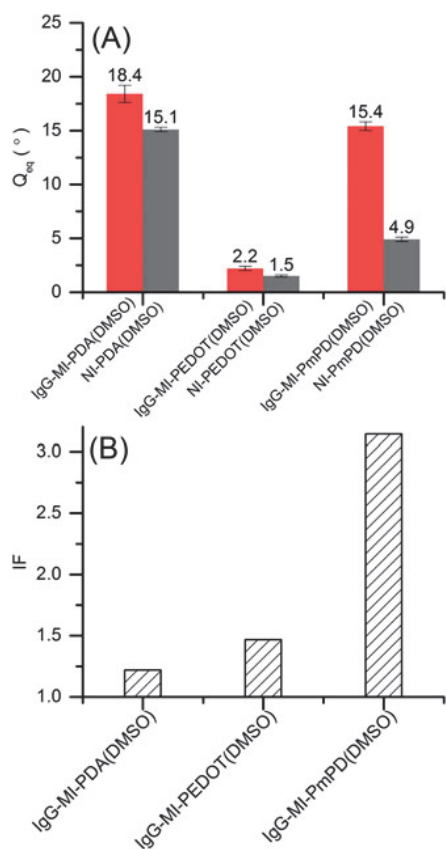


FIGURE 5 A, Q_{eq} values derived from the kinetic analysis of the sensorgram association phase (Figure S5) upon injection of IgG (53.3nM) as measured by surface acoustic wave for the immunoglobulin G-molecularly imprinted polymers (IgG-MI-PDA (DMSO), IgG-MI-PEDOT(DMSO), IgG-MI-PmPD(DMSO)) and for the reference nonimprinted polymer films. The respective films were synthesized from dopamine (DA), 3,4-ethylenedioxythiophene (EDOT), or m-phenylenediamine (mPD) and subjected to the additional DMSO treatment. B, The values of imprinting factors for the respective pairs of immunoglobulin G-molecularly imprinted polymers and nonimprinted polymer films as calculated by Equation 3

5 | CONCLUSIONS

A computational approach based on the combination of MD and QCCs was developed for the rational selection of an optimal monomer for synthesis of a protein-MIP. The optimal binding poses of the monomer on the different regions of IgG, its distribution over IgG molecule, and energies of noncovalent interactions were estimated using MD. Although all 3 studied monomers demonstrated almost similar GScore values ranging between -19.54 and -22.38 kJ mol⁻¹, mPD molecules were found to be arranged more uniformly around IgG as compared to DA and EDOT. Additionally, the comparison of the association energies (ΔE) of interaction between the polar amino acid or monosaccharide residues of IgG and the different monomers calculated by QCC showed that mPD formed the strongest network of H-bond interactions around IgG molecule, versus the other 2 monomers that further justified the selection of mPD as an optimal monomer for the synthesis of IgG-MIP. The complementary treatments, used to extend the removal of the templates from the polymer matrix, revealed that among the solvents, NaOH, HCl, and DMSO, the latter was found to be a more suitable solvent to disrupt the multiple H-bond interactions between IgG and the polymer matrix, while minimally affecting the binding properties of the control polymer (NIP). The results of the computational studies were in good agreement with the experiments revealing the higher IgG-specific binding to IgG-MI-PmPD (IF = 3.1) as compared to IgG-MI-PDA (IF = 1.2) and IgG-MI-PEDOT (IF = 1.5).

ACKNOWLEDGEMENTS

This work was supported by the Estonian Research Council grant (PUT150). The authors acknowledge Schrödinger Inc for providing trial license software used for MD simulation presented in the manuscript.

REFERENCES

- Alexander C, Andersson HS, Andersson LI, et al. Molecular imprinting science and technology: a survey of the literature for the years up to and including 2003. *J Mol Recognit*. 2006;19(2):106-180. <https://doi.org/10.1002/jmr.760>
- Cai D, Ren L, Zhao HZ, et al. A molecular-imprint nanosensor for ultra-sensitive detection of proteins. *Nat Nanotechnol*. 2010;5(8):597-601. <https://doi.org/10.1038/nnano.2010.114>
- Haupt K. Biomaterials: plastic antibodies. *Nat Mater*. 2010;9(8):612-614.
- Mahon CS, Fulton DA. Mimicking nature with synthetic macromolecules capable of recognition. *Nat Chem*. 2014;6(8):665-672. <https://doi.org/10.1038/nchem.1994>
- Mosbach K, Ramstrom O. The emerging technique of molecular imprinting and its future impact on biotechnology. *Biotechnology*. 1996;14(2):163-170. <https://doi.org/10.1038/nbt0296-163>
- Ye L, Haupt K. Molecularly imprinted polymers as antibody and receptor mimics for assays, sensors and drug discovery. *Anal Bioanal Chem*. 2004;378(8):1887-1897. <https://doi.org/10.1007/s00216-003-2450-8>
- Zhang HQ, Ye L, Mosbach K. Non-covalent molecular imprinting with emphasis on its application in separation and drug development. *J Mol Recognit*. 2006;19(4):248-259. <https://doi.org/10.1002/jmr.793>
- Kryscio DR, Peppas NA. Critical review and perspective of macromolecularly imprinted polymers. *Acta Biomater*. 2012;8(2):461-473. <https://doi.org/10.1016/j.actbio.2011.11.005>
- Whitcombe MJ, Chianella I, Larcombe L, et al. The rational development of molecularly imprinted polymer-based sensors for protein detection. *Chem Soc Rev*. 2011;40(3):1547-1571. <https://doi.org/10.1039/c0cs00049c>
- Karim K, Breton F, Rouillon R, et al. How to find effective functional monomers for effective molecularly imprinted polymers? *Adv Drug Deliv Rev*. 2005;57(12):1795-1808. <https://doi.org/10.1016/j.addr.2005.07.013>
- Hoshino Y, Kodama T, Okahata Y, Shea KJ. Peptide imprinted polymer nanoparticles: a plastic antibody. *J Am Chem Soc*. 2008;130(46):15242+. <https://doi.org/10.1021/ja8062875>
- Ukmar T, Gaberscek M, Merzel F, Godec A. Modus operandi of controlled release from mesoporous matrices: a theoretical perspective. *Phys Chem Chem Phys*. 2011;13(33):15311-15317. <https://doi.org/10.1039/c1cp20636b>
- Ukmar T, Maver U, Planinsek O, Kaucic V, Gaberscek M, Godec A. Understanding controlled drug release from mesoporous silicates: theory and experiment. *J Control Release*. 2011;155(3):409-417. <https://doi.org/10.1016/j.jconrel.2011.06.038>
- Wheeler SE, Seguin TJ, Guan YF, Doney AC. Noncovalent interactions in organocatalysis and the prospect of computational catalyst design. *Acc Chem Res*. 2016;49(5):1061-1069. <https://doi.org/10.1021/acs.accounts.6b00096>
- Holthoff EL, Bright FV. Molecularly templated materials in chemical sensing. *Anal Chim Acta*. 2007;594(2):147-161. <https://doi.org/10.1016/j.aca.2007.05.044>
- Uzun L, Turner AP. Molecularly-imprinted polymer sensors: realising their potential. *Biosens Bioelectron*. 2016;76131-76144. <https://doi.org/10.1016/j.bios.2015.07.013>
- Cheong WJ, Yang SH, Ali F. Molecular imprinted polymers for separation science: a review of reviews. *J Sep Sci*. 2013;36(3):609-628. <https://doi.org/10.1002/jssc.201200784>
- Tamayo FG, Turiel E, Martin-Esteban A. Molecularly imprinted polymers for solid-phase extraction and solid-phase microextraction: recent developments and future trends. *J Chromatogr A*. 2007;1152(1-2):32-40. <https://doi.org/10.1016/j.chroma.2006.08.095>
- Alvarez-Lorenzo C, Concheiro A. Molecularly imprinted polymers for drug delivery. *J Chromatogr B*. 2004;804(1):231-245. <https://doi.org/10.1016/j.jchromb.2003.12.032>
- Puoci F, Cirillo G, Curcio M, Parisi OI, lemma F, Picci N. Molecularly imprinted polymers in drug delivery: state of art and future perspectives. *Expert Opin Drug Deliv*. 2011;8(10):1379-1393. <https://doi.org/10.1517/17425247.2011.609166>
- Kan XW, Zhao Q, Shao DL, Geng Z, Wang ZL, Zhu JJ. Preparation and recognition properties of bovine hemoglobin magnetic molecularly imprinted polymers. *J Phys Chem B*. 2010;114(11):3999-4004. <https://doi.org/10.1021/jp910060c>
- Kirsch N, Hedin-Dahlstrom J, Henschel H, Whitcombe MJ, Wikman S, Nicholls IA. Molecularly imprinted polymer catalysis of a Diels-Alder reaction. *J Mol Catal B-Enzym*. 2009;58(1-4):110-117. <https://doi.org/10.1016/j.molcatb.2008.12.002>
- Li SJ, Ge Y, Turner AP. A catalytic and positively thermosensitive molecularly imprinted polymer. *Adv Funct Mater*. 2011;21(6):1194-1200. <https://doi.org/10.1002/adfm.201001906>
- Tong KJ, Xiao S, Li SJ, Wang J. Molecular recognition and catalysis by molecularly imprinted polymer catalysts: thermodynamic and kinetic surveys on the specific behaviors. *J Inorg Organomet Polym Mater*. 2008;18(3):426-433. <https://doi.org/10.1007/s10904-008-9217-9>
- Wulff G, Liu JQ. Design of biomimetic catalysts by molecular imprinting in synthetic polymers: the role of transition state stabilization. *Acc Chem Res*. 2012;45(2):239-247. <https://doi.org/10.1021/ar200146m>
- Li SJ, Cao SS, Whitcombe MJ, Piletsky SA. Size matters: challenges in imprinting macromolecules. *Prog Polym Sci*. 2014;39(1):145-163. <https://doi.org/10.1016/j.progpolymsci.2013.10.002>
- Menger M, Yarman A, Erdosy J, Yildiz HB, Gyurcsanyi RE, Scheller FW. MIPs and aptamers for recognition of proteins in biomimetic sensing. *Biosensors-Basel*. 2016;6(3):35. <https://doi.org/10.3390/bios6030035>
- Zhang HQ. Water-compatible molecularly imprinted polymers: promising synthetic substitutes for biological receptors. *Polymer*. 2014;55(3):699-714. <https://doi.org/10.1016/j.polymer.2013.12.064>
- Olsson GD, Niedergall K, Bach M, Karlsson BCG, Tovar G, Nicholls IA. Simulation of imprinted emulsion prepolymerization mixtures. *Polym J*. 2015;47(12):827-830. <https://doi.org/10.1038/pj.2015.63>
- Azimi A, Javanbakht M. Computational prediction and experimental selectivity coefficients for hydroxyzine and cetirizine molecularly imprinted polymer based potentiometric sensors. *Anal Chim Acta*. 2014;812184-812190. <https://doi.org/10.1016/j.aca.2013.12.042>
- Cowen T, Karim K, Piletsky S. Computational approaches in the design of synthetic receptors—a review. *Anal Chim Acta*. 2016;93662-93674. <https://doi.org/10.1016/j.aca.2016.07.027>
- Subrahmanyam S, Guerreiro A, Poma A, Moczko E, Piletska E, Piletsky S. Optimisation of experimental conditions for synthesis of high affinity MIP nanoparticles. *Eur Polym J*. 2013;49(1):100-105. <https://doi.org/10.1016/j.eurpolymj.2012.09.022>
- Subrahmanyam S, Karim K, Piletsky S. Computational Approaches in the Design of Synthetic Receptors. In: S.A. Piletsky and M.J. Whitcombe, ed. *Designing Receptors for the Next Generation of Biosensors*. Berlin, Heidelberg: Springer Berlin Heidelberg; 2013:131-165. <https://doi.org/10.1007/978-3-642-20122-22>
- Piletsky SA, Karim K, Piletska EV, et al. Recognition of ephedrine enantiomers by molecularly imprinted polymers designed using a computational approach. *Analyst*. 2001;126(10):1826-1830. <https://doi.org/10.1039/b102426b>
- Piletsky SA, Piletska EV, Karim K, Foster G, Legge C, Turner AP. Custom synthesis of molecular imprinted polymers for biotechnological application—preparation of a polymer selective for tylosin. *Anal Chim Acta*. 2004;504(1):123-130. [https://doi.org/10.1016/s0003-2670\(03\)00814-6](https://doi.org/10.1016/s0003-2670(03)00814-6)

36. Dong CK, Li X, Guo ZC, Qi JY. Development of a model for the rational design of molecular imprinted polymer: computational approach for combined molecular dynamics/quantum mechanics calculations. *Anal Chim Acta*. 2009;647(1):117-124. <https://doi.org/10.1016/j.aca.2009.05.040>
37. Sobiech M, Zolek T, Lulinski P, Maciejewska D. A computational exploration of imprinted polymer affinity based on voriconazole metabolites. *Analyst*. 2014;139(7):1779-1788. <https://doi.org/10.1039/c3an01721d>
38. Barkaline VV, Douhaya YV, Tsakalof A. Computer simulation based selection of optimal monomer for imprinting of tri-O-acetyladenosine in polymer matrix: vacuum calculations. *J Mol Model*. 2013;19(1):359-369. <https://doi.org/10.1007/s00894-012-1561-6>
39. Dong WG, Yan M, Zhang ML, Liu Z, Li YM. A computational and experimental investigation of the interaction between the template molecule and the functional monomer used in the molecularly imprinted polymer. *Anal Chim Acta*. 2005;542(2):186-192. <https://doi.org/10.1016/j.aca.2005.03.032>
40. Liu Y, Wang F, Tan TW, Lei M. Study of the properties of molecularly imprinted polymers by computational and conformational analysis. *Anal Chim Acta*. 2007;581(1):137-146. <https://doi.org/10.1016/j.aca.2006.08.015>
41. Monti S, Cappelli C, Bronco S, Giusti P, Ciardelli G. Towards the design of highly selective recognition sites into molecular imprinting polymers: a computational approach. *Biosens Bioelectron*. 2006;22(1):153-163. <https://doi.org/10.1016/j.bios.2006.05.017>
42. Hsu CY, Lin HY, Thomas JL, Wu BT, Chou TC. Incorporation of styrene enhances recognition of ribonuclease A by molecularly imprinted polymers. *Biosens Bioelectron*. 2006;22(3):355-363. <https://doi.org/10.1016/j.bios.2006.05.008>
43. Kryscio DR, Shi Y, Ren PY, Peppas NA. Molecular docking simulations for macromolecularly imprinted polymers. *Ind Eng Chem Res*. 2011;50(24):13877-13884. <https://doi.org/10.1021/ie201858n>
44. Pan J, Xue XH, Wang JH, Me HM, Wu ZY. Recognition property and preparation of *Staphylococcus aureus* protein A-imprinted polyacrylamide polymers by inverse-phase suspension and bulk polymerization. *Polymer*. 2009;50(11):2365-2372. <https://doi.org/10.1016/j.polymer.2009.04.004>
45. Levi L, Srebnik S. Simulation of protein-imprinted polymers. 1. Imprinted pore properties. *J Phys Chem B*. 2010;114(1):107-114. <https://doi.org/10.1021/jp9087767>
46. Unzue A, Lafleur K, Zhao HT, et al. Three stories on Eph kinase inhibitors: from in silico discovery to in vivo validation. *Eur J Med Chem*. 2016;112347-112366. <https://doi.org/10.1016/j.ejmech.2016.01.057>
47. Hao MH. Theoretical calculation of hydrogen-bonding strength for drug molecules. *J Chem Theory Comput*. 2006;2(3):863-872. <https://doi.org/10.1021/ct0600262>
48. *Maestro v10.4*. Schrodinger. New York, NY, USA: LLC; 2016.
49. *LigPrep v3.6*. Schrodinger. New York, NY, USA: LLC; 2015.
50. *QMPL*. Schrodinger. New York, NY, USA: LLC; 2015.
51. Cho AE, Guallar V, Berne BJ, Friesner R. Importance of accurate charges in molecular docking: quantum mechanical/molecular mechanical (QM/MM) approach. *J Comput Chem*. 2005;26(9):915-931. <https://doi.org/10.1002/jcc.20222>
52. Friesner RA, Banks JL, Murphy RB, et al. Glide: a new approach for rapid, accurate docking and scoring. 1. Method and assessment of docking accuracy. *J Med Chem*. 2004;47(7):1739-1749. <https://doi.org/10.1021/jm0306430>
53. Jorgensen WL, Tiradorives J. The OPLS potential functions for proteins—energy minimizations for crystals of cyclic-peptides and crambin. *J Am Chem Soc*. 1988;110(6):1657-1666. <https://doi.org/10.1021/ja00214a001>
54. Kaminski GA, Friesner RA, Tirado-Rives J, Jorgensen WL. Evaluation and reparametrization of the OPLS-AA force field for proteins via comparison with accurate quantum chemical calculations on peptides. *J Phys Chem B*. 2001;105(28):6474-6487. <https://doi.org/10.1021/jp003919d>
55. *Jaguar, Schrödinger*. New York, NY: LLC; 2016.
56. *Glide5.5 User Manual*. 2009.
57. Vass M, Tarcsay A, Keseru GM. Multiple ligand docking by Glide: implications for virtual second-site screening. *J Comput Aided Mol Des*. 2012;26(7):821-834. <https://doi.org/10.1007/s10822-012-9578-6>
58. Tretjakov A, Syritski V, Reut J, Boroznjak R, Opik A. Molecularly imprinted polymer film interfaced with surface acoustic wave technology as a sensing platform for label-free protein detection. *Anal Chim Acta*. 2016;902182-902188. <https://doi.org/10.1016/j.aca.2015.11.004>
59. Tretjakov A, Syritski V, Reut J, Boroznjak R, Volobujeva O, Opik A. Surface molecularly imprinted polydopamine films for recognition of immunoglobulin G. *Microchim Acta*. 2013;180(15-16):1433-1442. <https://doi.org/10.1007/s00604-013-1039-y>
60. Chernov I, Greb H, Janssen-Bienhold U, Parisi J, Weiler R, von Hauff E. Binding and potential-triggered release of L-glutamate with molecularly imprinted polypyrrole in neutral pH solutions. *Sens Actuator B-Chem*. 2014;203327-203332. <https://doi.org/10.1016/j.snb.2014.06.030>
61. Menaker A, Syritski V, Reut J, Opik A, Horvath V, Gyurcsanyi RE. Electrosynthesized surface-imprinted conducting polymer microrods for selective protein recognition. *Adv Mater*. 2009;21(22):2271+. <https://doi.org/10.1002/adma.200803597>
62. Ratautaite V, Plausinaitis D, Baleviciute I, Mikoluniyte L, Ramanaviciene A, Ramanavicius A. Characterization of caffeine-imprinted polypyrrole by a quartz crystal microbalance and electrochemical impedance spectroscopy. *Sens Actuator B-Chem*. 2015;21263-21271. <https://doi.org/10.1016/j.snb.2015.01.109>

SUPPORTING INFORMATION

Additional Supporting Information may be found online in the supporting information tab for this article.

How to cite this article: Boroznjak R, Reut J, Tretjakov A, Lomaka A, Öpik A, Syritski V. A computational approach to study functional monomer-protein molecular interactions to optimize protein molecular imprinting. *J Mol Recognit*. 2017; e2635. <https://doi.org/10.1002/jmr.2635>

PAPER II

A. Tretjakov, V. Syriski, J. Reut, **R. Borožnjak**, O. Volobujeva, A. Öpik, Surface molecularly imprinted polydopamine films for recognition of immunoglobulin G. *Microchim Acta* 2013, 180. 1433-1442, DOI: 10.1007/s00604-013-1039-y.

Surface molecularly imprinted polydopamine films for recognition of immunoglobulin G

Aleksei Tretjakov · Vitali Syritski · Jekaterina Reut · Roman Boroznjak · Olga Volobujeva · Andres Öpik

Received: 5 November 2012 / Accepted: 30 June 2013 / Published online: 14 July 2013
© Springer-Verlag Wien 2013

Abstract We have prepared a surface imprinted polymer (SIP) film for label-free recognition of immunoglobulin G (IgG). The IgG-SIPs were obtained by covalent immobilization of IgG via a cleavable covalent bond and a suitable spacer unit to a gold electrode, followed by electrodeposition of a nm-thin film of polydopamine (PDA). The IgG was then removed by destruction of the cleavable bond so that complementary binding sites were created on the surface of the film. IgG-SIPs with various thicknesses of the PDA films were compared with respect to their affinity to IgG using a quartz crystal microbalance combined with flow injection analysis. The films were also characterized by cyclic voltammetry and scanning electron microscopy. The IgG-SIPs with a film thickness of around 17 nm showed the most pronounced imprinting effect (IF 1.66) and a binding constant of 296 nM.

Keywords Molecularly imprinted polymers · IgG · Polydopamine · EQCM · QCM · FIA · Electrochemical polymerization

Introduction

Today, the concept of molecular imprinting has been widely recognized as a promising strategy for developing robust

molecular recognition materials with high specificity toward the analyte [1]. Molecular imprinting consists in polymerization of a mixture of functional monomers in the presence of a target molecule that acts as a template. During polymerization, the template induces binding sites in the reticulated polymer that are capable to selectively recognize the target molecules or similar structures after removal of the templates from the polymer. The main benefits of these so-called Molecularly Imprinted Polymers (MIPs), are related to their synthetic nature, i.e., excellent chemical and thermal stability associated with reproducible, cost-effective fabrication. Therefore, MIPs have a substantial potential for application in various fields such as chemical analysis and detection [2], separation and purification [3], drug delivery [4], and catalysis [5]. In addition, MIPs have been shown to be a promising alternative to natural biological receptors (e.g. enzymes, DNA, antibodies) in biosensors providing more stable and low-cost recognition elements [1].

However, there remain many unsolved issues in the development of MIP-based biosensors, especially concerning the imprinting of high molecular weight templates, proteins or whole cells. The main drawbacks in protein imprinting including permanent entrapment, poor mass transfer, denaturation, and heterogeneity in binding sites, are commonly attributed to the inherent properties of proteins such as conformational instability, large size, and complexity. Moreover the need of synthesis in aqueous media can present serious difficulties as aqueous solutions significantly reduce the binding strength of the non-covalent template—monomer interactions. The surface imprinting approach resulting in polymer with the imprinted sites situated at or close to the surface—Surface Imprinted Polymers (SIPs)—as well as introducing new biocompatible monomers are promising ways to overcome these difficulties. SIPs have many advantages such as monoclonal binding sites; faster mass transfer and hence stronger

Electronic supplementary material The online version of this article (doi:10.1007/s00604-013-1039-y) contains supplementary material, which is available to authorized users.

A. Tretjakov · V. Syritski (✉) · J. Reut · R. Boroznjak · O. Volobujeva · A. Öpik
Department of Materials Science, Tallinn University of Technology, Ehitajate tee 5, 19086 Tallinn, Estonia
e-mail: syritski@gmail.com

binding capacity as compared to traditional MIPs [6]. SIPs for selective protein recognition were realized by implementing various protocols based on immobilization of a target protein on different support materials acting either as a sacrificial [7], or a transfer material [6]. Li et al. has prepared the SIP nanowires exhibiting highly selective recognition for a variety of template proteins, including albumin, hemoglobin, and cytochrome *c* [8]. Qin et al. demonstrated a possibility to combine surface initiated living-radical polymerization with a protein SIP and prepared the lysozyme-SIP beads capable of separating the template from competitive proteins in a chromatographic column [9]. Sellergren's group introduced hierarchical imprinting to produce MIP particles with surface-confined binding sites for a small molecule of amino acid [10], as well as for peptide [11] and protein [12]. Recently, we have achieved success in the development of surface imprinted poly(3,4-ethylenedioxythiophene) microstructures for avidin specific recognition [13, 14].

Immunoglobulin G (IgG) is the most plentiful class of antibodies present in human serum, and protects organism against bacterial and viral infections. Analyzing the presence of specific IgG molecules in the body fluids can be useful in diagnosing infections or certain illnesses. Despite the numerous successful reports on molecular imprinting of different kinds of proteins, only a few attempts have been made to imprint IgG [12, 15]. The difficulties in producing of the complementary cavities for IgG in a polymer matrix are mainly attributed to the complex Y-shape structure of an antibody molecule as well as the considerable amount of chemically identical groups in one molecule. A significant progress has been recently achieved by Dickert and co-workers who produced artificial antibody replicas by applying IgG-imprinted nanoparticles as templates in a surface imprinting process to generate SIP thin films directly on the sensor electrodes of a quartz crystal microbalance (QCM) [15].

QCM technique is a widely applied for the investigation of biomolecular interactions allowing the real-time analysis of reactions without labeling requirements [16]. Furthermore, a QCM sensor integrated in a FIA system (QCM-FIA) provides the advantage to monitor on-line the binding events of an analyte and could be applied to analysis of specific interactions such as antigen-antibody [17], protein-drug [18] as well as between MIP films and template molecules [19].

Although the significant achievements were reported for preparation of different protein MIPs formats, the use of thin MIP films seems to be preferred for sensing applications. MIP films can be easily integrated with different sensor transducers (e.g. optical, piezoelectric) allowing real-time label-free monitoring of protein binding events. Electrochemical polymerization is one of the prospective approaches for combining a MIP film with a sensor transducer surface. In this method, the conducting surface of a transducer is used as an electrode, where a polymeric film with well controlled thickness can be easily

formed by varying amount of charge passed during the electrodeposition. There are a number of successful reports on the application of the electropolymerization method in molecular imprinting, where various types of polymer were used, such as overoxidized polypyrrole [19], poly(*o*-phenylenediamine) [20], and polydopamine (PDA) [21]. PDA appears to be especially attractive for protein-SIPs formation due to its high hydrophilicity and high biocompatibility as well as the existence of a wide variety of functional groups (amino-, hydroxy-, and π - π bonds), compatibility with aqueous solutions, the possibility to obtain an ultrathin compact polymer film by the controlled self-limiting growth. Until now there are only a few reports on PDA based MIP films and most of them however concern the PDA prepared by chemical or self-polymerization of dopamine at weak alkaline pH [22, 23]. The application of the electrosynthesized PDA based MIP film as a recognition element for the capacitive sensing of nicotine was firstly reported by Liu et al. [21].

The aim of this work was to elaborate a strategy that gives a possibility to create IgG surface imprinted polymer (IgG-SIP) thin films using PDA controlled electrodeposition on QCM sensor electrodes for real-time label-free IgG recognition. The specific rebinding of IgG to the prepared IgG-SIPs was analyzed by QCM-FIA technique. In order to optimize the strategy a series of the IgG-SIPs based on the various thicknesses of PDA films were compared in terms of their affinity to IgG molecule.

Materials and methods

Materials

IgG from human serum, IgA from human serum, 4-aminothiophenol (4-ATP), 2-mercaptoethanol, phosphate buffer saline tablets (PBS), sodium chloride and sodium dodecyl sulfate were obtained from Sigma-Aldrich (<http://www.sigmaaldrich.com>). 3,3'-dithiobis [sulfosuccinimidylpropionate] (DTSSP) was purchased from ThermoFisher Scientific Inc (<http://www.thermoscientific.com>). 4-(2-aminoethyl)benzene-1,2-diol (dopamine) was supplied from Fluka (<http://www.sigmaaldrich.com>). All chemicals were of analytical grade or higher and were used as received without any further purification. Ultrapure Milli-Q water (resistivity 18.2 M Ω · cm, Millipore, USA) was used for preparation of all aqueous solutions. PBS solution (0.01 M, pH 7.4) was prepared by dissolving one tablet in 200 mL of Milli-Q water.

IgG immobilization on the gold electrode surface

The gold electrode of a 5 MHz quartz crystal microbalance (QCM) sensor (Maxtek, Inc.) served as a substrate for IgG immobilization. The electrode was cleaned by immersion in

fresh piranha solution (97 % H₂SO₄:30 % H₂O₂, 3:1 volume ratio) for 10 min and then rinsed abundantly with Milli-Q water. Then the electrode was electrochemically treated in 0.1 M H₂SO₄ by cycling the potential between -0.2 and +1.5 V (vs Ag/AgCl) until the gold oxide formation region of the voltammograms displayed three distinct peaks and successive scans showed minimal to no change. Finally, the electrode was rinsed with distilled water and dried in a nitrogen stream. The modification of the QCM electrode surface with amino-groups was carried out by immersing the cleaned electrode in ethanolic solution of 0.1 M 4-ATP for 1 h to form the self-assembled monolayer, after which the electrode was thoroughly rinsed with ethanol to remove the unreacted thiols. The attachment of DTSSP crosslinker to the 4-ATP- modified electrode was achieved by subsequent incubation in PBS buffer (pH 7.4) containing 10 mM of DTSSP for 30 min followed by rinsing with PBS buffer. Then, 100 μ L of PBS containing 1 mg mL⁻¹ of IgG was dropped onto the modified electrode surface and allowed to react for 30 min, following which the unbound IgG was washed out from the electrode surface by additional rinsing with PBS buffer.

Electrochemical measurements

Gold electrode modification steps were characterized electrochemically by cyclic voltammetry (CV) and electrochemical impedance spectroscopy (EIS). Electrochemical measurements were made in a custom-made 8 mL Teflon electrochemical cell connected with Reference 600 Potentiostat (Gamry Instruments, USA). A conventional three-electrode system was used with QCM sensor electrode as working electrode, a rectangular shaped platinum plate (4 \times 1.5 cm²) as counter electrode, and a Ag/AgCl/KCl_{sat} reference electrode. Also, gold disk electrodes with diameter either 2 mm or 7 mm were used as working electrodes for CV and EIS studies (see experimental details in ESM).

Electrochemical deposition of PDA film

Dopamine electrochemical polymerization on the IgG-modified electrode was monitored by the Electrochemical Quartz Crystal Microbalance (EQCM). EQCM measurements were performed using the QCM100 system (Stanford Research Systems, Inc., Sunnyvale, CA, USA) connected to the Reference 600TM potentiostat (Gamry Instruments, Inc.) and PM 6680B counter (Fluke Corporation) as described [19]. Electropolymerization was carried out on the IgG-modified QCM sensors by cycling the potential between -0.45 and +0.55 V at a scan rate of 50 mV \cdot s⁻¹ in PBS buffer solution containing 5 mM of dopamine until the resonant frequency dropped a designated value. The thickness of the deposited PDA film T_f was believed to be uniform and

estimated from the resonant frequency shift Δf according to the equation Eq. 1:

$$T_f = -\frac{\Delta f}{C_f \cdot \rho} \quad (1)$$

where C_f is the sensitivity factor for a 5 MHz quartz crystal resonator, $C_f=56.6$ Hz cm² μ g⁻¹; the PDA film density ρ is assumed to be 1.2 g cm⁻³ as polyaniline density [24].

After polymer film electrochemical deposition, the electrode was rinsed with distilled water and dried in a nitrogen stream. When not in use, the IgG-PDA modified QCM sensors were stored under nitrogen atmosphere in the refrigerator.

Template protein removal

Removal of the template protein, IgG, from polymeric matrix of the electrodeposited PDA film was carried out in order to create IgG-SIP films. For this purpose the IgG-PDA modified electrode was immersed in 0.1 M solution of 2-mercaptoethanol in ethanol, and heated in water bath up to 100 $^{\circ}$ C. The reaction was maintained under stirring for 15 min. After rinsing with ethanol and distilled water, the electrode was immersed into 3 M NaCl aqueous solution containing 0.1 % sodium dodecyl sulfate and the same parameters of heating were applied. The protein washing out procedure was maintained under stirring for 15 min and repeated twice. Finally, the resulting IgG-SIP sensor was washed thoroughly with distilled water and subjected to protein rebinding studies. To compare the IgG-SIPs in terms of their affinity to IgG molecule, a non-imprinted polymer (NIP) structure was also created. The NIP was formed under very same conditions as the IgG-SIP, excluding protein subsequent removal. In this case the PDA film still contains the target protein, but has no cavities on its surface.

IgG rebinding studies by QCM-FIA technique

Template protein rebinding on the prepared IgG-SIP films modified QCM sensors was studied by a QCM-FIA technique. The analysis was carried out in a QCM-FIA system comprising programmable precision pump (M6, VICI[®] Valco Instruments Company Inc., USA), a motorized six-way port injection valve controlled by a microelectric actuator (C22-3186EH, VICI[®] Valco Instruments Company Inc., USA) and a small volume (150 μ L) axial flow cell attached to the QCM sensor holder (Stanford Research Systems, Inc.) [19]. All elements of the system were connected to a PC and controlled by software written in Labview. A constant flow of degassed PBS buffer solution (pH=7.4) flowed over the sensor at a flow rate of 12 μ L \cdot min⁻¹ until a constant baseline of the QCM sensor resonance frequency was reached. Subsequently, various concentrations of analyte samples (IgG solution in PBS buffer) was injected into the flow stream via an injection loop (250 μ L) and allowed to interact with the IgG-SIP or NIP modified QCM sensor for 2,500 s.

Scanning electron microscopy

Scanning Electron Microscope Zeiss Ultra 55 (Carl Zeiss AG, Germany, Oberkochen) with ultra high resolution imaging was used for the surface investigation of the IgG-SIP and NIP modified as well as bare Au electrodes. A series of images at 100,000 \times magnification were obtained and analyzed.

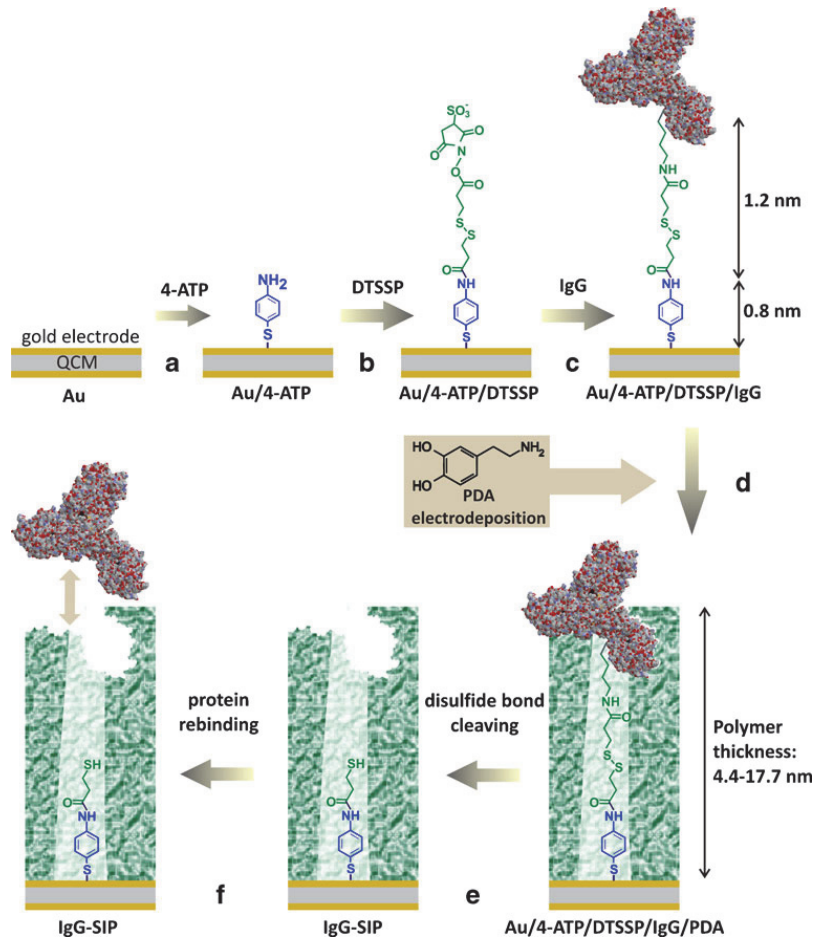
Results and discussion

Strategy for preparation of IgG-SIP thin films

Our approach for an IgG-SIP thin film formation is based on covalent immobilization of the target protein using a cleavable cross-linker to a gold electrode surface followed by electrochemical deposition of a nanometer thin PDA film. Figure 1 sketches

the concept of the strategy and gives theoretically estimated values of attached layers thicknesses. Thus, a gold electrode surface was modified with amino-groups by formation a self-assembled monolayer of 4-ATP (a). Then, a homobifunctional crosslinker with a cleavable disulfide bond and a suitable spacer unit, DTSSP, was attached to the amino-modified surface (b). The target protein was immobilized by the formation of covalent amide bond between succinimide group of DTSSP and amino-group of lysine residues of IgG (c). A polymer matrix was formed by electrochemical polymerization of dopamine around the immobilized IgG (d). It was expected that the multiple non-covalent interactions (hydrogen bonding, van der Waals interactions, electrostatic and hydrophobic) between PDA and IgG molecule ensure the formation of complementary cavities in the growing polymer films. After subsequent removal of the protein by destruction of the DTSSP cleavable bond using 2-mercaptoethanol, and non-covalent bonds by the surfactant

Fig. 1 The strategy for preparation of the IgG-SIP thin films: (a) 4-ATP self-assembled monolayer creation Au electrode (b) attachment of DTSSP cleavable linker (c) IgG covalent immobilization (d) PDA electrodeposition (e) washing out the IgG molecules (f) rebinding of IgG



containing NaCl solution, the complementary binding sites of the target protein confined in the surface of the polymer film were created (e).

In order to choose the appropriate thickness of the electrodeposited PDA layer the length of immobilized structure—4-ATP/DTSSP/IgG—was theoretically estimated. The previously reported AFM and ellipsometry studies indicated a perpendicular orientation of 4-ATP molecules to the metal surface [25], suggesting thus that thickness of a 4-ATP monolayer would be close to the length of the 4-ATP molecule (0.7–0.8 nm). The DTSSP linker has a spacer arm length of 1.2 nm. IgG covalent attachment to a succinimidyl group of the DTSSP proceeds through lysine residues that are abundant in antibody, resulting in random immobilization with multiple orientations of IgG on the surface. Therefore, two limiting cases of antibody possible orientations were considered to estimate the size of the immobilized IgG by RasMol software: “end-on” (Fc fragment closer to the surface) or “head-on” (Fab fragment closer to the surface) orientations with the size approx. 18 nm and “side-on” orientation (Fc and one of the Fabs closer to the surface while another Fab is away from the surface) with size approx. 8.5 nm. Thus, the theoretically estimated height of the whole immobilized structure can vary from approx. 10.5 to 20 nm. The choice for the range of thicknesses of the electrodeposited PDA film needed to achieve surface imprinting of the target protein is determined, from one side, by the linker system length, and, from the other side, by the height of the whole immobilized structure. In this work the polymer films with thicknesses ranging from 4.4 to 22.1 nm (Fig. 1d) were applied in order to evaluate the different extent of polymer coverage on the IgG-modified surface.

IgG immobilization on the gold electrode surface. Cyclic voltammetry and electrochemical impedance spectroscopy studies

IgG immobilization on the QCM gold electrode was accomplished by a multistep procedure including electrode modification with 4-ATP self-assembled monolayer, DTSSP crosslinker attachment, and finally antibody covalent immobilization. CV and EIS techniques were employed to evaluate the changes of gold electrode electrochemical behavior after each modification step. It was already shown that CV and EIS techniques are effective methods for testing the blocking ability towards the electron transfer reactions across a surface modified electrode/electrolyte interface using the ferro/ferri cyanide redox couple as a probe molecule [26].

Figure 2 shows cyclic voltammograms of the Au electrode after the different modification stages. It can be seen that the bare Au electrode (Fig. 2a) shows a reversible peak for the redox couple indicating that the electron transfer reaction is under diffusion-controlled. Reversibility of the reaction at the Au/4-ATP is almost the same as that at the bare Au electrode, indicating that the 4-ATP monolayer exhibits rather poor

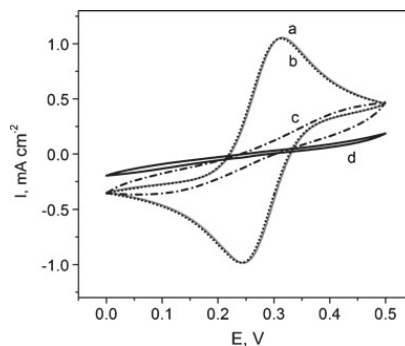


Fig. 2 Cyclic voltammograms of the bare Au (a), 4-ATP (b), 4-ATP/DTSSP (c), and 4-ATP/DTSSP/IgG (d) modified electrodes. The data were recorded in 1 M KCl containing 4 mM $\text{Fe}(\text{CN})_6^{3-/4-}$ at scan rate of $50 \text{ mV} \cdot \text{s}^{-1}$

blocking ability. The poor barrier properties of a 4-ATP monolayer towards the redox reaction were reported earlier [26]. The CV and EIS studies of aromatic thiols SAMs on a gold surface performed by the authors demonstrated that the 4-ATP monolayer is formed with low surface coverage implying the existence of a large number of pinholes and defects within the monolayer. After subsequent attachment of the DTSSP linker to the 4-ATP modified electrode no well-defined current peaks were observed on the voltammogram indicating a significant barrier to a charge-transfer reaction involving the redox couple due to partial surface blocking and thicker layer formation. It is supposed that some DTSSP molecules were disrupted through S-S bond cleavage by contact with uncovered gold surface thus filling the defects of the 4-ATP monolayer and producing so called mixed monolayer, while the intact DTSSP molecules are attached directly to the amino-group of 4-ATP forming the outerlayer intended for IgG binding. When IgG was immobilized through covalent binding between the succinimidyl groups of DTSSP and the amino-groups of the protein, a denser insulating layer is formed on the electrode surface inhibiting more strongly the faradic process as indicates the featureless voltammogram (Fig. 2d).

The EIS spectra (Fig. S1 in the ESM) are in well agreement with the CV measurements, which further confirm the successful immobilization of the IgG via the DTSSP linker on the electrode surface. In spite of significant perturbation to electronic transport at the modified electrode surface, it is evidently not completely blocked, since an electronic current is still observed on the cyclic voltammogram (Fig. 2d). Thus, polymer matrix formation around the immobilized IgG by dopamine electropolymerization is expected to be feasible.

PDA films electrodeposition. Electrochemical QCM study

The PDA films on the 4-ATP/DTSSP/IgG-modified QCM electrodes were formed by electrochemical polymerization of

dopamine in order to provide a more accurate control of polymer film growth. The electrochemical QCM technique was used to simultaneously monitor voltamperometric and gravimetric responses during the polymer growth. Electrochemical QCM has proved to be a valuable in-situ tool to study electropolymerization processes, redox behaviour of electroactive polymers etc., which relates the mass changes during the electrochemical transformations at a QCM electrode to the observed changes in resonant frequency [27]. Considering the theoretical estimations for the range of a polymer bulk needed (Strategy for preparation of IgG-SIP thin films section), the PDA films with thicknesses of 4.4, 8.8, 13.3, 17.7 and 22.1 nm that correspond to the QCM frequency changes of 30, 60, 90, 120 and 150 Hz respectively, were electrodeposited on the 4-ATP/DTSSP/IgG modified QCM sensor electrode. Figure 3 shows a typical resonance frequency response of the QCM during PDA electrodeposition on its electrode. As it can be seen from Fig. 3a the PDA film grows non-linearly demonstrating a faster growth in the beginning of the process, following by its gradual slowing-down until the constant resonant frequency value is reached indicating the self-limiting polymerization. For comparison, the PDA film that is formed on a bare Au electrode, grows significantly faster as shown by Fig. 3b, due to lack of any layer hindering electron transfer at the electrode. In addition, it should be noted that due its insulating nature the PDA film electrochemical growth is self-limited achieving the maximum value of 22 nm in our experimental conditions. The SEM micrographs in Fig. S4 (see ESM) provide additional evidence for the PDA film deposition on the 4-ATP/DTSSP/IgG modified electrode, where this polymer with morphology of uniformly sized agglomerates of fine particles can be seen.

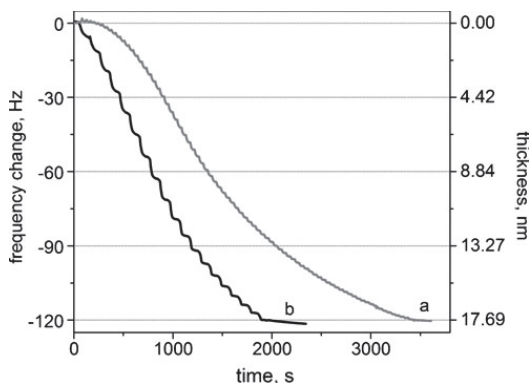


Fig. 3 The resonant frequency responses during dopamine electropolymerization on bare Au (b) and the Au/4-ATP/DTSSP/IgG modified (a) electrodes. The data were recorded with the QCM sensor upon potential cycling between -0.45 and $+0.55$ V at scan rate of $50 \text{ mV} \cdot \text{s}^{-1}$ in a PBS buffer solution containing 5 mM of dopamine

Evaluation of IgG-SIPs films rebinding capability

IgG rebinding capability of the IgG-SIPs prepared with the different PDA film thicknesses was studied by the QCM-FIA technique. To ascertain that the interaction between IgG and the IgG-SIP surface was specific, a control experiment was performed with the NIP modified electrode for each tested PDA film thickness. The sensor-to-sensor reproducibility reported as the relative standard deviation of the resonance frequency changes at saturation ($6.7 \mu\text{M}$ IgG) for the different sensors was 14.5% . Figure 4 shows typical frequency responses of the IgG-SIP and NIP modified QCM sensors with the thickness of PDA film of 8.8 nm upon consecutive injections of the solutions with increasing concentration of IgG in PBS buffer. A frequency drop associated with IgG binding is observed for the IgG-SIP modified QCM sensor already after the injection of $6.4 \cdot 10^{-5} \text{ mg} \cdot \text{mL}^{-1}$ IgG concentration, while the NIP modified sensor shows the non-significant frequency change. With the increasing concentration of IgG the frequency drop becomes more pronounced for both SIP and NIP films but at the same time the noticeably difference between the frequency responses of the IgG-SIP and NIP modified sensors is still observed. The higher rebinding capability of the IgG-SIP is more likely attributed to the presence of the imprint sites on the surface. However, there is also evidence of the significant non-specific adsorption appeared as the considerable frequency decrease recorded by the NIP modified QCM sensor.

Considering the experimental conditions of the QCM-FIA rebinding study, in particular, the low flow rate ($12 \mu\text{L} \cdot \text{min}^{-1}$) and the construction of the axial flow cell, where an injected solution flows about stagnation point, it can be assumed that the adsorption equilibrium is achieved after each successive injection of IgG. Therefore, the adsorption isotherm can be generated by plotting the appropriate accumulated frequency changes that are related to the amount of the bound protein on the Y axis, and the

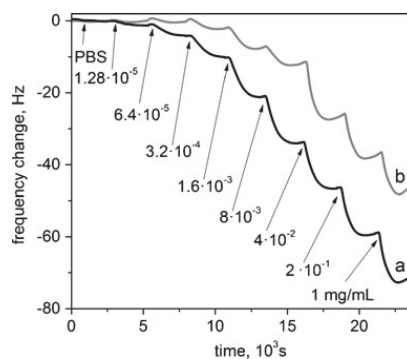


Fig. 4 The resonant frequency response of the IgG-SIP (a) and NIP (b) modified QCM Au electrode. The IgG-SIP and NIP are prepared with PDA film thickness of 8.8 nm . The data were upon successive injections of the different concentrations of IgG in 10 mM PBS buffer

IgG solution concentrations on the X axis (Fig. 5). Adsorption isotherms are useful in understanding the adsorption interaction mechanism of a template with a MIP surface.

A number of different models such as Langmuir [28], bi-Langmuir [29], Freundlich [30] and Freundlich-Langmuir (FL) [31] was used in order to obtain comparable and physically interpretable parameters, which describe the adsorption process. Since most of MIPs have heterogeneous binding sites, the models that account for heterogeneity (Freundlich and FL) should be considered primarily [32]. According to Shimidzu and co-workers [33] FL model (Eq. 2) is more universally applicable in characterizing MIPs

because it can provide heterogeneity information and is able to model adsorption behavior over the entire concentration range up to saturation:

$$B = \frac{B_{\max}(K_{FL}C)^m}{1 + (K_{FL}C)^m} \quad (2)$$

where C is the concentration of a protein in a solution, B and B_{\max} the fraction of bound protein and its saturation value, respectively, m is the heterogeneity index, which varies from 0 to 1 and with values <1 , the material is heterogeneous. K_{FL} is the association constant, which relates to the equilibrium

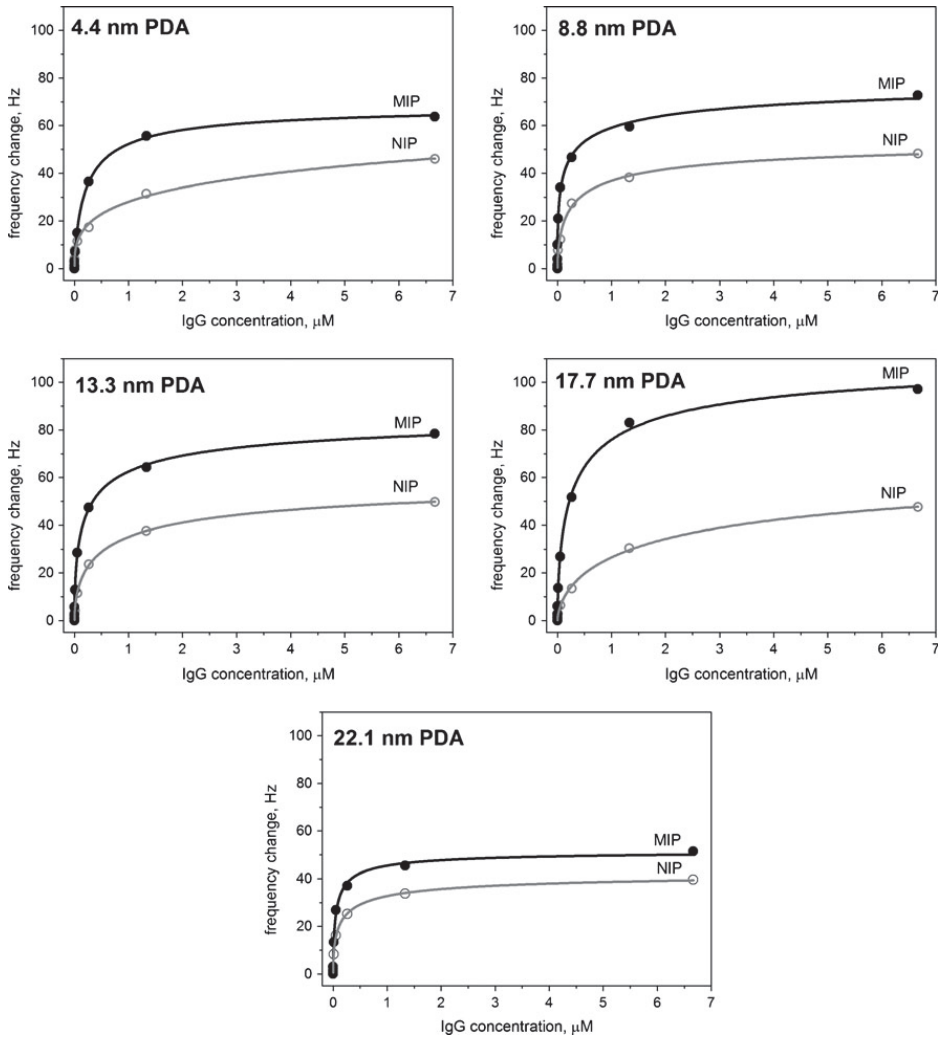


Fig. 5 The IgG adsorption isotherms for the IgG-SIP (*black circle*) and NIP (*hollow circle*) of the PDA various thicknesses. The curves represent fits of the data to Freundlich-Langmuir (FL) isotherm model

Table 1 The fitted binding parameters and corresponding correlation coefficients using the FL isotherm model

PDA thickness, nm	B_{\max} , Hz	m	K_{FL} , L μmol^{-1}	K_D , nmol L $^{-1}$	R^2	IF
IgG-SIP						
4.4	70.1 (2.0)	0.780 (0.049)	4.127 (0.488)	242 (28.6)	0.998	0.89
8.8	82.0 (3.9)	0.457 (0.032)	7.848 (2.239)	127 (36.3)	0.997	1.52
13.3	88.2 (1.8)	0.578 (0.020)	5.374 (0.546)	186 (18.9)	0.999	1.38
17.7	117.0 (4.0)	0.621 (0.035)	3.376 (0.531)	296 (46.6)	0.998	1.66
22.1	52.1 (1.9)	0.676 (0.064)	17.261 (3.277)	57.9 (11.0)	0.995	1.19
NIP						
4.4	78.1 (22.1)	0.459 (0.072)	0.262 (0.329)	3813 (4794)	0.990	–
8.8	53.8 (2.6)	0.621 (0.051)	3.813 (0.865)	262 (59.5)	0.996	–
13.3	64.0 (4.0)	0.566 (0.040)	1.413 (0.393)	708 (197)	0.998	–
17.7	70.3 (3.5)	0.583 (0.021)	0.394 (0.075)	2537 (481)	0.999	–
22.1	43.9 (1.1)	0.567 (0.024)	6.690 (0.843)	149 (18.9)	0.999	–

Values in parentheses are standard errors

dissociation constant (K_D) as $K_{FL}=1/K_D$. In this work K_D was used to assess the affinity of the prepared IgG-SIP film to the template protein. The experimental data of the adsorption isotherms were fitted to the FL model using a nonlinear regression and plotted in both normal and logarithmic forms (Figs. 5 and S5 in ESM for log plot). The fitted parameters are presented in the Table 1. The imprinting factor (IF) was calculated according to the following equation [34]:

$$IF = \frac{B_{\max}(MIP)}{B_{\max}(NIP)} \quad (3)$$

It can be seen from the graphical evaluation that for all tested IgG-SIPs and NIPs the FL model gives an excellent fit, which is confirmed by the high correlation coefficient R^2 values (0.990–0.999). The benefit of using the FL fitting model is also supported by the graphs presented in the log plot of the binding isotherms (Fig. S5 in ESM), which show both the linear regions at the low concentrations and the curvature at the high concentrations [33]. The values of m index in the range of 0.457 to 0.78 indicate that the adsorption sites along the IgG-SIPs and NIPs surface are energetically heterogeneous. Nevertheless, all the IgG-SIPs differing in PDA film thickness show somewhat higher binding capacity compared to the corresponding NIPs, that is most likely caused by the presence of the complementary cavities on the surface of the SIP films due to the imprinting phenomenon. Among the IgG-SIPs prepared with different PDA film thicknesses the most pronounced imprinting effect (IF 1.66) was observed for the IgG-SIP with PDA film of 17.7 nm thick. For this case the value of K_D , which is considered as a measure of IgG affinity toward the SIP, is found to be approximately one order of magnitude higher for the IgG-SIP than that for the corresponding NIP. Probably, at such PDA

film thickness the immobilized IgG molecules are appropriately confined in the polymer and high-affinity binding sites are formed at the polymer surface after the IgG removal procedure. However, binding isotherms observed for the IgG-SIP and NIP pair built-up of the thinnest PDA film (4.4 nm) are clearly inconsistent with the other ones showing the highest difference between the binding affinities of the SIP and NIP while the B_{\max} value of NIP exceeds B_{\max} of MIP giving the IF less than unity. This is perhaps due to the non-uniformity of the ultrathin polymer film that may contain significant number of the uncovered areas on the surface, enhancing thus the non-specific adsorption. On the other hand, the lower value of IF was obtained for the IgG-SIP with PDA film of 22 nm thick compared to the IgG-SIPs with other PDA film thicknesses (excl. 4.4 nm thick PDA). This may be explained by the decreasing of the number of the specific cavities on the surface of the polymer film supporting our hypothesis that the polymer film with thickness exceeding the height of the whole immobilized structure (approx. 18 nm) may entrap the template more rigorously.

A selectivity test for IgG-SIPs as well as IgA-SIP prepared by the described approach was carried out with respect to IgA and IgG. The preliminary study showed (Fig. S6 in the ESM) that the IgG-SIP binds ca. 2 times more IgG than IgA while the IgA-SIP binds ca. 1.5 times more IgA than IgG.

Conclusion

In summary, we have demonstrated a possibility of preparing the SIP thin films for IgG specific recognition based on a covalent immobilization of IgG through a cleavable cross-linker to a gold electrode of a QCM followed by controlled electropolymerization of the monomer to yield an ultrathin

polymeric matrix. The IgG rebinding study performed by the QCM-FIA revealed that the IgG-SIPs built-up of PDA film thickness starting from 8.8 nm and higher demonstrated an apparently enhanced affinity towards IgG when they are compared to the corresponding NIP films. The nanomolar range of K_D , estimated by fitting the adsorption isotherms to FL model, indicated strong polymer-template interaction that was expected to result from the multipoint attachment (multiple non-covalent bonds) of the protein to the polymer matrix. IgG-SIPs prepared with PDA thickness of 17.7 nm showed the most pronounced imprinting effect (IF 1.66) compared to other studied IgG-SIPs as well as the nanomolar range binding affinity (K_D 296 nM). It was concluded that at such PDA film thickness the immobilized IgG molecules were appropriately confined in the polymer and the more specific binding sites were formed at the polymer surface after the subsequent IgG removal procedure. Although further research is required in this field, we believe that the presented strategy offers a great promise for SIP-based biosensor development demonstrating a way for formation of SIP thin films directly on a sensor transducer surface, which in turn enables convenient real-time label-free detection of a target protein.

Acknowledgements This work has been supported by the Estonian Ministry of Education and Research (grant PUT150) and the Estonian Science Foundation (grant ETF8249).

References

- Ye L, Mosbach K (2008) Molecular imprinting: synthetic materials as substitutes for biological antibodies and receptors. *Chem Mater* 20(3):859–868. doi:10.1021/Cm703190w
- Tamayo FG, Turiel E, Martin-Esteban A (2007) Molecularly imprinted polymers for solid-phase extraction and solid-phase microextraction: recent developments and future trends. *J Chromatogr A* 1152(1–2):32–40. doi:10.1016/j.chroma.2006.08.095
- Pichon V, Haupt K (2006) Affinity separations on molecularly imprinted polymers with special emphasis on solid–phase extraction. *J Liq Chromatogr Relat Technol* 29(7–8):989–1023. doi:10.1080/10826070600574739
- Sellergren B, Allender CJ (2005) Molecularly imprinted polymers: a bridge to advanced drug delivery. *Adv Drug Deliv Rev* 57(12):1733–1741. doi:10.1016/j.addr.2005.07.010
- Wulff G (2002) Enzyme-like catalysis by molecularly imprinted polymers. *Chem Rev* 102(1):1–27. doi:10.1021/Cr980039a
- Shi H, Tsai WB, Garrison MD, Ferrari S, Ratner BD (1999) Template-imprinted nanostructured surfaces for protein recognition. *Nature* 398:593–597. doi:10.1038/19267
- Yilmaz E, Haupt K, Mosbach K (2000) The Use of immobilized templates—new approach in molecular imprinting. *Angew Chem Int Ed* 39:2115–2118
- Li Y, Yang HH, You QH, Zhuang ZX, Wang XR (2006) Protein recognition via surface molecularly imprinted polymer nanowires. *Anal Chem* 78:317–320
- Qin L, He X-W, Zhang W, Li W-Y, Zhang Y-K (2009) Surface-modified polystyrene beads as photografting imprinted polymer matrix for chromatographic separation of proteins. *J Chromatogr A* 1216:807–814. doi:10.1016/j.chroma.2008.12.007
- Titirici MM, Hall AJ, Sellergren B (2002) Hierarchically imprinted stationary phases: mesoporous polymer beads containing surface-confined binding sites for adenine. *Chem Mater* 14(1):21–23. doi:10.1021/Cm011207+
- Titirici MM, Sellergren B (2004) Peptide recognition via hierarchical imprinting. *Anal Bioanal Chem* 378:1913–1921. doi:10.1007/s00216-003-2445-5
- Nematollahzadeh A, Sun W, Aureliano CSA, Lutkemeyer D, Stute J, Abdekhodaie MJ, Shojaei A, Sellergren B (2011) High-capacity hierarchically imprinted polymer beads for protein recognition and capture. *Angew Chem Int Ed* 50(2):495–498. doi:10.1002/anie.201004774
- Lautner G, Kaev J, Reut J, Öpik A, Rappich J, Syritski V, Gyurcsányi RE (2011) Selective artificial receptors based on micropatterned surface-imprinted polymers for label-free detection of proteins by SPR imaging. *Adv Funct Mater* 21(3):591–597. doi:10.1002/adfm.201001753
- Menaker A, Syritski V, Reut J, Öpik A, Horváth V, Gyurcsányi RE (2009) Electrosynthesized surface-imprinted conducting polymer microrods for selective protein recognition. *Adv Mater* 21(22):2271–2275. doi:10.1002/adma.200803597
- Schirhagl R, Lieberzeit PA, Blaas D, Dickert FL (2010) Chemosensors for viruses based on artificial immunoglobulin copies. *Adv Mater* 22:2078–2081. doi:10.1002/adma.200903517
- Marx KA (2003) Quartz crystal microbalance: a useful tool for studying thin polymer films and complex biomolecular systems at the solution-surface interface. *Biomacromolecules* 4:1099–1120
- Arce L, Zougagh M, Arce C, Moreno A, Ríos A, Valcárcel M (2007) Self-assembled monolayer-based piezoelectric flow immunosensor for the determination of canine immunoglobulin. *Biosens Bioelectron* 22(12):3217–3223. doi:10.1016/j.bios.2007.02.014
- Zhang Q, Huang Y, Zhao R, Liu G, Chen Y (2008) Determining binding sites of drugs on human serum albumin using FIA-QCM. *Biosens Bioelectron* 24:48–54. doi:10.1016/j.bios.2008.03.009
- Syritski V, Reut J, Menaker A, Gyurcsányi RE, Öpik A (2008) Electrosynthesized molecularly imprinted polypyrrole films for enantioselective recognition of L-aspartic acid. *Electrochim Acta* 53(6):2729–2736. doi:10.1016/j.electacta.2007.10.032
- Malitesta C, Losito I, Zambonin PG (1999) Molecularly imprinted electrosynthesized polymers: new materials for biomimetic sensors. *Anal Chem* 71:1366–1370
- Liu K, Zeng J-X, Wei W-Z, Liu X-Y, Gao Y-P (2006) Application of a novel electrosynthesized polydopamine-imprinted film to the capacitive sensing of nicotine. *Anal Bioanal Chem* 385:724–729. doi:10.1007/s00216-006-0489-z
- Ouyang R, Lei J, Ju H (2008) Surface molecularly imprinted nanowire for protein specific recognition. *Chemical Communications*. 5761–5763. doi:10.1039/b810248a
- Zhou W-H, Tang S-F, Yao Q-H, Chen F-R, Yang H-H, Wang X-R (2010) A quartz crystal microbalance sensor based on mussel-inspired molecularly imprinted polymer. *Biosens Bioelectron* 26:585–589. doi:10.1016/j.bios.2010.07.024
- Orata D, Buttry DA (1987) Determination of ion populations and solvent content as functions of redox state and pH in polyaniline. *J Am Chem Soc* 109(12):3574–3581. doi:10.1021/ja00246a013
- Valério E, Abrantes LM, Viana AS (2008) 4-Aminothiophenol self-assembled monolayer for the development of a DNA biosensor aiming the detection of cylindrospermopsin producing cyanobacteria. *Electroanalysis* 20:2467–2474. doi:10.1002/elan.200804350
- Sabatani E, Cohen-Boulakia J, Bruening M, Rubinstein I (1993) Thioaromatic monolayers on gold: a new family of self-assembling monolayers. *Langmuir* 9:2974–2981
- Buttry DA, Ward MD (1992) Measurement of interfacial processes at electrode surfaces with the electrochemical quartz crystal microbalance. *Chem Rev* 92(6):1355–1379. doi:10.1021/cr00014a006

28. Langmuir I (1918) The adsorption of gases on plane surfaces of glass, mica and platinum. *J Am Chem Soc* 40(9):1361–1403. doi:[10.1021/ja02242a004](https://doi.org/10.1021/ja02242a004)
29. Shea KJ, Spivak DA, Sellergren B (1993) Polymer complements to nucleotide bases—selective binding of adenine-derivatives to imprinted polymers. *J Am Chem Soc* 115(8):3368–3369
30. Freundlich H (1906) Over the adsorption in solution. *Z Phys Chem* 57:385–471
31. Sips R (1948) On the structure of a catalyst surface. *J Chem Phys* 16(5):490–495
32. Umpleby RJ, Baxter SC, Chen YZ, Shah RN, Shimizu KD (2001) Characterization of molecularly imprinted polymers with the Langmuir-Freundlich isotherm. *Anal Chem* 73(19):4584–4591
33. Umpleby RJ, Baxter SC, Rampey AM, Rushton GT, Chen YZ, Shimizu KD (2004) Characterization of the heterogeneous binding site affinity distributions in molecularly imprinted polymers. *J Chromatogr B* 804(1):141–149. doi:[10.1016/j.jchromb.2004.01.064](https://doi.org/10.1016/j.jchromb.2004.01.064)
34. Muhammad T, Nur Z, Piletska EV, Yimit O, Piletsky SA (2012) Rational design of molecularly imprinted polymer: the choice of cross-linker. *Analyst* 137(11):2623–2628

PAPER III

A. Tretjakov, V. Syritski, J. Reut, **R. Boroznjak**, A. Öpik, Molecularly imprinted polymer film interfaced with Surface Acoustic Wave technology as a sensing platform for label-free protein detection. *Anal Chim Acta* 2016, 902. 182-188, DOI: 10.1016/j.aca.2015.11.004.



Molecularly imprinted polymer film interfaced with Surface Acoustic Wave technology as a sensing platform for label-free protein detection



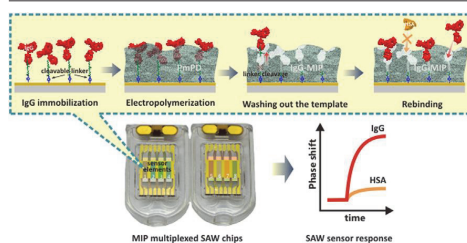
Aleksei Tretjakov, Vitali Syritski*, Jekaterina Reut, Roman Boroznjak, Andres Öpik

Department of Materials Science, Tallinn University of Technology, Ehitajate tee 5, 19086 Tallinn Estonia

HIGHLIGHTS

- A facile integration of protein-MIPs with SAW technology was firstly reported.
- IgG-MIP ultrathin films were interfaced with the multiplexed SAW chips by an electrosynthesis approach.
- The selectivity of IgG-MIP films toward IgG over IgA and HSA was demonstrated.

GRAPHICAL ABSTRACT



ARTICLE INFO

Article history:

Received 18 July 2015

Received in revised form 29 October 2015

Accepted 4 November 2015

Available online 17 November 2015

Keywords:

Molecularly imprinted polymer

Electrochemical polymerization

Immunoglobulin G

Surface acoustic wave

ABSTRACT

Molecularly imprinted polymer (MIP)-based synthetic receptors integrated with Surface Acoustic Wave (SAW) sensing platform were applied for the first time for label-free protein detection. The ultrathin polymeric films with surface imprints of immunoglobulin G (IgG-MIP) were fabricated onto the multiplexed SAW chips using an electrosynthesis approach. The films were characterized by analyzing the binding kinetics recorded by SAW system. It was revealed that the capability of IgG-MIP to specifically recognize the target protein was greatly influenced by the polymer film thickness that could be easily optimized by the amount of the electrical charge consumed during the electrodeposition. The thickness-optimized IgG-MIPs demonstrated imprinting factors towards IgG in the range of 2.8–4, while their recognition efficiencies were about 4 and 10 times lower toward the interfering proteins, IgA and HSA, respectively. Additionally, IgG-MIP preserved its capability to recognize selectively the template after up to four regeneration cycles. The presented approach of the facile integration of the protein-MIP sensing layer with SAW technology allowed observing the real-time binding events of the target protein at relevant sensitivity levels and can be potentially suitable for cost effective fabrication of a biosensor for analysis of biological samples in multiplexed manner.

© 2015 Elsevier B.V. All rights reserved.

1. Introduction

Today label-free detection of proteins has become of extensive demand in fundamental research as well as in clinical practice

providing an alternative to the widely used label-based detection methods that involves laborious, lengthy procedure and can influence the interfacial activity of the resulting protein–label complexes, and consequently the accuracy of measurement results [1]. Label-free detection can be implemented with the help of various transduction mechanisms, including, but not limited to, optical, electrochemical or piezoelectric, where the biochemical interaction between an analyte and a recognition element of the sensor

* Corresponding author.

E-mail address: vitali.syritski@ttu.ee (V. Syritski).

is recorded as a change in e.g., refractive index (SPR sensors), impedance (electrochemical sensors) or resonance frequency (QCM sensors), respectively.

Common recognition elements in biosensors are biomacromolecules such as antibodies, enzymes, or DNA, that can capture target analyte with very high affinity and specificity. However, due to the restricted operating conditions and high production cost of these biological receptors, the development of artificial systems with molecular recognition capability, so-called synthetic receptors, have gained a lot of interest as potential alternatives for biological recognition elements. Among a number of existing techniques for design of synthetic receptors, high expectations are set in the development of molecularly imprinted polymers (MIPs). The technique of molecular imprinting allows the formation of specific molecular recognition sites in highly reticulated polymeric network grown in the presence of analyte molecules, which are subsequently removed leaving behind the analyte specific cavities. MIPs have been shown to possess several advantages as an alternative recognition material for biosensor including low cost, the ease of preparation, storage stability, repeated operations without loss of activity, high mechanical strength, durability to heat and pressure, as well as applicability in harsh chemical media [2,3].

Although synthesis of MIP materials recognizing small molecular weight compounds has proven to be very successful, molecular imprinting of biomacromolecules, in particular proteins, obviously has encountered challenges due their inherent properties such as molecular size, complexity, conformational flexibility, and solubility [4]. Thus, the hindered mass transfer of a large biomolecule in highly reticulated polymeric networks prepared by conventional bulk imprinting leads to their entrapment during imprinting rather than to binding sites permitting free ligand exchange with the sample solution. A number of imprinting strategies were elaborated in order to address the issues associated with protein imprinting [4,5]. The surface imprinting approach leading to the formation of polymer with imprinted sites located at or close to the surface of MIPs, enabling easy access to the target macromolecules, was shown to be a promising way for protein-MIP preparation [6–8].

Many of the reported surface imprinting strategies take advantage of the facile integration of protein-MIP sensing layer with a transducer that is a key aspect in the design of a MIP-based sensor. Thus, the microcontact surface imprinting approach based on photopolymerization has been widely studied to prepare a surface imprinted polymer thin film directly on the surface for selective recognition of C-reactive protein [6], trypsin [9], bovine serum albumin [10]. In another surface imprinting approach, the sol-gel method was combined with a self-assembly technology to prepare a human serum albumin (HSA)-imprinted film on the surface of a QCM [11]. Electrosynthesis has been introduced recently as a convenient strategy for effectively interfacing protein-MIPs with transducers allowing rapid and controlled deposition of polymer films with tunable thickness [7,12–17]. It is worth to mention that in the most of the reported works using protein-MIPs for sensing applications QCM, SPR or electrochemical sensors are preferential choice. Meanwhile, Surface Acoustic Waves (SAW) may provide advances in fabrication of MIP-based sensors over these technologies. Generally, SAW devices share the similar principle of operation as QCMs, but utilize acoustic waves at surfaces rather than in the bulk of a piezoelectric material allowing to increase operating frequencies of SAW devices to the range of 100–500 MHz without compromising in their mechanical fragility. The Love Wave sensor, a special class of the shear-horizontal SAW having the acoustic energy propagation path strictly confined inside of the guiding layer coated onto the top of the sensor. This layer minimizes the energy dissipation losses into environmental media making thus the Love Wave sensors, besides their ex-

tremely high sensitivity towards surface effects, well suited for operation in liquids. Usually, owing to high operation frequencies SAW offers about an order of magnitude higher mass resolution than QCMs, while keeps sensor cost low and at the same time is fully compatible with large-scale fabrication and multiplexing technologies [18,19]. As compared to SPR, SAW technology is not limited to detect only mass loading onto the surface, but also useful to follow structural insights of sensing layers through use of dissipation factor of the acoustic wave propagating along the sensor surface.

Despite of the mentioned advantages, integration of SAW sensors with polymeric synthetic receptor materials has not yet been sufficiently displayed. While SAW gas sensors with a MIP-based recognition layer have been reported [20,21], there is no a report, however, on a sensor of similar type designed for protein selective recognition. To fill this void, here we have integrated the IgG-MIPs with SAW technology by facile electrochemical synthesis approach. The special attention was paid to the careful choice of optimal polymer thickness to prepare IgG-MIP with the improved recognition properties. The binding kinetics were analyzed to differentiate the equilibrium binding capacities and affinities of the targets to IgG-MIP and NIP surfaces. The regeneration, and thus reusability of the IgG-MIP-modified SAW chips after the repeated regeneration cycles was also examined.

2. Experimental

2.1. Chemicals and materials

IgG from human serum, IgA from human serum, HSA from human serum, 4-aminothiophenol (4-ATP), *m*-phenylenediamine (mPD), 2-mercaptoethanol, phosphate buffer saline (PBS) tablets, sodium chloride were obtained from Sigma-Aldrich. 3,3'-dithiobis[sulfosuccinimidylpropionate] (DTSSP) was purchased from ThermoFisher Scientific Inc. All chemicals were of analytical grade or higher and were used as received without any further purification. Ultrapure water (resistivity 18.2 M Ω cm, Millipore, USA) was used for preparation of all aqueous solutions. Phosphate buffered saline (PBS) solution (0.01 M, pH 7.4) was used to prepare synthesis and analyte solutions.

2.2. IgG-MIP film preparation

IgG-MIP films were fabricated directly on Love Wave-configured SAW chips (NanoTemper Technologies GmbH, München, Germany) according to the previously developed procedure (Fig. 1) [14]. The procedure was undergone some modifications with intention to improve analytical performance of the resulting films. In brief, the gold sensing surface of SAW chip consisting of four sensor elements was preliminary cleaned by a fresh base piranha solution (25% NH₄OH:30% H₂O₂:H₂O, 1:1:5 volume ratio) for 15 min, rinsed abundantly with ultrapure water, and treated in an UV/ozone cleaner followed by rinsing with ultrapure water and drying in a nitrogen stream. Then, IgG was immobilized on the cleaned surface through DTSSP cleavable crosslinker. For this purpose, the surface was functionalized with amino-groups by immersion in the ethanolic solution of 0.1 M 4-ATP for 1 h and then, DTSSP crosslinker was covalently attached by incubation in PBS buffer (pH 7.4) containing 10 mM of DTSSP for 30 min. After that, 0.1 mL of PBS containing 1 mg mL⁻¹ of IgG was dropped onto the modified sensing surface and allowed to react for 30 min, followed by additional rinsing with PBS buffer to remove the unbound IgG. The protein-modified SAW chip was placed into the 5-mL electrochemical cell designed to expose the modified sensing surface to the synthesis solution. The electrochemical cell accommodated

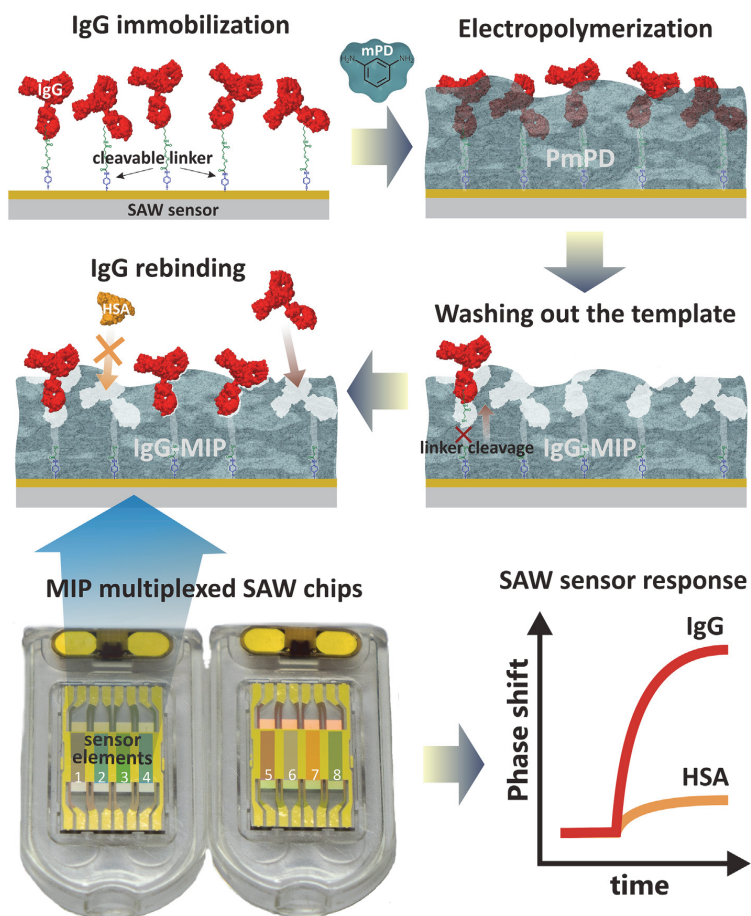


Fig. 1. Schematic representation of the synthesis concept for IgG-MIP sensing layer integration with SAW chip.

three electrodes, i.e. the sensing surface of SAW chip as a working electrode, a spiral shaped Pt wire as a counter electrode, and Ag/AgCl/KCl_{sat} as a reference electrode, all connected to an electrochemical workstation (Reference 600TM, Gamry Instruments, Inc., USA). *m*-PD electropolymerization on the IgG-modified surface was carried out in PBS buffer solution containing 10 mM of mPD by imposing the constant potential of 0.9 V to the working electrode.

To yield the polymeric structures of defined thickness their growth were controlled by charge passed through the working electrode. Thicknesses were determined by a spectroscopic ellipsometer (SE 850 DUV, Sentech Instruments GmbH, Berlin, Germany). Ellipsometric parameters ψ and Δ were measured from three spots for each sample in ambient air confining the wavelength range between 380 and 850 nm at the angle of incidence of 70°. The spectra were fitted (SpectraRay 3 software) with the optical model containing a one-layer Cauchy layer on the top of the gold and the thicknesses were determined.

After the electrodeposition the PmPD film coated sensing surface was rinsed with ultrapure water and dried in a nitrogen stream. To remove the template protein, IgG, from the electrode-

posited PmPD film the modified sensing surface was immersed in aqueous solution of 0.1 M 2-mercaptoethanol, and heated in water bath up to 100 °C with stirring for 15 min. After that, the sensing surface was washed additionally in 3 M NaCl aqueous solution for 15 min and in DMSO for 30 min. The resulting IgG-MIP SAW chip was washed thoroughly with ultrapure water and subjected to the protein rebinding studies. To assess the IgG-MIPs in terms of their affinity to IgG molecule, control non-imprinted polymer (NIP) structures were also created using the very same conditions as for the IgG-MIP but excluding the linker cleavage stage by mercaptoethanol. In this case, the NIP films still contained the covalently bound target protein, but had no specific cavities on its surface.

2.3. IgG rebinding studies

Real-time rebinding of IgG on the prepared IgG-MIP-modified SAW chips was performed using a SAW biosensor system (SamX[®], NanoTemper Technologies GmbH, München, Germany) capable to handle two SAW chips having four separate sensor elements each. The microfluidics of the system provided the option to deliver

analyte solutions to the modified sensor elements either individually or in serial fashion.

The sensor elements were preconditioned at constant flow (25 $\mu\text{L min}^{-1}$) of the degassed PBS buffer solution (pH = 7.4) until a constant baseline was reached. Subsequently, various concentrations (from 0.4 nM to 53 nM) of analytes prepared from the same buffer were injected into the flow stream via an autosampler using a 430 μL injection loop and allowed to interact with the IgG-MIP or IgG-NIP modified SAW chip.

The SAW sensor system capable of both phase and amplitude signal measurement, reflecting changes in mass and in viscoelastic properties of a material at the sensor surface, respectively. In this work, phase-shift response was analyzed to evaluate rebinding properties of IgG-MIPs. Data analysis was performed using Origin 9.1 (Northampton, MA). Raw data were exported, cut and analyzed by individual fits using two kinetic models for sorption from liquid solution represented by the first- and second-order equations as described in the Results and Discussion section. Affinity constants and K_D values were determined from plot of the equilibrium signal (Q_{eq}) versus analyte concentration using Langmuir–Freundlich equation for the data fitting. Regeneration of the film-modified chips was done by their immersion in 3 M NaCl aqueous solution for 2 h with stirring and heating up to 100 °C.

3. Results and discussion

3.1. IgG-MIP fabrication

In contrast to the previously reported synthesis strategy [14], some modifications were introduced here in order to improve the selectivity of the resulting IgG-MIPs. mPD was used as a functional monomer for polymer matrix formation instead of dopamine. Electropolymerization of mPD proceeds faster than that of dopamine therefore the surface-immobilized IgG is less exposed to the synthesis solution as well as to the applied potential that significantly reduces the possibility of conformational changes of IgG. In addition, the computational modeling using molecular docking and quantum chemical approach revealed that mPD as a functional monomer minimally affected the conformation of IgG and was able to create molecular memory via multiple hydrogen bonds, van der Waal's and lipophilic interactions between the polymer matrix and IgG [22]. Moreover, taking into account the types of possible interactions between PmPD and IgG, the template washing out procedure was also modified by including the treatment with 3 M NaCl solution and DMSO in addition to the cleavage of DTSSP linker with mercaptoethanol.

The electrosynthesis approach to the preparation of MIP films allowed a fine control of the polymer thickness by monitoring the electrical charge passed during the synthesis. For the surface imprinting strategy used in this study the deposition of a polymer film with an appropriate thickness is one of the most important task in order to produce protein-MIP film with specific binding sites located on the surface [23,24]. The influence of the electrodeposited polymer thickness on the specific recognition properties of IgG-MIP has been already demonstrated in the previous study [14]. Thereby, in this study to avoid irreversible entrapment of the template the special attention was paid to the careful choice of optimal polymer thickness through control of the charge passed during the in-situ electrodeposition and subsequent correlation of the data with the *ex-situ* ellipsometry measurements (Fig. 2). As it can be seen, the deposited polymer thickness varied nearly linearly ($R^2 = 0.996$) across the applied electric charge range making thus its prediction between ca. 3 nm and 30 nm quite certain. Since the height of IgG with the immobilizing linker system above the surface may spread from ca. 10.5 till 20 nm [14] PmPD films with the thicknesses in the range of 5.7 nm and 28.4 nm were synthesized

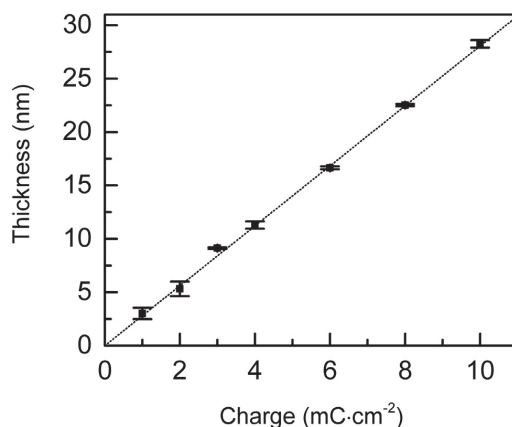


Fig. 2. The calibration graph representing the dependence of the polymeric film thickness, as measured by the spectroscopic ellipsometry, on the amount of the charge consumed during the electropolymerization of *m*-PD on IgG-modified gold electrode.

on the IgG-modified SAW chips by applying the respective charge between 2 and 10 mC cm^{-2} . The influence of the polymer film thickness on IgG-MIP capability to specifically recognize the target protein was evaluated in the course of IgG rebinding study as discussed below.

3.2. IgG rebinding study

The fabricated IgG-MIPs were characterized in term of their affinity to IgG by monitoring the binding kinetics with SAW system. Typical sensorgrams of IgG rebinding at the different concentrations to the surface of SAW chip modified with 11 nm thick IgG-MIP and NIP are presented in Fig. 3a. The association phase of the sensorgrams was analyzed in order to determine the equilibrium signal for the IgG to IgG-MIP and NIP surfaces by fitting the response to the pseudo-first order and pseudo second order kinetic Eqs. (1) and (2), respectively:

$$Q = Q_{eq}[1 - e^{-k_1 t}] \quad (1)$$

$$Q = [Q_{eq}^2 k_2 t] / [1 + Q_{eq} k_2 t] \quad (2)$$

where Q is the phase-shift response upon IgG rebinding at time t , Q_{eq} is its value at equilibrium, k_1 is a pseudo-first order rate constant, k_2 is a pseudo-second order rate constant. The first and second order rate models have been widely used to describe adsorption data obtained under non-equilibrium conditions [25]. According to the first order kinetics model, the adsorbate binds only to a single active site on the adsorbent surface and the interactions of adsorbate and adsorbent are of physical nature; the rate of occupation of adsorption sites is proportional to the number of unoccupied sites [26,27]. The pseudo-second order model recognizes that the rate-limiting step is chemisorption involving sharing or exchange of electrons between adsorbent and adsorbate and the rate of occupation of adsorption sites is proportional to the square of the number of unoccupied sites [27,28]. Both models have been applied to describe the adsorption kinetics on the MIP surfaces [29–31].

The kinetics parameters obtained by fitting the sensorgrams in Fig. 3a to the Eqs. (1) and (2) are listed in Table 1. As it can be seen both models provided excellent fit to the experimental data with the correlation coefficients (R^2) in the range of

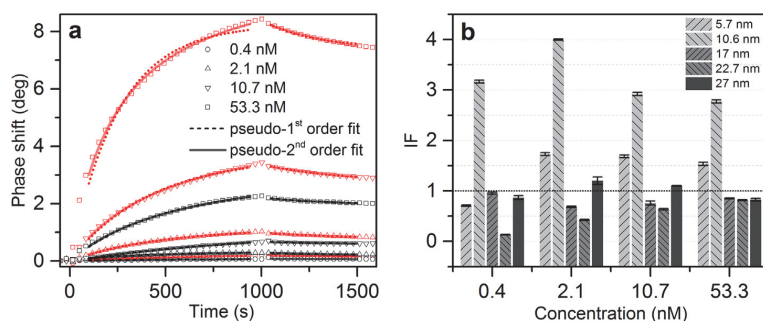


Fig. 3. (a) Typical phase-shift responses of the IgG-MIP (red) and NIP (black) modified SAW chips (PmPD film thickness of 11 nm) upon consecutive injections of IgG in PBS buffer. The dotted and solid lines represent the fits to the Eq. (1) and Eq. (2), respectively; (b) The calculated *IF* values for IgG-MIPs prepared with PmPD films of different thicknesses as a function of the IgG concentration. (For interpretation of the references to color in this figure legend, the reader is referred to the web version of this article.)

Table 1

The kinetics parameters obtained by fitting the sensorgrams in Fig. 3a to the pseudo-first order and pseudo-second order kinetic models.

C (nM)	Q_{eq} (MIP) (deg)	k^a	R^2	Q_{eq} (NIP) (deg)	k^a	R^2
Pseudo-first order model						
0.4	0.24	1.51E-03	0.994	0.08	1.83E-03	0.965
2.1	1.13	2.15E-03	0.998	0.30	3.01E-03	0.994
10.7	3.65	2.37E-03	0.994	1.06	9.90E-04	0.999
53.3	8.25	3.98E-03	0.978	2.58	2.09E-03	0.997
Pseudo-second order model						
0.4	0.38	2.72E-03	0.995	0.12	1.15E-02	0.965
2.1	1.64	1.00E-03	0.999	0.41	6.18E-03	0.995
10.7	5.17	3.66E-04	0.999	1.77	3.43E-04	0.999
53.3	10.43	3.90E-04	0.997	3.76	4.21E-04	0.999

^a Pseudo-first order rate constant (s^{-1}) or pseudo-second order rate constant ($deg^{-1} s^{-1}$).

0.965–0.999, although, at the higher analyte concentrations, somewhat higher values were obtained for the second order adsorption model. The latter might be explained by the fact that Q_{eq} in the pseudo-second order model can be determined independently of the kinetic mechanism of the adsorption process [32] and is less prone to the random experimental errors as compared to the first order rate equation [27]. Thus, Q_{eq} values determined by the pseudo-second rate model were used further to assess the degree of recognition capability of MIP towards the target molecule calculating imprinting factor (*IF*). Actually, *IF* shows a binding ratio between MIP and NIP:

$$IF = Q_{eq}(MIP)/Q_{eq}(NIP) \quad (3)$$

where Q_{eq} (MIP) and Q_{eq} (NIP) are phase-shift responses at equilibrium for MIP and NIP, respectively. As a measure of the presence of selective cavities, *IF* was taken into account to optimize the thickness of the PmPD film in IgG-MIP. SAW chips modified with IgG-MIP and NIP of different thicknesses in the range of ca 6 and 27 nm were subjected to interact with various IgG concentrations between 0.4 and 53.3 nM. Fig. 3b clearly indicates that for all IgG concentrations studied the highest *IF* values in the range of 2.8–4.0 were obtained for the IgG-MIP with PmPD film of 11 nm. This polymer thickness corresponds to the half of the height of immobilized IgG that was estimated to be around 20 nm assuming the IgG “end-on” orientation (through the Fc region). Obviously, at such polymer film thickness the immobilized IgG molecules might be appropriately confined in the polymer leading to the increasing number of high-affinity binding sites at the polymer surface after the IgG removal procedure. Thus, the thickness-optimized IgG-MIP films were employed for subsequent analysis of equilibrium parameters, regeneration and selectivity studies.

Adsorption isotherms are of particular interest as they represent the dependence of the equilibrium concentration of a bound analyte on the concentration of a free analyte in a solution and can provide useful information on the binding properties of the material by fitting the isotherm to specific binding models. The isotherm of IgG rebinding to IgG-MIP was constructed using the values of Q_{eq} determined from analysis of the experimental kinetic data fitting them to Eq. (2) (Fig. 4). Considering the binding site heterogeneity was frequently encountered in noncovalent MIPs [33] the analyte rebinding was modeled by the Langmuir–Freundlich (LF) isotherm (Eq. (4)).

$$Q = Q_{max}C^m / (K_D + C^m) \quad (4)$$

Here *C* is the concentration of an analyte in a solution, *Q* and Q_{max} the phase-shift responses upon IgG rebinding at concentration *C* and its saturation value, respectively, *m* is the heterogeneity index, which varies from 0 to 1 and with values < 1, the material is heterogeneous, K_D – equilibrium dissociation constant. According to Fig. 4 LF model gives an excellent fit ($R^2 = 0.999$) for both IgG-MIP and NIP films tested in this study. The calculated *m* value of IgG-MIP indicates the somewhat heterogeneity of the binding sites in comparison to NIP, whose heterogeneity index equals to 1 corresponding to a homogeneous material. This can be well explained through assumption that NIP films might possess the exclusively nonspecific binding sites of equal adsorption energy, while the imprinting process introduced the binding sites with varying degrees of affinity resulting in the heterogeneity of the polymer surface. Furthermore, the obtained value of the signal at saturated binding to IgG-MIP was about 3 times higher than that to corresponding NIP (15.0 vs 5.3 deg) while the only modest difference in the dissociation constants (K_D) between two polymers was observed. One possible explanation for the observed phenomenon could be that despite of the total number of binding sites was increased in MIP relative to the NIP, the fraction of the higher-affinity binding sites was still low to contribute significantly to the overall affinity of IgG-MIP. Similarly, Shimizu and co-workers reported on the inconsistency between the difference in binding capacities and binding affinities of MIP and corresponding NIP [34].

3.3. Regeneration of IgG-MIPs

In order to verify the stability and reusability of the fabricated IgG-MIPs, the films with the optimal thickness after first IgG rebinding were subjected to the regeneration procedure. Since the nature of the interactions between the imprinted material and the target protein was insufficiently known, the regeneration

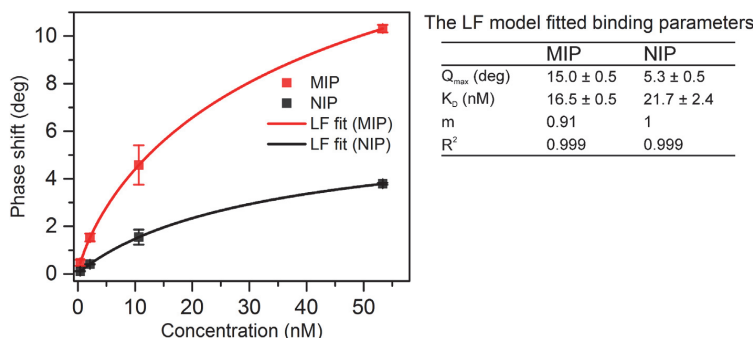


Fig. 4. The binding isotherms obtained using Q_{eq} determined from fitting of the kinetic data to Eq. (2). The solid lines represent fits of the data to Langmuir–Freundlich (LF) isotherm model. The table summarizes the fitted binding parameters.

experiments disrupting hydrogen, ionic and electrostatic bonds were performed. It was found that solutions of 1 M NaOH and 10 mM HCl affected significantly on reproducibility of further binding events making difference between MIP and NIP films barely noticed (results are not shown), while MIPs retained their affinity towards the target after the treatment in 3 M NaCl solution (100 °C) suggesting that electrostatic interactions might play a role in the given MIP-protein system. Therefore, the treatment in the hot 3 M NaCl solution was chosen as a method for regeneration of the fabricated IgG-MIPs. The changes in Q_{max} of the polymers for IgG after the subsequent rebinding-regeneration cycles are depicted in Fig. 5. As it can be seen, although both MIP and NIP polymers showed irreversible adsorption of the target, their rebinding capacities were about to stabilize after the 3rd regeneration cycle while still demonstrating MIP preferential affinity and relevant sensitivity levels towards the target. The noticed decrease in the adsorption capacity may indicate that the regeneration method left behind to some extent the target entrapped in the polymeric matrix altering thus the following rebinding. Still, the phenomenon cannot be explained purely by the target entrapment since the nonspecific adsorption, displayed by NIP film response, was suppressed significantly after the very 1st regeneration cycle. Thus, the films might also undergo morphological changes upon contact with the high temperature and ionic strength solutions resulting

in loss of a fraction of the polymeric material from the sensing surface.

3.4. Selectivity study

Selectivity of IgG imprinted films towards the template was studied by injecting $8 \mu\text{g mL}^{-1}$ solutions of other serum proteins: HSA and IgA that may cause serious interference when analyzing real samples. Selectivity factor S , which is the ratio of IF of an interfering substance to that toward the template molecule, was used to assess cross-reactivity of IgG-MIP:

$$S = IF_{(interf)} / IF_{(IgG)} \quad (5)$$

where $IF_{(IgG)}$ is the imprinting factor of IgG-MIP for IgG and $IF_{(interf)}$ is the imprinting factor of IgG-MIP for interfering protein, IgA or HSA. $IF_{(interf)}$ values for IgA and HSA were calculated according to Eq. (3), where the values of Q_{eq} upon HSA and IgA adsorption onto IgG-MIP and NIP were determined from the kinetics data using the similar analysis procedure as described for IgG rebinding study (Section 3.2). As it can be seen in Fig. 6, IgG-MIP demonstrated the preferential binding to the original template molecule (IgG) over the IgA and HSA with the S values of 0.3 and 0.09, respectively. The data suggests that the both interfering proteins have lower binding affinity to IgG-MIP than IgG, even though the molecular size and shape of IgG and IgA are similar. Thus, IgG-MIP can recognize the

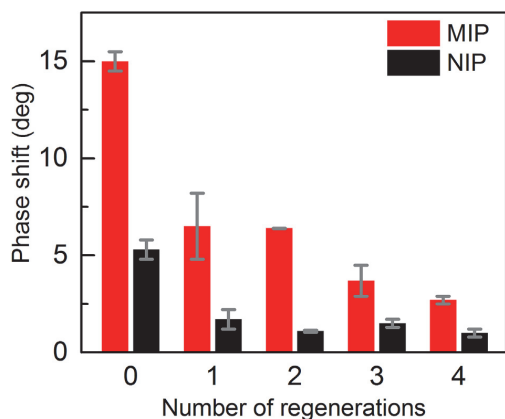


Fig. 5. SAW sensor response at saturated binding (Q_{max}) for IgG-MIP and NIP after various number of regeneration cycles. The initial responses of freshly fabricated sensors are presented at 0 value of regeneration cycle.

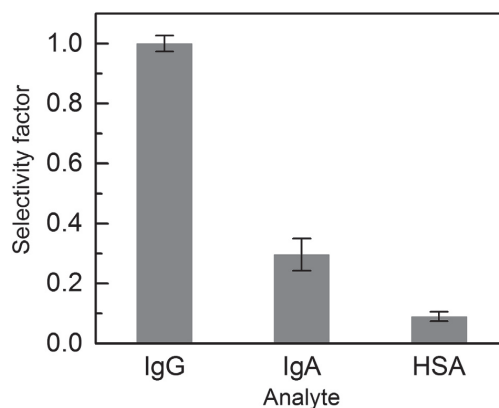


Fig. 6. Selectivity factors (S) of IgG-MIP for the template (IgG) and non-template (IgA, HSA) proteins.

target protein confirming the presence of IgG imprints in the polymer matrix that are able to discriminate on the basis of molecular shape and size as well as functional groups arrangement.

4. Conclusions

In this study, the protein imprinted polymers, IgG-MIPs, were used for the first time as sensing layers of SAW sensor platform. The thin films of IgG-MIP were successfully interfaced with SAW chips using the electrosynthesis approach. The binding kinetic analysis with the pseudo second-order rate model allowed the determination of equilibrium binding response and thus, the calculation and comparison of the imprinting factors for the IgG-MIP of different polymer thicknesses. It was found that IgG-MIP films with the thickness of 11 nm had higher specific recognition ability towards IgG as compared to the other studied IgG-MIP counterparts. The thickness optimized MIPs demonstrated imprinting factors in the range of 2.8–4.

The analysis of the isotherm data by fitting them to Langmuir-Freundlich adsorption model suggested a certain degree of heterogeneity of the binding sites in IgG-MIP films. Although, the binding capacity of IgG-MIP was about 3 times higher than that of NIP, their dissociation constants were somewhat comparable. This is more likely attributed to the disproportionately low contribution of the high affinity binding sites to the increased binding capacity of IgG-MIP. The prepared IgG-MIPs demonstrated good selectivity towards IgG over the interfering proteins such as IgA and HSA as well preserved their capability to recognize selectively the template after up to four regeneration cycles in hot 3 M NaCl solution.

The realized concept for facile integration of protein-MIPs with SAW technology allowed observing the real-time binding events of the target protein at relevant sensitivity levels and can be potentially suitable for cost effective fabrication of a biosensor for analysis of biological samples in multiplexed manner.

Acknowledgments

This work was supported by the Estonian Ministry of Education and Research (grant PUT150). The authors thank Dr. J. Rappich for the opportunity to perform the ellipsometry measurements at Helmholtz-Zentrum Berlin für Materialien und Energie GmbH.

References

- [1] S. Ray, G. Mehta, S. Srivastava, Label-free detection techniques for protein microarrays: prospects, merits and challenges, *Proteomics* 10 (2010) 731–748.
- [2] S. Li, Y. Ge, S.A. Piletsky, J. Lunec, *Molecularly Imprinted Sensors: Overview and Applications*, Elsevier, 2012, p. 388.
- [3] L. Ye, K. Haupt, Molecularly imprinted polymers as antibody and receptor mimics for assays, sensors and drug discovery, *Anal. Bioanal. Chem.* 378 (2004) 1887–1897.
- [4] N.W. Turner, C.W. Jeans, K.R. Brain, C.J. Allender, V. Hlady, D.W. Britt, From 3D to 2D: A review of the molecular imprinting of proteins, *Biotechnol. Prog.* 22 (2006) 1474–1489.
- [5] H. Nishino, C.S. Huang, K.J. Shea, Selective protein capture by epitope imprinting, *Angew. Chem. Int. Ed.* 45 (2006) 2392–2396.
- [6] P.C. Chou, J. Rick, T.C. Chou, C-reactive protein thin-film molecularly imprinted polymers formed using a micro-contact approach, *Anal. Chim. Acta* 542 (2005) 20–25.
- [7] G. Lautner, J. Kaev, J. Reut, A. Öpik, J. Rappich, V. Syritski, R.E. Gyurcsanyi, Selective Artificial receptors based on micropatterned surface-imprinted polymers for label-free detection of proteins by SPR imaging, *Adv. Funct. Mater.* 21 (2011) 591–597.
- [8] A. Menaker, V. Syritski, J. Reut, A. Öpik, V. Horvath, R.E. Gyurcsanyi, Electrosynthesized surface-imprinted conducting polymer microrods for selective protein recognition, *Adv. Mater.* 21 (2009) 2271–2275.
- [9] O. Hayden, C. Haderspock, S. Krassnig, X.H. Chen, F.L. Dickert, Surface imprinting strategies for the detection of trypsin, *Analyst* 131 (2006) 1044–1050.
- [10] D.R. Kryscio, N.A. Peppas, Surface imprinted thin polymer film systems with selective recognition for bovine serum albumin, *Anal. Chim. Acta* 718 (2012) 109–115.
- [11] Z.H. Zhang, Y.M. Long, L.H. Nie, S.Z. Yao, Molecularly imprinted thin film self-assembled on piezoelectric quartz crystal surface by the sol-gel process for protein recognition, *Biosens. Bioelectron.* 21 (2006) 1244–1251.
- [12] J. Rick, T.C. Chou, Using protein templates to direct the formation of thin-film polymer surfaces, *Biosens. Bioelectron.* 22 (2006) 544–549.
- [13] P.S. Sharma, A. Pietrzyk-Le, F. D'Souza, W. Kutner, Electrochemically synthesized polymers in molecular imprinting for chemical sensing, *Anal. Bioanal. Chem.* 402 (2012) 3177–3204.
- [14] A.S. Tretjakov, V. Syritski, J. Reut, O. Volobujeva, A. Öpik, Surface molecularly imprinted polydopamine films for recognition of immunoglobulin G, *Mikrochim. Acta* 180 (2013) 1433–1442.
- [15] J. Bognar, J. Szucs, Z. Dorko, V. Horvath, R.E. Gyurcsanyi, Nanosphere lithography as a versatile method to generate surface-imprinted polymer films for selective protein recognition, *Adv. Funct. Mater.* 23 (2013) 4703–4709.
- [16] D. Cai, L. Ren, H.Z. Zhao, C.J. Xu, L. Zhang, Y. Yu, H.Z. Wang, Y.C. Lan, M.F. Roberts, J.H. Chung, M.J. Naughton, Z.F. Ren, T.C. Chiles, A molecular-imprint nanosensor for ultrasensitive detection of proteins, *Nat. Nanotechnol.* 5 (2010) 597–601.
- [17] D. Dechtrirat, N. Gajovic-Eichelmann, F.F. Bier, F.W. Scheller, Hybrid material for protein sensing based on electrosynthesized MIP on a mannose terminated self-assembled monolayer, *Adv. Funct. Mater.* 24 (2014) 2233–2239.
- [18] T.M.A. Gronewold, Surface acoustic wave sensors in the bioanalytical field: recent trends and challenges, *Anal. Chim. Acta* 603 (2007) 119–128.
- [19] K. Länge, B.E. Rapp, M. Rapp, Surface acoustic wave biosensors: a review, *Anal. Bioanal. Chem.* 391 (2008) 1509–1519.
- [20] V.V. Losev, A.V. Medved, A.V. Roshchin, R.G. Kryshal, B.I. Zapadinski, I.D. Epinat'ev, I.V. Kumpnenko, An acoustic study of the selective absorption of vapors by microporous polymer films, *Russ. J. Phys. Chem. B* 3 (2009) 990–1003.
- [21] W. Wen, S.T. He, S.Z. Li, M.H. Liu, P. Yong, Enhanced sensitivity of SAW gas sensor coated molecularly imprinted polymer incorporating high frequency stability oscillator, *Sens. Actuators B Chem.* 125 (2007) 422–427.
- [22] R. Boroznjak, A. Tretjakov, V. Syritski, J. Reut, A. Öpik, Unpublished results, (2015).
- [23] M. Bosserdt, J. Erdossy, G. Lautner, J. Witt, K. Kohler, N. Gajovic-Eichelmann, A. Yarman, G. Wittstock, F.W. Scheller, R.E. Gyurcsanyi, Microelectrospotting as a new method for electrosynthesis of surface-imprinted polymer microarrays for protein recognition, *Biosens. Bioelectron.* 73 (2015) 123–129.
- [24] K.J. Jetzschmann, G. Jagerszki, D. Dechtrirat, A. Yarman, N. Gajovic-Eichelmann, H.D. Gilsing, B. Schulz, R.E. Gyurcsanyi, F.W. Scheller, Vectorially Imprinted Hybrid Nanofilm for Acetylcholinesterase Recognition, *Adv. Funct. Mater.* 25 (2015) 5178–5183.
- [25] Y. Liu, L. Shen, From Langmuir kinetics to first- and second-order rate equations for adsorption, *Langmuir ACS J. Surf. Coll.* 24 (2008) 11625–11630.
- [26] S. Lagergren, Zur theorie der sogenannten adsorption gelöster stoffe, *Kungliga Svenska Vetenskapsakademiens Handlingar* 24 (1898) 1–39.
- [27] W. Plazinski, W. Rudzinski, A. Plazinska, Theoretical models of sorption kinetics including a surface reaction mechanism: a review, *Adv. Colloid Interfac.* 152 (2009) 2–13.
- [28] Y.S. Ho, Review of second-order models for adsorption systems, *J. Hazard Mater.* 136 (2006) 681–689.
- [29] C.Y. Chen, C.H. Wang, A.H. Chen, Recognition of molecularly imprinted polymers for a quaternary alkaloid of berberine, *Talanta* 84 (2011) 1038–1046.
- [30] K. da Mata, M.Z. Corazza, F.M. de Oliveira, A.L. de Toffoli, C.R.T. Tarley, A.B. Moreira, Synthesis and characterization of cross-linked molecularly imprinted polyacrylamide for the extraction/preconcentration of glyphosate and aminomethylphosphonic acid from water samples, *React. Funct. Polym.* 83 (2014) 76–83.
- [31] Q.P. You, Y.P. Zhang, Q.W. Zhang, J.F. Guo, W.H. Huang, S.Y. Shi, X.Q. Chen, High-capacity thermo-responsive magnetic molecularly imprinted polymers for selective extraction of curcuminoids, *J. Chromatogr. A* 1354 (2014) 1–8.
- [32] W. Rudzinski, W. Plazinski, On the applicability of the pseudo-second order equation to represent the kinetics of adsorption at solid/solution interfaces: a theoretical analysis based on the statistical rate theory, *Adsorption* 15 (2009) 181–192.
- [33] R.J. Umpleby 2nd, S.C. Baxter, Y. Chen, R.N. Shah, K.D. Shimizu, Characterization of molecularly imprinted polymers with the Langmuir–Freundlich isotherm, *Anal. Chem.* 73 (2001) 4584–4591.
- [34] A.M. Rampey, R.J. Umpleby, G.T. Rushton, J.C. Iseman, R.N. Shah, K.D. Shimizu, Characterization of the imprint effect and the influence of imprinting conditions on affinity, capacity, and heterogeneity in molecularly imprinted polymers using the Freundlich isotherm-affinity distribution analysis, *Anal. Chem.* 76 (2004) 1123–1133.

APPENDIX B

CURRICULUM VITAE

1. Personal data

Name Roman Boronzjak
Date and place of birth 20.08.1980, Tallinn
E-mail address roman.boroznjak@ttu.ee

2. Education

Educational institution	Graduation year	Education (field of study/degree)
Tallinn University of Technology	2011 - ...	Chemical and Materials Technology / Doctoral studies
Tallinn University of Technology	2007	Organic Chemistry / Master degree
Tallinn University	2002	Chemistry / Bachelor degree
Tallinn 15th Secondary School	1998	Secondary education

3. Language competence/skills

Language	Level
Russian	Native
Estonian	Fluent
English	Average

4. Special courses

Period	Educational or other organisation
2012-2017	Graduate school “Functional materials and technologies FMTDK”, Tallinn University of Technology, Estonia

5. Professional employment

Period	Organisation	Position
2010–2011	Tallinn University of Technology, Department of Materials Science	Engineer
2007-2009	Tallinn University of Technology, Department of Chemistry	Technician
2005-2005	Mustjõe Secondary School	Chemistry/biology teacher

6. Research activity, including honours and thesis supervised

Projects

01.01.2010 - 31.12.2012	Surface-Imprinted Electrosynthesized Conducting Polymers for Biorecognition	ETF8249
01.01.2012 - 31.12.2012	Advanced Functional Materials and Devices Based on Molecularly Imprinted Polymers and Organic-inorganic Hybrid Structures	SF0140033s12
01.01.2012 -	p-type ZnO and ZnS	ETF9243

31.12.2015		
01.01.2013 - 31.12.2016	Investigation and development of new generation biosensing selective recognition elements based on Molecularly Imprinted Polymers	PUT150

Honours

Award for the best publication in the field of natural and exact sciences in 2015 at Tallinn University of Technology: Akinrinade George Ayankajo, Aleksei Tretjakov, Jekaterina Reut, **Roman Boroznjak**, Andres Öpik, Jörg Rappich, Andreas Furchner, Karsten Hinrichs, and Vitali Syriski, Molecularly Imprinted Polymer Integrated with a Surface Acoustic Wave Technique for Detection of Sulfamethizole, *Analytical Chemistry*, 88(2) (2016) 1476–1484.

ELULOOKIRJELDUS

1. Isikuandmed

Ees- ja perekonnanimi Roman Boroznjak
Sünniaeg ja -koht 20.08.1980, Tallinn
Kodakondsus Eesti
E-posti aadress roman.boroznjak@ttu.ee

2. Hariduskäik

Õppeasutus (nimetus lõpetamise ajal)	Lõpetamise aeg	Haridus (eriala/kraad)
Tallinna Tehnikaülikool	2011 - ...	Keemia- ja materjalitehnoloogia / doktoriõpe
Tallinna Tehnikaülikool	2007	Orgaaniline keemia / Magistrikraad
Tallinna Ülikool	2002	Loodusteaduslike ainete õpetaja / Bakalaureusekraad
Tallinna 15. keskkool	1998	Keskharidus

3. Keelteoskus

Keel	Tase
Vene	Emakeel
Eesti	Kõrgtase
Inglise	Keskase

4. Täiendusõpe

Õppimise aeg	Täiendusõppe korraldaja nimetus
2012-2017	TÜ ja TTÜ doktorikool "Funktsionaalsed materjalid ja tehnoloogiad" (FMTDK), Eesti

5. Teenistuskäik

Töötamise aeg	Tööandja nimetus	Ametikoht
2010-2011	Tallinna Tehnikaülikool, Materjaaliteaduse instituut	Insener
2007-2009	Tallinna Tehnikaülikool, keemiasstituut	Tehnik
2005	Tallinna Mustjõe Gümnaasium	Keemia ja bioloogia õpetaja

6. Teadustegevus, sh tunnustused ja juhendatud lõputööd

Projektid

01.01.2010 - 31.12.2012	Biotundlikud süsteemid pindmiste mälupesadega molekulaarselt jäljendatud elektrit juhtivatest polümeeridest	ETF8249
01.01.2012 - 31.12.2012	Kaasaegsed funktsionaalsed materjalid ja seadised molekulaarselt jäljendatud polümeeride ja orgaaniliste/anorgaaniliste hübriidsete struktuuride baasil	SF0140033s12
01.01.2012 - 31.12.2015	p-tüüpi ZnO ja ZnS	ETF9243

01.01.2013 31.12.2016	- Uue põlvkonna biotundlike süsteemide uurimine ja väljatöötamine molekulaarselt jäljendatud polümeeride baasil	PUT150
--------------------------	---	--------

Tunnustused

TTÜ 2015 aasta parim teadusartikkel loodus-, täppis- ja terviseteaduste valdkonnas: Akinrinade George Ayankajo, Aleksei Tretjakov, Jekaterina Reut, **Roman Boroznjak**, Andres Öpik, Jörg Rappich, Andreas Furchner, Karsten Hinrichs, and Vitali Syritski, Molecularly Imprinted Polymer Integrated with a Surface Acoustic Wave Technique for Detection of Sulfamethizole, *Analytical Chemistry*, 88(2) (2016) 1476–1484.

**DISSERTATIONS DEFENDED AT
TALLINN UNIVERSITY OF TECHNOLOGY ON
NATURAL AND EXACT SCIENCES**

1. **Olav Kongas**. Nonlinear Dynamics in Modeling Cardiac Arrhythmias. 1998.
2. **Kalju Vanatalu**. Optimization of Processes of Microbial Biosynthesis of Isotopically Labeled Biomolecules and Their Complexes. 1999.
3. **Ahto Buldas**. An Algebraic Approach to the Structure of Graphs. 1999.
4. **Monika Drews**. A Metabolic Study of Insect Cells in Batch and Continuous Culture: Application of Chemostat and Turbidostat to the Production of Recombinant Proteins. 1999.
5. **Eola Valdre**. Endothelial-Specific Regulation of Vessel Formation: Role of Receptor Tyrosine Kinases. 2000.
6. **Kalju Lott**. Doping and Defect Thermodynamic Equilibrium in ZnS. 2000.
7. **Reet Koljak**. Novel Fatty Acid Dioxygenases from the Corals *Plexaura homomalla* and *Gersemia fruticosa*. 2001.
8. **Anne Paju**. Asymmetric oxidation of Prochiral and Racemic Ketones by Using Sharpless Catalyst. 2001.
9. **Marko Vendelin**. Cardiac Mechanoenergetics *in silico*. 2001.
10. **Pearu Peterson**. Multi-Soliton Interactions and the Inverse Problem of Wave Crest. 2001.
11. **Anne Menert**. Microcalorimetry of Anaerobic Digestion. 2001.
12. **Toomas Tiivel**. The Role of the Mitochondrial Outer Membrane in *in vivo* Regulation of Respiration in Normal Heart and Skeletal Muscle Cell. 2002.
13. **Olle Hints**. Ordovician Scolecodonts of Estonia and Neighbouring Areas: Taxonomy, Distribution, Palaeoecology, and Application. 2002.
14. **Jaak Nõlvak**. Chitinozoan Biostratigraphy in the Ordovician of Baltoscandia. 2002.
15. **Liivi Kluge**. On Algebraic Structure of Pre-Operad. 2002.
16. **Jaanus Lass**. Biosignal Interpretation: Study of Cardiac Arrhythmias and Electromagnetic Field Effects on Human Nervous System. 2002.
17. **Janek Peterson**. Synthesis, Structural Characterization and Modification of PAMAM Dendrimers. 2002.
18. **Merike Vaher**. Room Temperature Ionic Liquids as Background Electrolyte Additives in Capillary Electrophoresis. 2002.
19. **Valdek Mikli**. Electron Microscopy and Image Analysis Study of Powdered Hardmetal Materials and Optoelectronic Thin Films. 2003.
20. **Mart Viljus**. The Microstructure and Properties of Fine-Grained Cermets. 2003.
21. **Signe Kask**. Identification and Characterization of Dairy-Related *Lactobacillus*. 2003.
22. **Tiiu-Mai Laht**. Influence of Microstructure of the Curd on Enzymatic and Microbiological Processes in Swiss-Type Cheese. 2003.
23. **Anne Kuusksalu**. 2–5A Synthetase in the Marine Sponge *Geodia cydonium*. 2003.
24. **Sergei Bereznev**. Solar Cells Based on Polycrystalline Copper-Indium Chalcogenides and Conductive Polymers. 2003.

25. **Kadri Kriis.** Asymmetric Synthesis of C₂-Symmetric Bimorpholines and Their Application as Chiral Ligands in the Transfer Hydrogenation of Aromatic Ketones. 2004.
26. **Jekaterina Reut.** Polypyrrole Coatings on Conducting and Insulating Substrates. 2004.
27. **Sven Nõmm.** Realization and Identification of Discrete-Time Nonlinear Systems. 2004.
28. **Olga Kijatkina.** Deposition of Copper Indium Disulphide Films by Chemical Spray Pyrolysis. 2004.
29. **Gert Tamberg.** On Sampling Operators Defined by Rogosinski, Hann and Blackman Windows. 2004.
30. **Monika Übner.** Interaction of Humic Substances with Metal Cations. 2004.
31. **Kaarel Adamberg.** Growth Characteristics of Non-Starter Lactic Acid Bacteria from Cheese. 2004.
32. **Imre Vallikivi.** Lipase-Catalysed Reactions of Prostaglandins. 2004.
33. **Merike Peld.** Substituted Apatites as Sorbents for Heavy Metals. 2005.
34. **Vitali Syritski.** Study of Synthesis and Redox Switching of Polypyrrole and Poly(3,4-ethylenedioxythiophene) by Using *in-situ* Techniques. 2004.
35. **Lee Põllumaa.** Evaluation of Ecotoxicological Effects Related to Oil Shale Industry. 2004.
36. **Riina Aav.** Synthesis of 9,11-Secosterols Intermediates. 2005.
37. **Andres Braunbrück.** Wave Interaction in Weakly Inhomogeneous Materials. 2005.
38. **Robert Kitt.** Generalised Scale-Invariance in Financial Time Series. 2005.
39. **Juss Pavelson.** Mesoscale Physical Processes and the Related Impact on the Summer Nutrient Fields and Phytoplankton Blooms in the Western Gulf of Finland. 2005.
40. **Olari Ilison.** Solitons and Solitary Waves in Media with Higher Order Dispersive and Nonlinear Effects. 2005.
41. **Maksim Säkki.** Intermittency and Long-Range Structurization of Heart Rate. 2005.
42. **Enli Kiipli.** Modelling Seawater Chemistry of the East Baltic Basin in the Late Ordovician–Early Silurian. 2005.
43. **Igor Golovtsov.** Modification of Conductive Properties and Processability of Polyparaphenylene, Polypyrrole and polyaniline. 2005.
44. **Katrin Laos.** Interaction Between Furcellaran and the Globular Proteins (Bovine Serum Albumin β -Lactoglobulin). 2005.
45. **Arvo Mere.** Structural and Electrical Properties of Spray Deposited Copper Indium Disulphide Films for Solar Cells. 2006.
46. **Sille Ehala.** Development and Application of Various On- and Off-Line Analytical Methods for the Analysis of Bioactive Compounds. 2006.
47. **Maria Kulp.** Capillary Electrophoretic Monitoring of Biochemical Reaction Kinetics. 2006.
48. **Anu Aaspõllu.** Proteinases from *Vipera lebetina* Snake Venom Affecting Hemostasis. 2006.
49. **Lyudmila Chekulayeva.** Photosensitized Inactivation of Tumor Cells by Porphyrins and Chlorins. 2006.

50. **Merle Uudsemaa.** Quantum-Chemical Modeling of Solvated First Row Transition Metal Ions. 2006.
51. **Tagli Pitsi.** Nutrition Situation of Pre-School Children in Estonia from 1995 to 2004. 2006.
52. **Angela Ivask.** Luminescent Recombinant Sensor Bacteria for the Analysis of Bioavailable Heavy Metals. 2006.
53. **Tiina Lõugas.** Study on Physico-Chemical Properties and Some Bioactive Compounds of Sea Buckthorn (*Hippophae rhamnoides* L.). 2006.
54. **Kaja Kasemets.** Effect of Changing Environmental Conditions on the Fermentative Growth of *Saccharomyces cerevisiae* S288C: Auxo-accelerostat Study. 2006.
55. **Ildar Nisamedtinov.** Application of ^{13}C and Fluorescence Labeling in Metabolic Studies of *Saccharomyces* spp. 2006.
56. **Alar Leibak.** On Additive Generalisation of Voronoï's Theory of Perfect Forms over Algebraic Number Fields. 2006.
57. **Andri Jagomägi.** Photoluminescence of Chalcopyrite Tellurides. 2006.
58. **Tõnu Martma.** Application of Carbon Isotopes to the Study of the Ordovician and Silurian of the Baltic. 2006.
59. **Marit Kauk.** Chemical Composition of CuInSe_2 Monograin Powders for Solar Cell Application. 2006.
60. **Julia Kois.** Electrochemical Deposition of CuInSe_2 Thin Films for Photovoltaic Applications. 2006.
61. **Ilona Oja Açıık.** Sol-Gel Deposition of Titanium Dioxide Films. 2007.
62. **Tiia Anmann.** Integrated and Organized Cellular Bioenergetic Systems in Heart and Brain. 2007.
63. **Katrin Trummal.** Purification, Characterization and Specificity Studies of Metalloproteinases from *Vipera lebetina* Snake Venom. 2007.
64. **Gennadi Lessin.** Biochemical Definition of Coastal Zone Using Numerical Modeling and Measurement Data. 2007.
65. **Enno Pais.** Inverse problems to determine non-homogeneous degenerate memory kernels in heat flow. 2007.
66. **Maria Borissova.** Capillary Electrophoresis on Alkylimidazolium Salts. 2007.
67. **Karin Valmsen.** Prostaglandin Synthesis in the Coral *Plexaura homomalla*: Control of Prostaglandin Stereochemistry at Carbon 15 by Cyclooxygenases. 2007.
68. **Kristjan Piirimäe.** Long-Term Changes of Nutrient Fluxes in the Drainage Basin of the Gulf of Finland – Application of the PolFlow Model. 2007.
69. **Tatjana Dedova.** Chemical Spray Pyrolysis Deposition of Zinc Sulfide Thin Films and Zinc Oxide Nanostructured Layers. 2007.
70. **Katrin Tomson.** Production of Labelled Recombinant Proteins in Fed-Batch Systems in *Escherichia coli*. 2007.
71. **Cecilia Sarmiento.** Suppressors of RNA Silencing in Plants. 2008.
72. **Vilja Mardla.** Inhibition of Platelet Aggregation with Combination of Antiplatelet Agents. 2008.
73. **Maie Bachmann.** Effect of Modulated Microwave Radiation on Human Resting Electroencephalographic Signal. 2008.
74. **Dan Hüvonen.** Terahertz Spectroscopy of Low-Dimensional Spin Systems. 2008.

75. **Ly Villo.** Stereoselective Chemoenzymatic Synthesis of Deoxy Sugar Esters Involving *Candida antarctica* Lipase B. 2008.
76. **Johan Anton.** Technology of Integrated Photoelasticity for Residual Stress Measurement in Glass Articles of Axisymmetric Shape. 2008.
77. **Olga Volobujeva.** SEM Study of Selenization of Different Thin Metallic Films. 2008.
78. **Artur Jõgi.** Synthesis of 4'-Substituted 2,3'-dideoxynucleoside Analogues. 2008.
79. **Mario Kadastik.** Doubly Charged Higgs Boson Decays and Implications on Neutrino Physics. 2008.
80. **Fernando Pérez-Caballero.** Carbon Aerogels from 5-Methylresorcinol-Formaldehyde Gels. 2008.
81. **Sirje Vaask.** The Comparability, Reproducibility and Validity of Estonian Food Consumption Surveys. 2008.
82. **Anna Menaker.** Electrosynthesized Conducting Polymers, Polypyrrole and Poly(3,4-ethylenedioxythiophene), for Molecular Imprinting. 2009.
83. **Lauri Ilison.** Solitons and Solitary Waves in Hierarchical Korteweg-de Vries Type Systems. 2009.
84. **Kaia Ernits.** Study of In₂S₃ and ZnS Thin Films Deposited by Ultrasonic Spray Pyrolysis and Chemical Deposition. 2009.
85. **Veljo Sinivee.** Portable Spectrometer for Ionizing Radiation "Gammamapper". 2009.
86. **Jüri Virkepu.** On Lagrange Formalism for Lie Theory and Operadic Harmonic Oscillator in Low Dimensions. 2009.
87. **Marko Piirsoo.** Deciphering Molecular Basis of Schwann Cell Development. 2009.
88. **Kati Helmja.** Determination of Phenolic Compounds and Their Antioxidative Capability in Plant Extracts. 2010.
89. **Merike Sõmera.** Sobemoviruses: Genomic Organization, Potential for Recombination and Necessity of P1 in Systemic Infection. 2010.
90. **Kristjan Laes.** Preparation and Impedance Spectroscopy of Hybrid Structures Based on CuIn₃Se₅ Photoabsorber. 2010.
91. **Kristin Lippur.** Asymmetric Synthesis of 2,2'-Bimorpholine and its 5,5'-Substituted Derivatives. 2010.
92. **Merike Luman.** Dialysis Dose and Nutrition Assessment by an Optical Method. 2010.
93. **Mihhail Berezovski.** Numerical Simulation of Wave Propagation in Heterogeneous and Microstructured Materials. 2010.
94. **Tamara Aid-Pavlidis.** Structure and Regulation of BDNF Gene. 2010.
95. **Olga Bragina.** The Role of Sonic Hedgehog Pathway in Neuro- and Tumorigenesis. 2010.
96. **Merle Randrüüt.** Wave Propagation in Microstructured Solids: Solitary and Periodic Waves. 2010.
97. **Marju Laars.** Asymmetric Organocatalytic Michael and Aldol Reactions Mediated by Cyclic Amines. 2010.
98. **Maarja Grossberg.** Optical Properties of Multinary Semiconductor Compounds for Photovoltaic Applications. 2010.

99. **Alla Maloverjan.** Vertebrate Homologues of Drosophila Fused Kinase and Their Role in Sonic Hedgehog Signalling Pathway. 2010.
100. **Priit Pruunsild.** Neuronal Activity-Dependent Transcription Factors and Regulation of Human *BDNF* Gene. 2010.
101. **Tatjana Knjazeva.** New Approaches in Capillary Electrophoresis for Separation and Study of Proteins. 2011.
102. **Atanas Katerski.** Chemical Composition of Sprayed Copper Indium Disulfide Films for Nanostructured Solar Cells. 2011.
103. **Kristi Timmo.** Formation of Properties of CuInSe_2 and $\text{Cu}_2\text{ZnSn}(\text{S},\text{Se})_4$ Monograin Powders Synthesized in Molten KI. 2011.
104. **Kert Tamm.** Wave Propagation and Interaction in Mindlin-Type Microstructured Solids: Numerical Simulation. 2011.
105. **Adrian Popp.** Ordovician Proetid Trilobites in Baltoscandia and Germany. 2011.
106. **Ove Pärn.** Sea Ice Deformation Events in the Gulf of Finland and Their Impact on Shipping. 2011.
107. **Germo Väli.** Numerical Experiments on Matter Transport in the Baltic Sea. 2011.
108. **Andrus Seiman.** Point-of-Care Analyser Based on Capillary Electrophoresis. 2011.
109. **Olga Katargina.** Tick-Borne Pathogens Circulating in Estonia (Tick-Borne Encephalitis Virus, *Anaplasma phagocytophilum*, *Babesia* Species): Their Prevalence and Genetic Characterization. 2011.
110. **Ingrid Sumeri.** The Study of Probiotic Bacteria in Human Gastrointestinal Tract Simulator. 2011.
111. **Kairit Zovo.** Functional Characterization of Cellular Copper Proteome. 2011.
112. **Natalja Makarytseva.** Analysis of Organic Species in Sediments and Soil by High Performance Separation Methods. 2011.
113. **Monika Mortimer.** Evaluation of the Biological Effects of Engineered Nanoparticles on Unicellular Pro- and Eukaryotic Organisms. 2011.
114. **Kersti Tepp.** Molecular System Bioenergetics of Cardiac Cells: Quantitative Analysis of Structure-Function Relationship. 2011.
115. **Anna-Liisa Peikolainen.** Organic Aerogels Based on 5-Methylresorcinol. 2011.
116. **Leeli Amon.** Palaeoecological Reconstruction of Late-Glacial Vegetation Dynamics in Eastern Baltic Area: A View Based on Plant Macrofossil Analysis. 2011.
117. **Tanel Peets.** Dispersion Analysis of Wave Motion in Microstructured Solids. 2011.
118. **Liina Kaupmees.** Selenization of Molybdenum as Contact Material in Solar Cells. 2011.
119. **Allan Olsper.** Properties of VPg and Coat Protein of Sobemoviruses. 2011.
120. **Kadri Koppel.** Food Category Appraisal Using Sensory Methods. 2011.
121. **Jelena Gorbatošova.** Development of Methods for CE Analysis of Plant Phenolics and Vitamins. 2011.
122. **Karin Viipsi.** Impact of EDTA and Humic Substances on the Removal of Cd and Zn from Aqueous Solutions by Apatite. 2012.

123. **David Schryer**. Metabolic Flux Analysis of Compartmentalized Systems Using Dynamic Isotopologue Modeling. 2012.
124. **Ardo Illaste**. Analysis of Molecular Movements in Cardiac Myocytes. 2012.
125. **Indrek Reile**. 3-Alkylcyclopentane-1,2-Diones in Asymmetric Oxidation and Alkylation Reactions. 2012.
126. **Tatjana Tamberg**. Some Classes of Finite 2-Groups and Their Endomorphism Semigroups. 2012.
127. **Taavi Liblik**. Variability of Thermohaline Structure in the Gulf of Finland in Summer. 2012.
128. **Priidik Lagemaa**. Operational Forecasting in Estonian Marine Waters. 2012.
129. **Andrei Errapart**. Photoelastic Tomography in Linear and Non-linear Approximation. 2012.
130. **Külliki Krabbi**. Biochemical Diagnosis of Classical Galactosemia and Mucopolysaccharidoses in Estonia. 2012.
131. **Kristel Kaseleht**. Identification of Aroma Compounds in Food using SPME-GC/MS and GC-Olfactometry. 2012.
132. **Kristel Kodar**. Immunoglobulin G Glycosylation Profiling in Patients with Gastric Cancer. 2012.
133. **Kai Rosin**. Solar Radiation and Wind as Agents of the Formation of the Radiation Regime in Water Bodies. 2012.
134. **Ann Tiiman**. Interactions of Alzheimer's Amyloid-Beta Peptides with Zn(II) and Cu(II) Ions. 2012.
135. **Olga Gavrilova**. Application and Elaboration of Accounting Approaches for Sustainable Development. 2012.
136. **Olesja Bondarenko**. Development of Bacterial Biosensors and Human Stem Cell-Based *In Vitro* Assays for the Toxicological Profiling of Synthetic Nanoparticles. 2012.
137. **Katri Muska**. Study of Composition and Thermal Treatments of Quaternary Compounds for Monograin Layer Solar Cells. 2012.
138. **Ranno Nahku**. Validation of Critical Factors for the Quantitative Characterization of Bacterial Physiology in Accelerostat Cultures. 2012.
139. **Petri-Jaan Lahtvee**. Quantitative Omics-level Analysis of Growth Rate Dependent Energy Metabolism in *Lactococcus lactis*. 2012.
140. **Kerti Orumets**. Molecular Mechanisms Controlling Intracellular Glutathione Levels in Baker's Yeast *Saccharomyces cerevisiae* and its Random Mutagenized Glutathione Over-Accumulating Isolate. 2012.
141. **Loreida Timberg**. Spice-Cured Sprats Ripening, Sensory Parameters Development, and Quality Indicators. 2012.
142. **Anna Mihhalevski**. Rye Sourdough Fermentation and Bread Stability. 2012.
143. **Liisa Arike**. Quantitative Proteomics of *Escherichia coli*: From Relative to Absolute Scale. 2012.
144. **Kairi Otto**. Deposition of In₂S₃ Thin Films by Chemical Spray Pyrolysis. 2012.
145. **Mari Sepp**. Functions of the Basic Helix-Loop-Helix Transcription Factor TCF4 in Health and Disease. 2012.
146. **Anna Suhhova**. Detection of the Effect of Weak Stressors on Human Resting Electroencephalographic Signal. 2012.
147. **Aram Kazarjan**. Development and Production of Extruded Food and Feed Products Containing Probiotic Microorganisms. 2012.

148. **Rivo Uiboupin**. Application of Remote Sensing Methods for the Investigation of Spatio-Temporal Variability of Sea Surface Temperature and Chlorophyll Fields in the Gulf of Finland. 2013.
149. **Tiina Kriščiunaite**. A Study of Milk Coagulability. 2013.
150. **Tuuli Levandi**. Comparative Study of Cereal Varieties by Analytical Separation Methods and Chemometrics. 2013.
151. **Natalja Kabanova**. Development of a Microcalorimetric Method for the Study of Fermentation Processes. 2013.
152. **Himani Khanduri**. Magnetic Properties of Functional Oxides. 2013.
153. **Julia Smirnova**. Investigation of Properties and Reaction Mechanisms of Redox-Active Proteins by ESI MS. 2013.
154. **Mervi Sepp**. Estimation of Diffusion Restrictions in Cardiomyocytes Using Kinetic Measurements. 2013.
155. **Kersti Jääger**. Differentiation and Heterogeneity of Mesenchymal Stem Cells. 2013.
156. **Victor Alari**. Multi-Scale Wind Wave Modeling in the Baltic Sea. 2013.
157. **Taavi Päll**. Studies of CD44 Hyaluronan Binding Domain as Novel Angiogenesis Inhibitor. 2013.
158. **Allan Niidu**. Synthesis of Cyclopentane and Tetrahydrofuran Derivatives. 2013.
159. **Julia Geller**. Detection and Genetic Characterization of *Borrelia* Species Circulating in Tick Population in Estonia. 2013.
160. **Irina Stulova**. The Effects of Milk Composition and Treatment on the Growth of Lactic Acid Bacteria. 2013.
161. **Jana Holmar**. Optical Method for Uric Acid Removal Assessment During Dialysis. 2013.
162. **Kerti Ausmees**. Synthesis of Heterobicyclo[3.2.0]heptane Derivatives via Multicomponent Cascade Reaction. 2013.
163. **Minna Varikmaa**. Structural and Functional Studies of Mitochondrial Respiration Regulation in Muscle Cells. 2013.
164. **Indrek Koppel**. Transcriptional Mechanisms of BDNF Gene Regulation. 2014.
165. **Kristjan Pilt**. Optical Pulse Wave Signal Analysis for Determination of Early Arterial Ageing in Diabetic Patients. 2014.
166. **Andres Anier**. Estimation of the Complexity of the Electroencephalogram for Brain Monitoring in Intensive Care. 2014.
167. **Toivo Kallaste**. Pyroclastic Sanidine in the Lower Palaeozoic Bentonites – A Tool for Regional Geological Correlations. 2014.
168. **Erki Kärber**. Properties of ZnO-nanorod/In₂S₃/CuInS₂ Solar Cell and the Constituent Layers Deposited by Chemical Spray Method. 2014.
169. **Julia Lehner**. Formation of Cu₂ZnSnS₄ and Cu₂ZnSnSe₄ by Chalcogenisation of Electrochemically Deposited Precursor Layers. 2014.
170. **Peep Pitk**. Protein- and Lipid-rich Solid Slaughterhouse Waste Anaerobic Co-digestion: Resource Analysis and Process Optimization. 2014.
171. **Kaspar Valgepea**. Absolute Quantitative Multi-omics Characterization of Specific Growth Rate-dependent Metabolism of *Escherichia coli*. 2014.
172. **Artur Noole**. Asymmetric Organocatalytic Synthesis of 3,3'-Disubstituted Oxindoles. 2014.
173. **Robert Tsanev**. Identification and Structure-Functional Characterisation of the Gene Transcriptional Repressor Domain of Human Gli Proteins. 2014.

174. **Dmitri Kartofelev**. Nonlinear Sound Generation Mechanisms in Musical Acoustic. 2014.
175. **Sigrid Hade**. GIS Applications in the Studies of the Palaeozoic Graptolite Argillite and Landscape Change. 2014.
176. **Agne Velthut-Meikas**. Ovarian Follicle as the Environment of Oocyte Maturation: The Role of Granulosa Cells and Follicular Fluid at Pre-Ovulatory Development. 2014.
177. **Kristel Hälvin**. Determination of B-group Vitamins in Food Using an LC-MS Stable Isotope Dilution Assay. 2014.
178. **Mailis Päre**. Characterization of the Oligoadenylate Synthetase Subgroup from Phylum Porifera. 2014.
179. **Jekaterina Kazantseva**. Alternative Splicing of *TAF4*: A Dynamic Switch between Distinct Cell Functions. 2014.
180. **Jaanus Suurväli**. Regulator of G Protein Signalling 16 (RGS16): Functions in Immunity and Genomic Location in an Ancient MHC-Related Evolutionarily Conserved Synteny Group. 2014.
181. **Ene Viiard**. Diversity and Stability of Lactic Acid Bacteria During Rye Sourdough Propagation. 2014.
182. **Kristella Hansen**. Prostaglandin Synthesis in Marine Arthropods and Red Algae. 2014.
183. **Helike Lõhelaid**. Allene Oxide Synthase-lipoxygenase Pathway in Coral Stress Response. 2015.
184. **Normunds Stivriņš**. Postglacial Environmental Conditions, Vegetation Succession and Human Impact in Latvia. 2015.
185. **Mary-Liis Kütt**. Identification and Characterization of Bioactive Peptides with Antimicrobial and Immunoregulating Properties Derived from Bovine Colostrum and Milk. 2015.
186. **Kazbulat Šogenov**. Petrophysical Models of the CO₂ Plume at Prospective Storage Sites in the Baltic Basin. 2015.
187. **Taavi Raadik**. Application of Modulation Spectroscopy Methods in Photovoltaic Materials Research. 2015.
188. **Reio Põder**. Study of Oxygen Vacancy Dynamics in Sc-doped Ceria with NMR Techniques. 2015.
189. **Sven Siir**. Internal Geochemical Stratification of Bentonites (Altered Volcanic Ash Beds) and its Interpretation. 2015.
190. **Kaur Jaanson**. Novel Transgenic Models Based on Bacterial Artificial Chromosomes for Studying BDNF Gene Regulation. 2015.
191. **Niina Karro**. Analysis of ADP Compartmentation in Cardiomyocytes and Its Role in Protection Against Mitochondrial Permeability Transition Pore Opening. 2015.
192. **Piret Laht**. B-plexins Regulate the Maturation of Neurons Through Microtubule Dynamics. 2015.
193. **Sergei Žari**. Organocatalytic Asymmetric Addition to Unsaturated 1,4-Dicarbonyl Compounds. 2015.
194. **Natalja Buhhalko**. Processes Influencing the Spatio-temporal Dynamics of Nutrients and Phytoplankton in Summer in the Gulf of Finland, Baltic Sea. 2015.
195. **Natalia Maticiuc**. Mechanism of Changes in the Properties of Chemically Deposited CdS Thin Films Induced by Thermal Annealing. 2015.

196. **Mario Öeren.** Computational Study of Cyclohexylhemicucurbiturils. 2015.
197. **Mari Kalda.** Mechanoenergetics of a Single Cardiomyocyte. 2015.
198. **Ieva Grudzinska.** Diatom Stratigraphy and Relative Sea Level Changes of the Eastern Baltic Sea over the Holocene. 2015.
199. **Anna Kazantseva.** Alternative Splicing in Health and Disease. 2015.
200. **Jana Kazarjan.** Investigation of Endogenous Antioxidants and Their Synthetic Analogues by Capillary Electrophoresis. 2016.
201. **Maria Safonova.** SnS Thin Films Deposition by Chemical Solution Method and Characterization. 2016.
202. **Jekaterina Mazina.** Detection of Psycho- and Bioactive Drugs in Different Sample Matrices by Fluorescence Spectroscopy and Capillary Electrophoresis. 2016.
203. **Karin Rosenstein.** Genes Regulated by Estrogen and Progesterone in Human Endometrium. 2016.
204. **Aleksei Tretjakov.** A Macromolecular Imprinting Approach to Design Synthetic Receptors for Label-Free Biosensing Applications. 2016.
205. **Mati Danilson.** Temperature Dependent Electrical Properties of Kesterite Monograin Layer Solar Cells. 2016.
206. **Kaspar Kevvai.** Applications of ¹⁵N-labeled Yeast Hydrolysates in Metabolic Studies of *Lactococcus lactis* and *Saccharomyces Cerevisiae*. 2016.
207. **Kadri Aller.** Development and Applications of Chemically Defined Media for Lactic Acid Bacteria. 2016.
208. **Gert Preegel.** Cyclopentane-1,2-dione and Cyclopent-2-en-1-one in Asymmetric Organocatalytic Reactions. 2016.
209. **Jekaterina Služenikina.** Applications of Marine Scatterometer Winds and Quality Aspects of their Assimilation into Numerical Weather Prediction Model HIRLAM. 2016.
210. **Erkki Kask.** Study of Kesterite Solar Cell Absorbers by Capacitance Spectroscopy Methods. 2016.
211. **Jürgen Arund.** Major Chromophores and Fluorophores in the Spent Dialysate as Cornerstones for Optical Monitoring of Kidney Replacement Therapy. 2016.
212. **Andrej Šamarin.** Hybrid PET/MR Imaging of Bone Metabolism and Morphology. 2016.
213. **Kairi Kasemets.** Inverse Problems for Parabolic Integro-Differential Equations with Instant and Integral Conditions. 2016.
214. **Edith Soosaar.** An Evolution of Freshwater Bulge in Laboratory Scale Experiments and Natural Conditions. 2016.
215. **Peeter Laas.** Spatiotemporal Niche-Partitioning of Bacterioplankton Community across Environmental Gradients in the Baltic Sea. 2016.
216. **Margus Voolma.** Geochemistry of Organic-Rich Metalliferous Oil Shale/Black Shale of Jordan and Estonia. 2016.
217. **Karin Ojamäe.** The Ecology and Photobiology of Mixotrophic Alveolates in the Baltic Sea. 2016.
218. **Anne Pink.** The Role of CD44 in the Control of Endothelial Cell Proliferation and Angiogenesis. 2016.
219. **Kristiina Kreek.** Metal-Doped Aerogels Based on Resorcinol Derivatives. 2016.
220. **Kaia Kukk.** Expression of Human Prostaglandin H Synthases in the Yeast *Pichia pastoris*. 2016.

221. **Martin Laasmaa**. Revealing Aspects of Cardiac Function from Fluorescence and Electrophysiological Recordings. 2016.
222. **Eeva-Gerda Kobrin**. Development of Point of Care Applications for Capillary Electrophoresis. 2016.
223. **Villu Kikas**. Physical Processes Controlling the Surface Layer Dynamics in the Stratified Gulf of Finland: An Application of Ferrybox Technology. 2016.
224. **Maris Skudra**. Features of Thermohaline Structure and Circulation in the Gulf of Riga. 2017.
225. **Sirje Sildever**. Influence of Physical-Chemical Factors on Community and Populations of the Baltic Sea Spring Bloom Microalgae. 2017.
226. **Nicolae Spalatu**. Development of CdTe Absorber Layer for Thin-Film Solar Cells. 2017.
227. **Kristi Luberg**. Human Tropomyosin-Related Kinase A and B: from Transcript Diversity to Novel Inhibitors. 2017.
228. **Andrus Kaldma**. Metabolic Remodeling of Human Colorectal Cancer: Alterations in Energy Fluxes. 2017.